Bachelor thesis

Implementation of the V52-control strategy in MATLAB

through co-simulation MATLAB-SIMPACK

Diese Arbeit wurde am Chair for Wind Power Drives vorgelegt von:

Javier Orera
Matrikelnummer: 399450

Fakultätsinterner Betreuer: Prof. Dr.-Ing. Ralf Schelenz
Betreuender wissenschaftlicher Mitarbeiter: Baher Azzam

Aachen, den 05.02.2019

Erklärung zur selbständigen Erstellung der Arbeit

Ich versichere, dass ich die vorliegende Arbeit einschließlich aller beigefügter Materialien selbstständig und ohne Benutzung anderer, als der angegebenen Hilfsmittel angefertigt habe. Alle Stellen, die wörtlich oder sinngemäß aus veröffentlichten oder unveröffentlichten Werken entnommen sind, sind in jedem Einzelfall unter Angabe der Quelle deutlich als solche kenntlich gemacht. Die Arbeit ist in gleicher oder ähnlicher Form noch nicht als Prüfungsarbeit eingereicht worden.

_____

Aachen, den 05.02.2019   Unterschrift

Contents

Symbols

Symbol	Unit	Description
$n_{measures}$	rad/s	Rotational speed in the main shaft from measurement data.
$n_{simpack}$	rad/s	Rotational speed in the main shaft from Simpack.
T_m, T_r, Tm	Nm	Mechanical torque in low-speed shaft.
T_e, T_g, Te, Me	Nm	Electrical or generator torque.
$M_{Turbine}$	kg	Sum of masses of the nacelle and the tower.
F_t	N	Thrust force in x-direction.
$c_T(\lambda, \beta)$	-	Thrust coefficient.
$c_p(\lambda, \beta)$	-	Power coefficient.
H_{Turm}	m	Tower height.
β	°	Pitch angle.
v_{wind}, u	m/s	Averaged wind speed.
P_m	W	Mechanical power in the low-speed shaft.
$c_q(\lambda, \beta)$	-	Torque coefficient.
ρ	kg/m^3	Densitiy of the air.
J	kgm^2	High-speed shaft inertia.
n	rad/s	High-speed shaft speed.

Abbreviations

Abbreviation	Description
WT(s)	Wind turbine(s)
V52 Simpack-Model	V52-SM
State-Space Model	SSM
Existing Simulated Controller	ESC
New Simulated Controller	NSC
Multi-Body Simulation	MBS
MATLAB-SIMPACK Co-simulation	MSC
Global State-Space Model	GSSM

Table index

Figure index

Abstract

Wind turbines (WTs) are complex and highly loaded systems, which leads to the importance of the task to determine the loads in the powertrain before operation. At CWD there are existing simulation models with a multi-body system approach, and simulated controllers which work parallel with them. In this case, a multibody SIMPACK-model is used to simulate the powertrain loads in the V52-testbench. Since the simulated controller for this model does not contain the operating strategy used in the real plant (V52-testbench), the thesis aims to design a new controller that reproduces this strategy. The existing simulated controller will be adapted to the real controller from the test bench.

The experimental measurements taken in the V52-testbench will be used to run the co-simulation MATLAB-SIMPACK needed for the development and implementation of a new simulated controller. The controller will get the simulated rotational speed in the low-speed shaft from the V52-testbench SIMPACK-model as input, and will output the torque in the generator that the model needs to produce the desired output rotational speed. A comparison between the response of the V52-testbench SIMPACK-model with the existing simulated controller and the new simulated controller will be investigated. The response of the controller to different rotational speed-input signals will be also tested and improved by means of another controller operating at a higher control level.

In order to determine if the method used to implement the new controller is transferable to the upcoming generator on the V52-testbench, the behavior of this new generator will be integrated in the V52-testbench SIMPACK-model by modifying the generator´s shaft moment of inertia in the model. A sensitivity analysis will be carried out in order to identify which parameters to change when adapting the controller to the new generator.

1. State of the art

This chapter provides some information about the current state of the wind turbine industry in subsection 1.1 and an overview of the most important control strategies used in the wind turbines in subsection 1.2.

1.1 Introduction

Wind turbines (WT) are becoming very relevant not only in the renewable energy industry, but also in the energy industry. There are currently about 539.581 globally installed MW, 52.573 of them in 2017 [GWE17]. Figure 1.1 shows the rapid increasement of the global annual installed wind capacity since the year 2001 (6.5 MW) until the year 2017 (52.573 MW). Furthermore, the current installed wind capacity can already cover more than 5% of the global electricity consumption [GWE17].
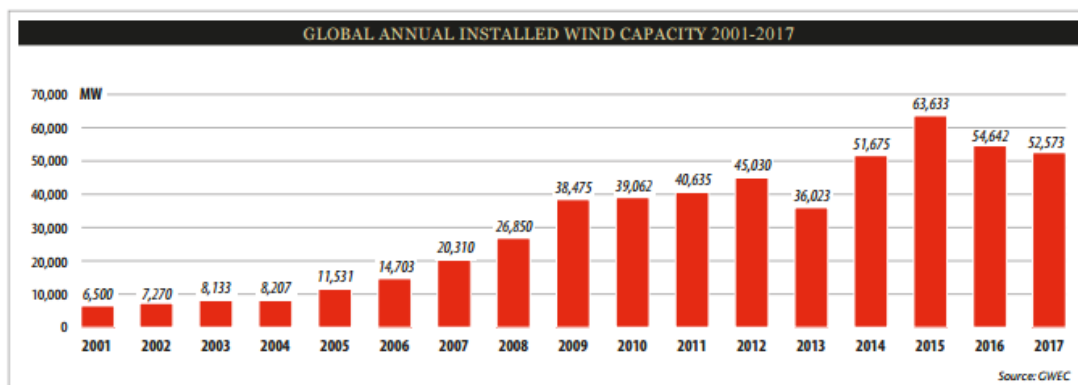
Figure 1.1:   Upward tendency of the installation of WTs in recent years 2001-2017, Source: [GWE17].

1.2 Control of wind turbines and new areas of research.

In this subsection the most important control strategies will be explained (subsection 1.2.1), as well as the relatively new individual pitch control strategy, described in subsection 1.2.2.

The controller plays an important role in a WT. Its influence determines the loads that appear on the components of the WT and the output generated electrical power [MMM02]. Therefore, the following regulation systems become relevant, as specified in [MMM02]:

- Sensors: wind speed, generator torque, power/current in the stator, temperature and speed in the generator or main shaft.

- Controllers: electrical and mechanical system and computers.

- Power Amplifiers: e.g. switches, pumps.

- Actuators: e.g. motors, magnets, coils, pistons.

There are two important different levels of wind turbine control: supervisory control and dynamic control [MMM02]. The supervisory control follows a sequence of commands to release the brakes or close the switches [MMM02]. This controller produces long-term changes in the wind turbine [MMM02]. The dynamic control measures different parameters from the dynamic operation and receives signals from the supervisory control [MMM02]. It generates certain signals for the positioning actuator and drive systems. In contrast with the supervisory control, this controller produces high-speed adjustments in the wind turbine actuators and components [MMM02]. In this thesis, the new simulated controller will try to

reproduce the supervisory and dynamic control, considering the global dynamic of the plant, and not the behavior of each component (e.g. brakes, switches and actuator).

The main goals of the control system are to maintain a safe operation of the turbine, to maximize the energy production, as well as to minimize the loads in the machine components to increase their fatigue life [MMM02].

1.2.1. Control basics

The aerodynamic torque can be regulated by means of the rotor tip speed ratio, rotor blade geometry, yaw and other additional parameters [MMM02].

To regulate this torque, there are various control strategies:

- **Fixed-speed turbines and variable speed turbines:**

  First, there is a difference between *fixed-speed* and *variable-speed* turbines. *Fixed-speed* turbines keep a constant rotational speed for all wind speeds [Wik]. The generator torque can only be changed in these turbines by regulation of the aerodynamic torque (change of pitch or yaw angle) [MMM02]. In the second one, both aerodynamic torque and generator torque can be changed by means of the generator control system [MMM02]. This is possible thanks to a power converter, specifically a inverter, which operates with Pulse-Width-Modulation technology [MMM02]. This power converter turns the non-constant frequency in the stator (as seen in Equation 1.1), determined by the number of poles and the rotational speed of the generator shaft, into the grid frequency (50 Hz or 60 Hz) so that the generator can be coupled to the grid.
  The frequency of the generated power in a wind turbine is determined by [MMM02]:

  $$f = \frac{N \cdot P}{120}$$ Equation 1.1

  where N is the rotational speed and P is the number of magnetic poles.

- **Stall-regulated rotor** (*power limitation by flow separation*) **and pitch-regulated rotor:**

  In the case of *stall-controlled fixed-speed turbines*, the blades are built up so that the power is regulated [MMM02]. Figure 1.2 shows the dependency of the coefficient of lift on the angle of attack. When the angle of attack reaches the stall angle, the coefficient of lift (which determines the rotor efficiency) decreases, and therefore the rotor efficiency decreases also [AE]. This effect will finally limit the output generated power [MMM02].

Chair for Wind Power Drives
Univ.-Prof. Dr.-Ing. Georg Jacobs

2
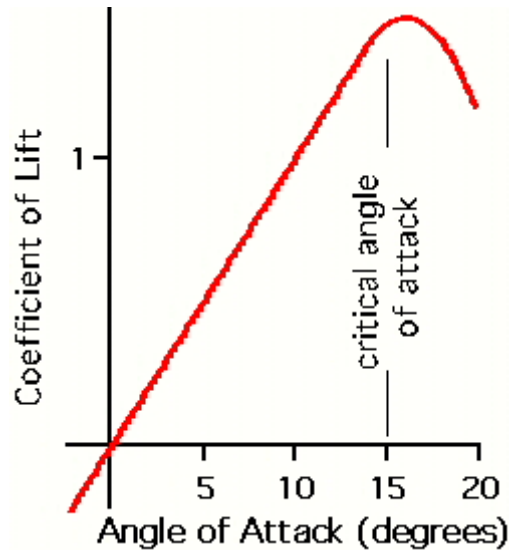
Figure 1.2: Dependence of the coefficient of lift on the angle of attack, Source: [AE].

Regarding *pitch-regulated fixed-speed* turbines, the power control provides some advantages in respect to *stall-regulated* turbines [REA15], because pitch control allows these turbines to have a constant power output above the rated wind speed, while *stall-regulated turbines* are not able to keep a constant power output at high winds [REA15], as shown in Figure 1.3.
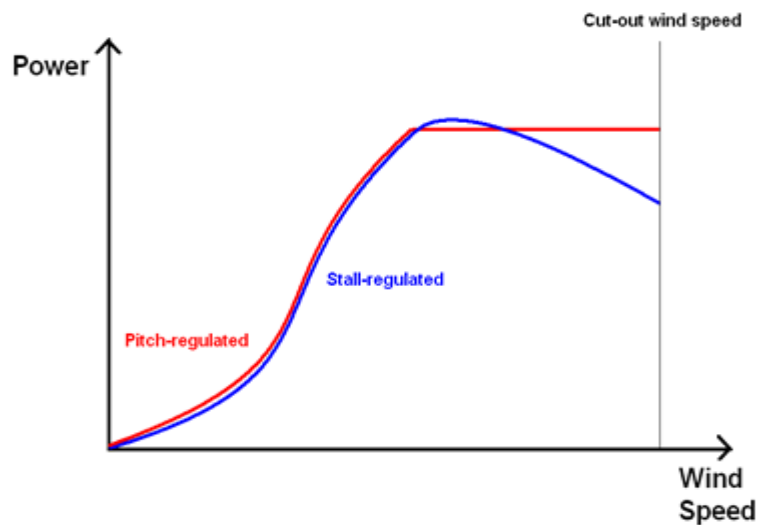
Figure 1.3: Power dependence on wind speed for pitch and stall-regulated turbines, Source: [REA15].

If we now consider *stall-regulated variable-speed* turbines, power electronics is used to control the generator torque so that the turbine can operate at the optimum speed [MMM02]. If the generator torque is lower than the aerodynamic torque, the rotor will accelerate according to Equation 4.1 (the difference of both torques is positive and therefore the angular acceleration is positive as well) [MMM02].

Regarding *pitch-regulated variable-speed* turbines, it is possible to distinguish between *active pitch-regulated* turbines and *passive pitch-regulated* turbines [MMM02]. V52 turbine belongs to the first group.

Chair for Wind Power Drives
Univ.-Prof. Dr.-Ing. Georg Jacobs

3

1.2.2. New strategies for control of WTs

The development of the pitch angle control strategies in the recent years has taken two different directions [Sel07]: limiting the aerodynamic torque in above rated wind speed conditions and optimizing the efficiency of the WT (maximum energy extracted from the wind) under rated wind speed conditions [Sel07].

Rotors have increasing diameters and because of that, asymmetrical loads appear [Sel07]. These loads reduce strongly the life of the WT [Sel07].

These asymmetric loads are caused by the following reasons [VES11]:

-Uneven wind distribution in the rotor plane.

-False yaw alignment.

-High turbulence.
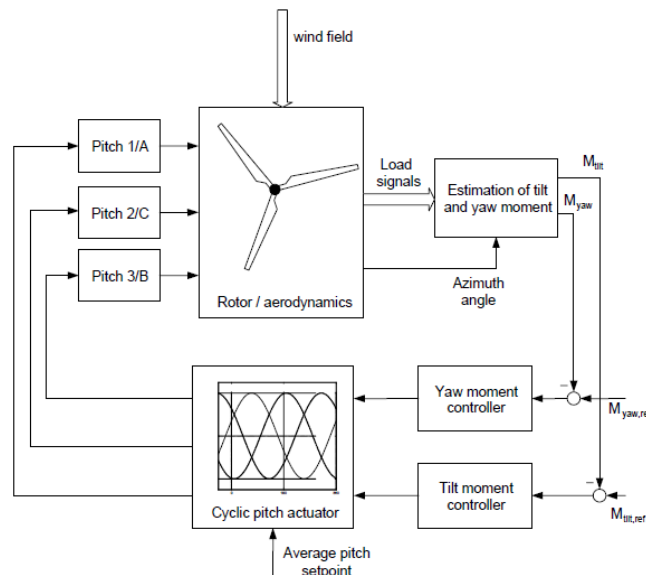
Figure 1.4:   Individual pitch control, Source: [VES11].

Overall, the individual pitch system works as shown in Figure 1.4 [VES11]: loads are calculated at the root of the blade by means of an estimator of a yawing moment and tilt torque [VES11]. The reference magnitudes for both are compared with the calculated yaw moment and tilt moment and adjusted to reference with two controllers [VES11]. Then, the *Cylic-pitch-actuator* block sets the 3 pitch systems (for each blade) to perform the cyclic pitch operation around the average pitch set-point [VES11]. The pitch angle for each blade A, B, C is a function of the azimuth angle and it moves sinusoidally. The three pitch angle waves are shifted 120º with each other [VES11]. Their amplitude is usually ± 2º, and ± 5º in some extreme cases [VES11].

2. Description and model of the V52-wind turbine

The following chapter attempts to give an overview of the systems that integrate the V52 turbine of the test rig, since that will be important for the understanding of the existing controller and the development of the new one. Information from the available V52-documentation will be summarized and analyzed. In subsection 2.1 the general operation of the turbine will be explained, and in subsection 2.2 the mathematical model of the main components of the turbine will be investigated. Subsection 2.3 describes the V52-Simpack model (V52-SM) and how will the co-simulation run.

2.1 Description of the turbine

This subsection aims to give an overview of the most important components of the V52 turbine as well as to provide with some useful information about its control strategy (subsection 2.1.1) and operation modes (subsection 2.1.2).

Technical specifications

❶ Ultrasonic wind sensor	❻ Oil and water coolers	⓫ Blade bearing	⓰ Machine foundation
❷ Service crane	❼ Gearbox	⓬ Blade	⓱ Mechanical disc brake
❸ VMP-Top controller with converter	❽ Main shaft	⓭ Rotor lock system	⓲ Yaw gear
❹ OptiSpeed® generator	❾ Pitch system	⓮ Hydraulic unit	⓳ Composite disc coupling
❺ Pitch cylinder	❿ Blade hub	⓯ Torque arm	

Figure 2.1:   Overview of the most relevant components, Source: [VESA3].

There are approximately 2100 VESTAS-52 (V52) turbines in the world [VESTCurve].

Figure 2.1 shows the most relevant components of the V52-turbine. The usual operation of the turbine works as follows (the following information is extracted from [LCK11]): wind speed is detected by the ultrasonic wind sensor as shown in Figure 2.1-mark 1. With this measurement, the controller calculates the correct pitch angle for the blades (12). After that, the rotor starts to rotate, as well as the low speed shaft (8). The gearbox (7) converts the speed of the rotor shaft into higher speed in the generator high-

speed shaft. In the generator (4), mechanical loads are converted into electrical torque through electromagnetic conversion.

The power generated depends on the wind speed as shown in Figure 2.2. If the wind speed is low (less than 4 m/s (cut-on wind speed), the turbine will not generate any power [VESChar; VESTCurve]. That keeps the power constant above the rated wind speed and bellow the shutdown speed (25 m/s), since it is pitch-regulated (see Figure 1.3) [VESTCurve].

Power curve V52-850 kW

Legend:
- 100.0 dB(A)
- 101.0 dB(A)
- 102.0 dB(A)
- 103.0 dB(A)
- 104.2 dB(A)
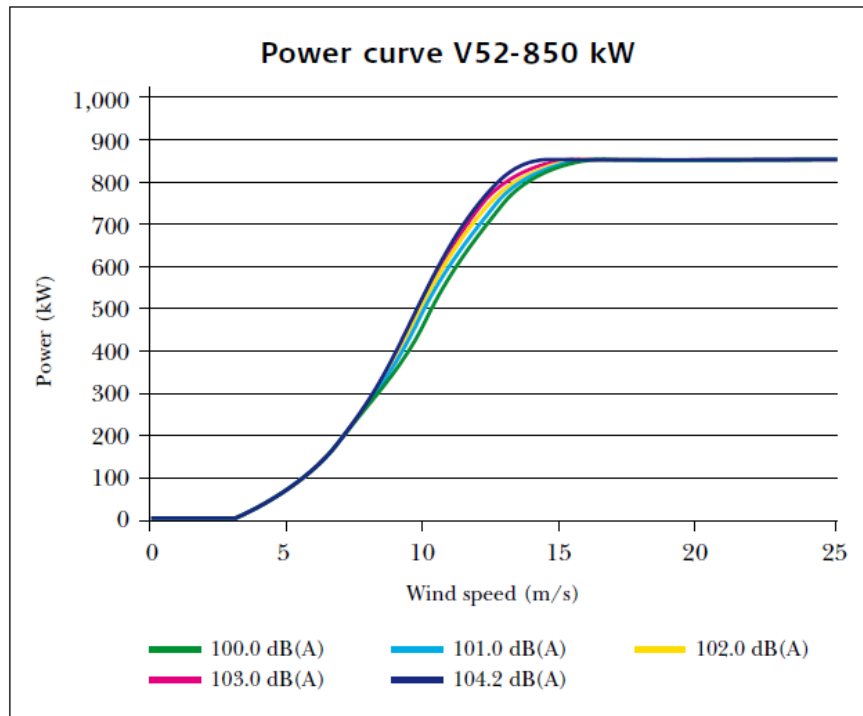
Figure 2.2:   Stationary-state power for different conditions of noise, Source: [VESA3].

The characteristics of this turbine are shown in Figure 2.3 and the most important ones are (the following information is extracted from Figure 2.3 in [VES]):

- The power control is controlled by the *Pitch/OptiSpeed* strategy. This control strategy will be explained in detail later.
- The nominal wind speed is v=16 m/s and the generator is asynchronous (it includes *OptiSpeed* control).
- The nacelle has different heights, respectively from 40 m to 65 m.
- The whole system weighs from 71 tons to 109 tons, depending on the nacelle´s height.
- V52 generates 850 KW of rated power and is a pitch-regulated variable-speed turbine [VEST] .
- V52 operates with variable speed thanks to the *OptiSpeed* strategy [Dut16].

2.1.1 Control strategy.

The main controller generates two signals, the reference for the pitch angle and the reference for the electrical power [VES11]. The pitch regulator and the power controller adjust the pitch angle and power generated according to the measured reference value [VES11]. The main controller contains most of the control loops and algorithms for the monitoring of the system. It has four specific tasks, described in [VES11]:

- Maximize the output power of the WT.

- Limit the mechanical loads occurring on the drive train.

- Limit acoustic noise.

- Maintain the quality of the high-power production.

Rotor	
Diameter:	52 m
Area swept:	2,124 m²
Speed of revolution:	26 o/min
Operational interval:	14.0-31.4 o/min
Number of blades:	3
Power regulation:	Pitch/OptiSpeed®
Air brake:	Feathered

Tower	
Hub height (approx.):	40 m, 44 m, 49 m, 55 m, 60 m, 65 m

Operational data	
Cut-in wind speed:	4 m/s
Nominal wind speed:	16 m/s
Stop wind speed:	25

Generator	
Type:	Asynchronous with OptiSpeed®
Nominal output:	850 kW
Operational data:	50 Hz/60 Hz
	690 V

Gearbox	
Type:	1 planet step/2-step parallel axle gears

Control	
Type:	Microprocessor-based monitoring of all turbine functions as well as OptiSpeed® output regulation and OptiTip® pitch regulation of the blades.

Weight (IEC IA/IEC IIA)						
	40 m	44 m	49 m	55 m	60 m	65 m
Tower:	39 t/-	44 t/-	50 t/-	57 t/52 t	69 t/-	77 t/-
Nacelle:	22 t	22 t	22 t	22 t	22 t	22 t
Rotor:	10 t	10 t	10 t	10 t	10 t	10 t
Total:	71 t/-	76 t/-	82 t/-	89 t/84 t	101 t/-	109 t/-

Figure 2.3: Characteristics of the V52-turbine, Source: [VES].

The main controller has the structure shown in Figure 2.4 [VES11] :

Chair for Wind Power Drives
Univ.-Prof. Dr.-Ing. Georg Jacobs

7
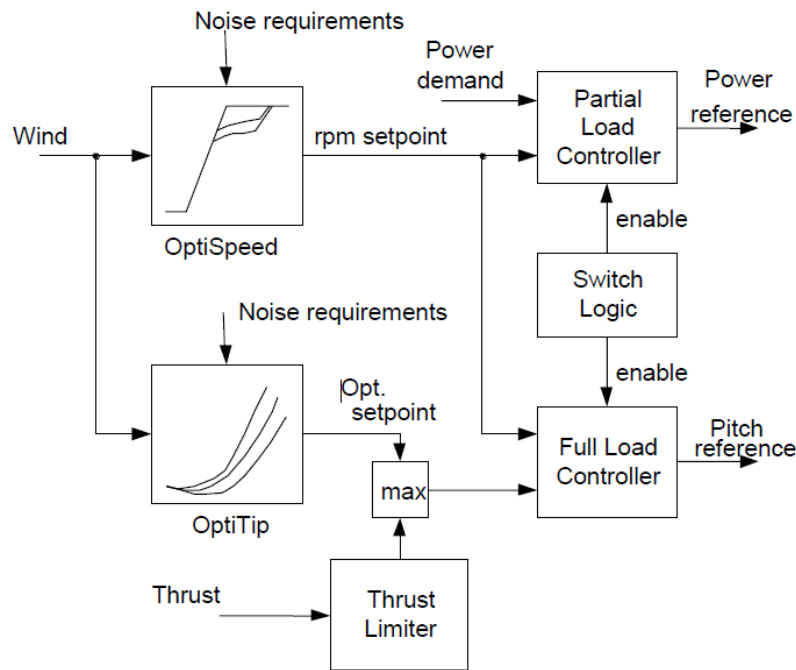
Figure 2.4:   Overview of the main controller structure, Source: [VES11].

OptiSpeed and **OptiTip** strategies mentioned in Figure 2.4 are relevant components of the main controller and calculate the optimal pitch angle (*OptiTip*) and rotational speed (*OptiSpeed*) both dependent on wind speed measurements and current noise emission specifications [VES11]. The *Optimal Set point* (optimal pitch and speed) is therefore calculated, with the objective of reaching maximum power efficiency [VES11].

The blocks on the right in Figure 2.4 are responsible for the adjustment of the turbine to *Pitch Optimal Set point* and the adjustment of the generated power to the grid requirements [VES11].

If the wind speed exceeds a certain level, the pitch angle increases above *Pitch Optimal Set point* [VES11]. When this happens, the required power equals the rated power and the wind speed is called *rated wind speed* [VES11]. Then *Switch Logic* switches the *Partial Load Controller* on to ensure maximum power efficiency [VES11]. The *Partial Load Controller* calculates only the power reference, which means that the pitch angle does not change [VES11].

However, wind speed may increase above rated wind speed [VES11]. In this case, *Switch Logic* switches the *Full Load Controller* on to limit power to nominal power and also its corresponding loads [VES11]. The *Full Load Controller* calculates only the pitch reference, which means that the output power does not change [VES11].

In the main controller, there is also a *Thrust Limiter* (shear force limiter), with which a different pitch angle is calculated according to the estimated thrust force [VES11]. The maximum required pitch angle between *Pitch Optimal Set point* and *Thrust Limiter* is selected and inputted into the *Full Load Controller*, as well as the speed (*OptiSpeed*) [VES11]. The *Full Load Controller* then outputs the pitch reference [VES11].

2.1.2. Partial load and Full load operation in the V52 system.

Specifying for the V52-turbine, the wind turbine never generates any power under wind speed less than 3 m/s [VES11]. Taking v as wind speed, if v <= v1 (v1=4 m/s), the rotor speed is minimal. In the case that v1<v<= v2 (v2=8m/s), *OptiSpeed* is activated but not *OptiTip*, since the pitch angle is kept almost constant [VES11]. Operation over *v2* leads the rotor speed through the nominal rotor speed [VES11].

Referring to the case that v>v2, the power output equals the required power, *Full Load operation* is activated, and pitch control adjusts the *Pitch Optimal Set point* [VES11]. Nevertheless, it is possible for the controller to change from *Full Load operation* to *Partial Load operation* under turbulence conditions [VES11].

In the following figures both operation modes can be distinguished:
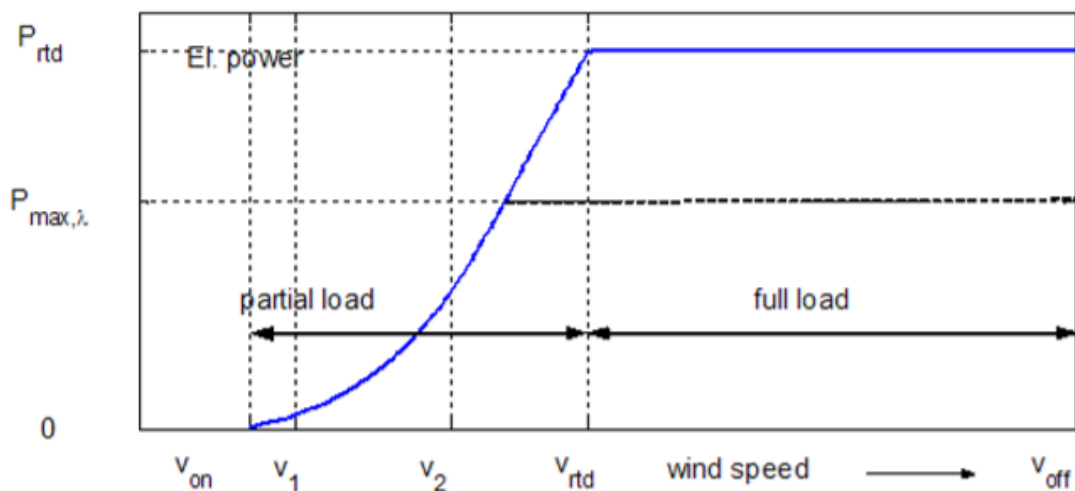
Figure 2.5:   Output electrical power for different wind speeds, Source: [VES11].
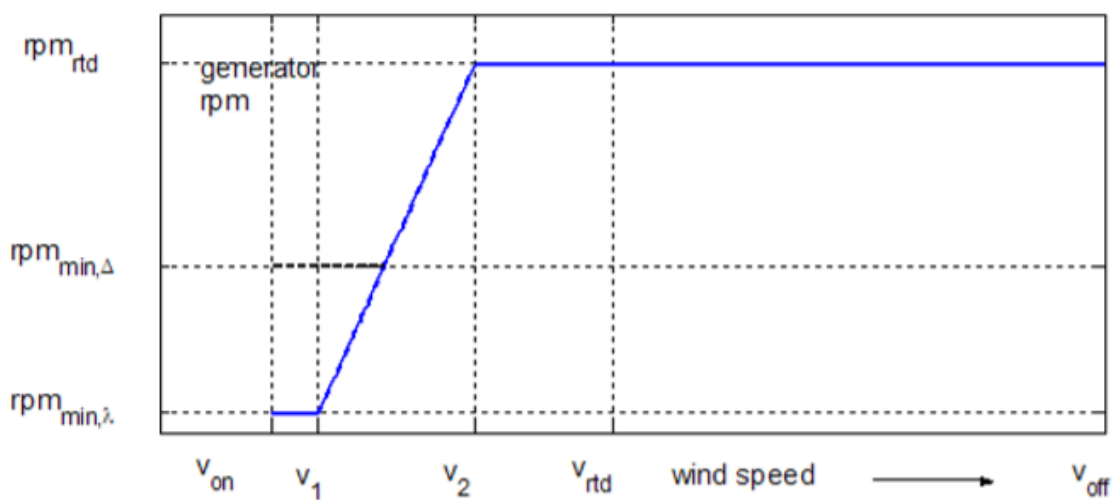
Figure 2.6:   Rotational speed in the high-speed shaft for different wind speeds, Source: [VES11].

2.2 Description of the components and their mathematical modelling.

A description of the main components of the V52-turbine (each subsection describes a component) will be done in this chapter, with a special focus on the mathematical model of each component and its possible use in the understanding of the existing simulated controller (ESC) and the implementation of the new one (NSC). Also the star-delta switch strategy will be analysed in subsection 2.2.6.

2.2.1. Tower (based on the model in [LCK11]).

First, wind speed is measured (V_{wind}). The tower model calculates the hub speed ($\dot{y}$) by means of the thrust (F_{tx}). Therefore, the effective wind speed at the rotor is calculated as $V_{eff} = V_{wind} - \dot{y}$ [LCK11]. When the second Newton's law, shown in Equation 2.1, is applied to the tower model shown in Figure 2.7, we obtain Equation 2.2.

$$\sum F_x = M_{Turbine} x \qquad \text{Equation 2.1}$$

$$F_{t-x} - K_{Feder-x} x - D_{Stoßdämpfer-x} \dot{x} = M_{Turbine} \ddot{x} \qquad \text{Equation 2.2}$$

where $F_{t-x}(N)$ is the thrust force; $K_{Feder-x}\left(\frac{N}{m}\right)$ is the rigidity of the tower; $D_{Stoßdämpfer-x}\left(\frac{\frac{N}{m}}{s}\right)$ is the dampening of the tower; $M_{Turbine}$ is the sum of masses of the nacelle and the tower.
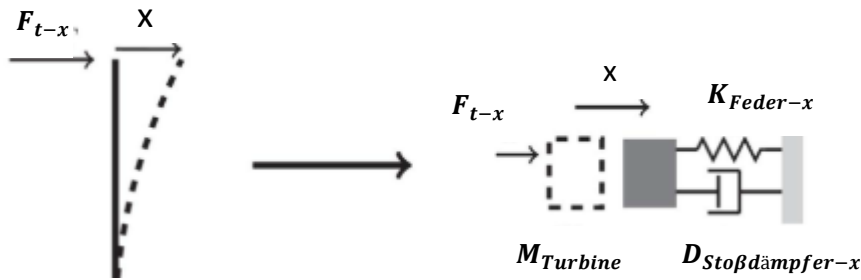
Figure 2.7:   On the left: tower bending; On the right: tower one-mass oscillator model, Source: [Sim16].

It is possible to calculate the thrust force in the hub as specified in [DMS15]:

$$F_t = F_t(v_{wind}, \lambda, \beta) = \frac{1}{2}\rho\pi r_t^2 v_{wind}^2 c_T(\lambda, \beta) \qquad \text{Equation 2.3}$$

where $\rho = 1.225\frac{kg}{m^3}$, $r_t = \frac{\phi_{rotor}}{2} = \frac{52}{2} = 26\ m$ [VES].

$c_T(\lambda, \beta)$ is called *thrust coefficient* and is calculated through $c_p(\lambda, \beta)$, called *power coefficient*, as specified in [Pie06] :

$$c_p\ (\lambda, \beta) = \frac{1}{2}\left(1 + \sqrt{1 - c_T(\lambda, \beta)}\right) c_T(\lambda, \beta)$$

Equation 2.4

The curve graphical representation is shown in Figure 2.8.
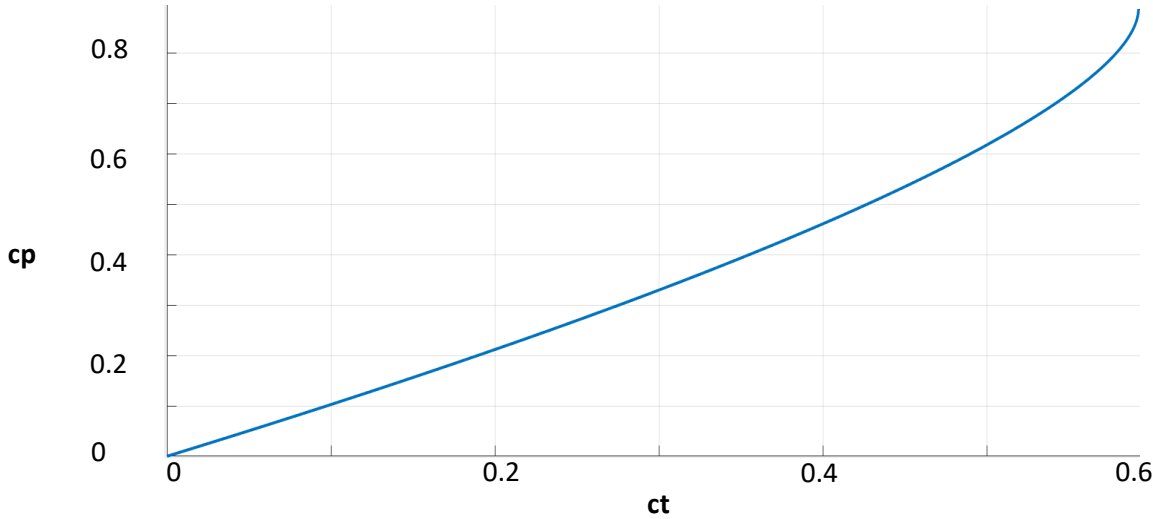
Figure 2.8:   *ct* curve.

with $c_p(\lambda, \beta) < \frac{16}{27}$ und $c_T(\lambda, \beta) < \frac{8}{9}$

Furthermore, it is possible to calculate the total force over the whole tower by integrating the distribution of the thrust over the tower, taking this distribution as (information extracted from [ŞAE]):

$$U_2 = U_1 \left(\frac{z_2}{z_1}\right)^{\alpha} = U_{Gondel} \left(\frac{z}{H_{Turm}}\right)^{\frac{1}{7}}$$

Equation 2.5

where U_1 the wind speed at the height is z_1, U_2 is the wind speed at the height z_2 , H_{Turm} is the height of the hub and α is the altitude exponent $(\alpha = 1/7)$.

The altitude exponent depends on various parameters: time of day, season, temperature, atmospheric stability, climatology, terrain and surface roughness, environmental conditions, weather stability and altitude [ŞAE; KAB]. The bigger the exponent is, the larger the vertical gradient in the wind speed will be [KAB].

By means of Equation 2.3 and Equation 2.5, it is possible to get an analytic expression of the total thrust force that the tower experiments, as specified in [KMD08]:

$$F_T = F_{thrust}\ + f = \frac{1}{2}\rho\pi r_t^2 v_{wind}^2 c_T(\lambda, \beta) + \int_0^H f(h)dh = \frac{1}{2}\rho\pi r_t^2 v_{wind}^2 c_T(\lambda, \beta) +$$

$$\int_0^{H_{Turm}} \frac{1}{2}\rho\pi r_t^2 \left(U_{Gondel}\left(\frac{z}{H_{Turm}}\right)^{\frac{1}{7}}\right)^2 c_p(\lambda, \beta)dz = \frac{1}{2}\rho\pi r_t^2 v_{wind}^2 c_T(\lambda, \beta) +$$

$$\int_0^{H_{Turm}} [\frac{1}{2}\rho\pi r_t^2 \left(U_{Gondel}\left(\frac{z}{H_{Turm}}\right)^{\frac{1}{7}}\right)^2 [c_1[c_2 f(\lambda, \beta) - c_3\beta - c_4\beta^x - c_5]e^{-c_6 f(\lambda, \beta)}]]\, dh$$

Equation 2.6

CWD Chair for Wind Power Drives | RWTH AACHEN UNIVERSITY

Chair for Wind Power Drives
Univ.-Prof. Dr.-Ing. Georg Jacobs

11

2.2.2. Pitch angle-model [VES11].

In subsection, the pitch control strategy of the V52 will be explained.

The pitch angle β is regulated by means of the pitch control system [VES11]:
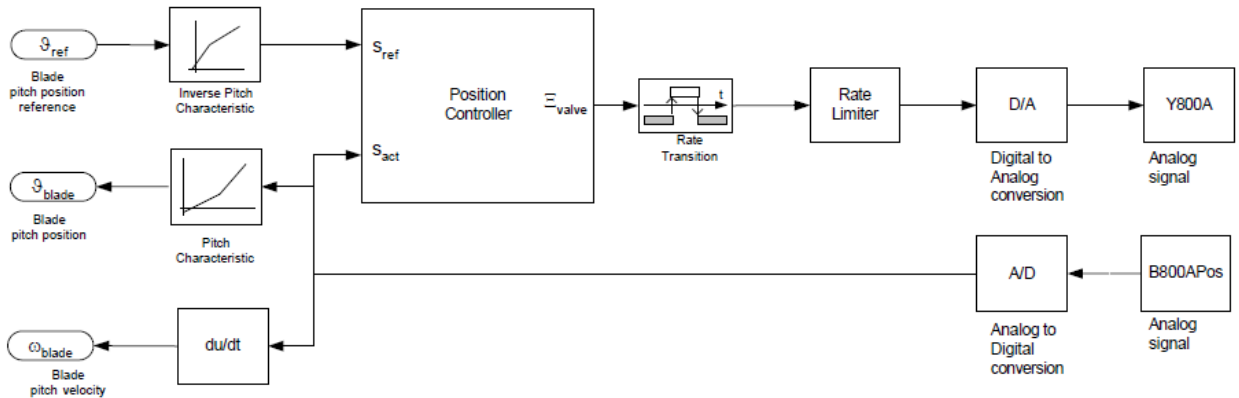
Table 1: *Pitch characteristics*, Source: [VES11].

Figure 2.9: Pitch control system, Source: [VES11].

The *pitch characteristics curve* is the following:

$$\beta(u) = \begin{cases} a_1u + b_1 & for\ u \le u_{cross} \\ a_2u + b_2 & for\ u \ge u_{cross} \end{cases} \qquad \text{Equation 2.7}$$

where $u_{cross} = (b_2 - b_1)/(a_2 - a_1);\ \beta_{cross} = \beta(u_{cross}) = a_1u_{cross} + b_1$

The manufacturer VESTAS gives the following table (**Table 1**), which assigns a piston position (position-mm) and a position transducer voltage (position-volts) for each possible pitch angle. **This** position transducer converts the piston position into a voltage signal [VES11]. The (Digital) Position Controller will get this reference voltage (s_{ref}) from the main control and calculate a suitable valve position signal using the current measured transducer voltage (s_{act}) (see Figure 2.9) [VES11].

The signal for the valve includes also a *Rate Transition* and *Rate Limiter,* shown in Figure 2.9. The rate limiter limits the derivative of the signal, what means that the pressure gradients in the hydraulic systems are reduced [VES11]. A D/A converter generates the analog signal for the valve actuator (servomotors) to control the piston position [VES11].

	V52	
Pitch [deg]	Position [mm]	Position [V]
-5	0	0,040
0	27	0,460
5	56	0,970
10	87	1,500
15	119	2,050
20	152	2,620
25	185	3,190
30	218	3,760
35	251	4,320
40	282	4,870
45	313	5,400
50	344	5,920
55	373	6,430
60	402	6,930
65	430	7,410
70	458	7,890
75	486	8,370
80	514	8,850
85	542	9,350
90	572	9,860

Figure 2.10 and Figure 2.11 show respectively the *pitch characteristics curve* and *inverse pitch characteristics curve* according to Equation 2.7.

Chair for Wind Power Drives
Univ.-Prof. Dr.-Ing. Georg Jacobs

12
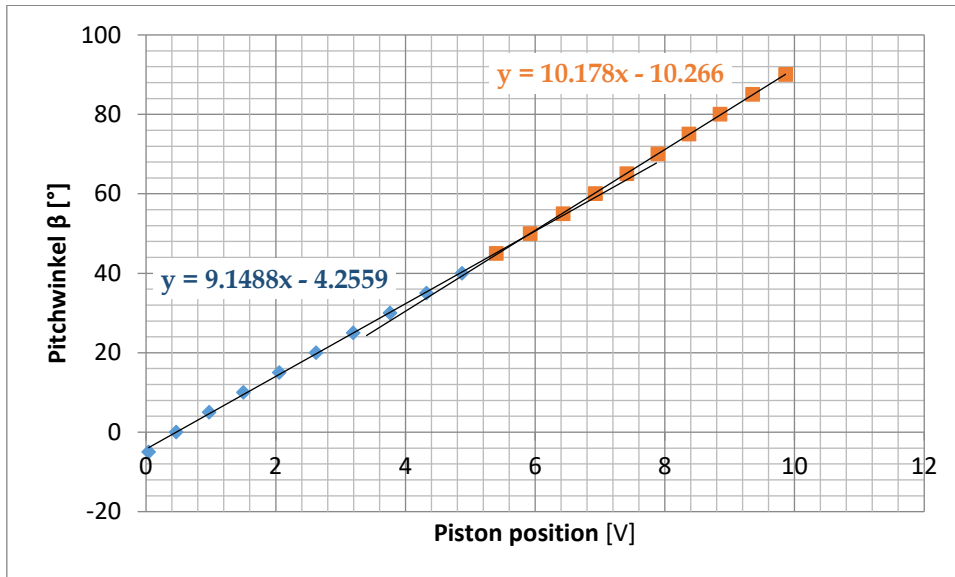
Figure 2.10: *Pitch characteristics curve* (linear interpolation).
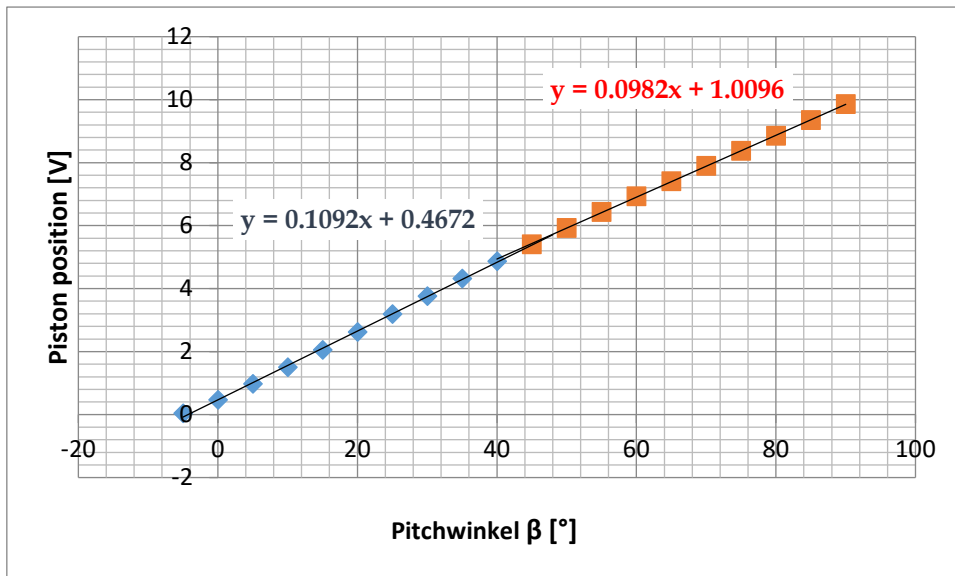
Figure 2.11: *Inverse pitch characteristic* curve (linear interpolation).

Figure 2.12 also shows the *pitch characteristics curve* but now the pitch position is in mm.

Chair for Wind Power Drives
Univ.-Prof. Dr.-Ing. Georg Jacobs

13
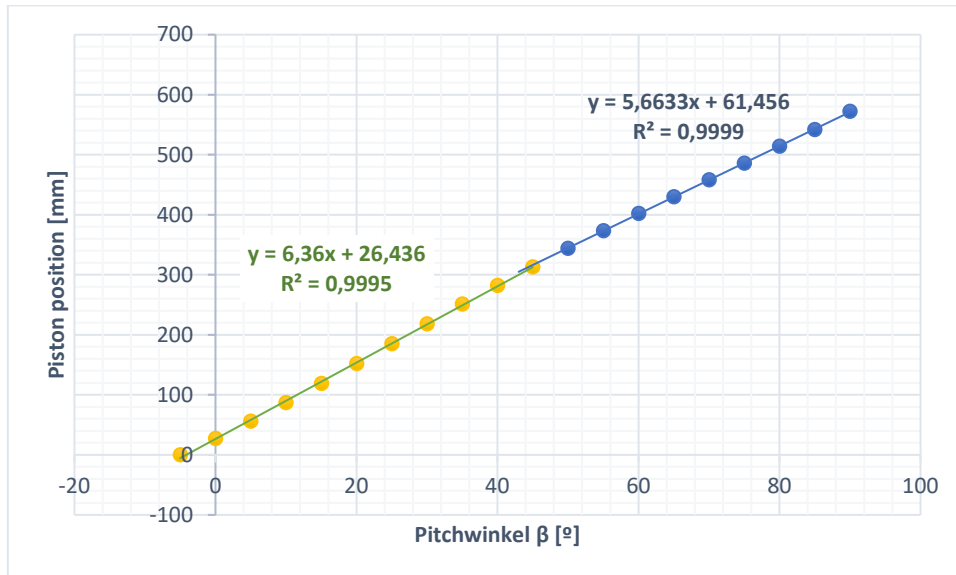
Figure 2.12: *Pitch characteristic curve* (linear interpolation).
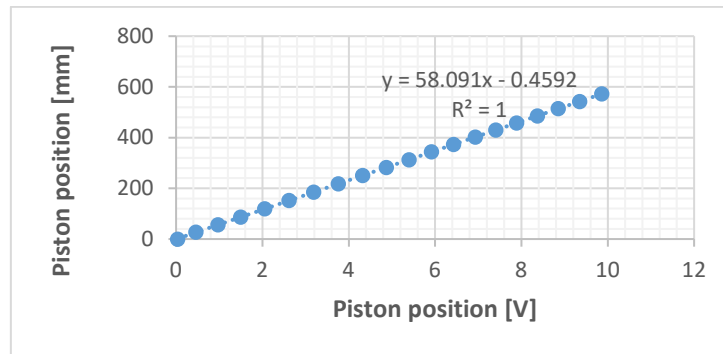
Figure 2.13: Piston analogic/position-converter characteristics.

The slope of the fitting line in Figure 2.13 is 58.3. This information is relevant for the pitch regulation control strategy, with which a pitch reference is converted into piston position. This conversion may be useful for the design of the new controller, because it describes the pitch actuator exactly.

The control strategy for the pitch regulation consists of a feedback control closed-loop with a controller [VES11]. The controller has different components depending on the operating state of the WEA *(Partial load operation* or *Full load operation)* [VES11].

Partial load operation usually uses the *Low Activity Position Controller* (LAPC) as seen in Figure 2.14.
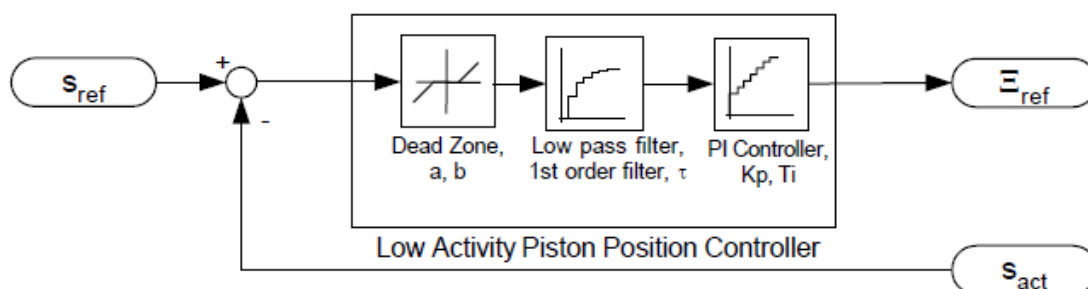
Figure 2.14: Pitch control loop for *Partial load operation* in V52 turbine, Source: [VES11].

Full load operation usually uses the *Fast Response Position Controller* (LAPC) shown in Figure 2.15. This controller ensures that the desired execution is carried out at the generator speed [VES11].
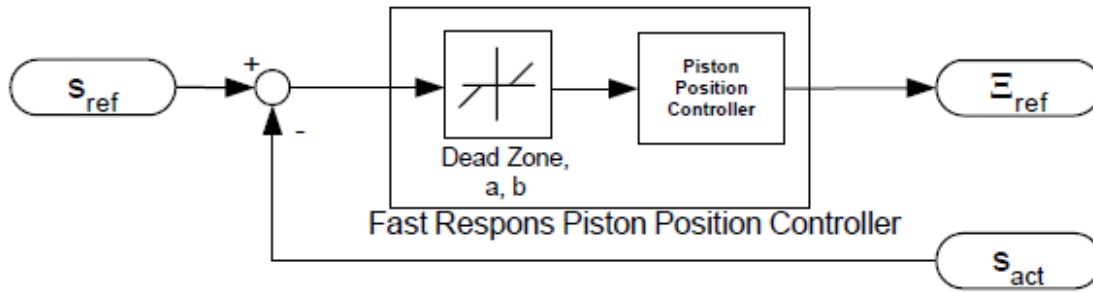
Figure 2.15: Pitch control loop for *Full Load operation* in V52 turbine, Source: [VES11].

The Dead Zone- Block models the non-linearity of the valve. Figure 2.16 represents the characteristic of the servomotor of the valve. It shows that the error position signal has a non-linearity versus the position of the valve.
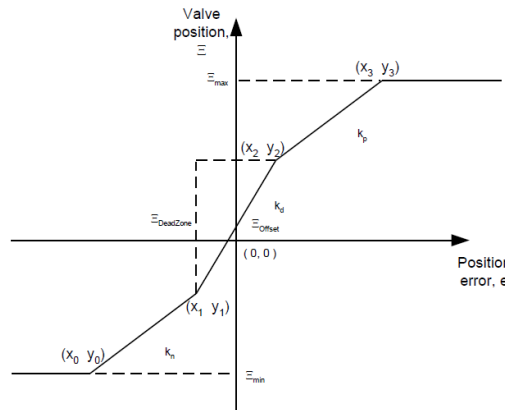
Figure 2.16: Dead Zone for the valve in V52-turbine pitch actuator system, Source: [VES11].

A general model for the pitch servomotor is described in [MPP18]:

$$\dot{\beta}_{unsaturated} = sat_{-\dot{\beta}_{max}}^{+\dot{\beta}_{max}}(\frac{\beta_{ref}(t)}{\tau} - \frac{\beta_{act}(t)}{\tau}) \qquad \text{Equation 2.8}$$

$$\beta_{act} = sat_{0º}^{90º}(\beta_{unsaturated}) \qquad \text{Equation 2.9}$$

where β_{act} is the current measured value of the pitch angle $\beta_{unsaturated}$ [º] is the unsaturated value of the pitch angle, β_{ref}[º] is the desired pitch angle and τ (delay-response model) $\cong$ *5 sec.* is the pitch control system time constant and $\dot{\beta}_{max}$ [º/s] is the feasible angle derivative. Figure 2.17 describes the pitch control loop which corresponds to the differential equation. It is expected to reproduce this controller loop in the new controller.

Chair for Wind Power Drives
Univ.-Prof. Dr.-Ing. Georg Jacobs

15
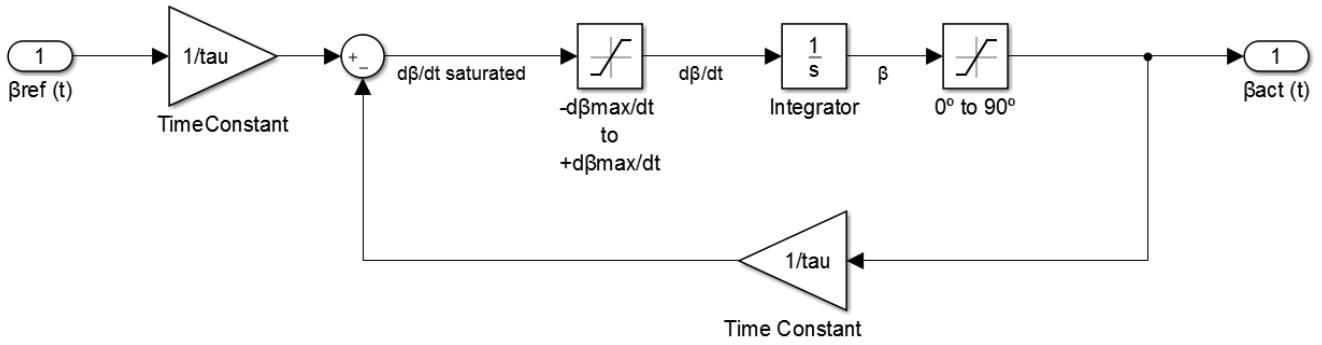
Figure 2.17: Pitch control loop.

2.2.3. Rotor model.

The rotor model (aerodynamic model): *cp* (performance coefficient) measurements plays an important role when detecting the efficiency of wind turbines. Its expression depends on the turbine. For a general turbine, the most general *cp* expression is found in Equation 2.10 and was extracted from [HK12; RUT14].

$$c_p(\lambda, \beta) = c_1[c_2 f(\lambda, \beta) - c_3 \beta - c_4 \beta^x - c_5]e^{-c_6 f(\lambda, \beta)} + c_9 \lambda \qquad \text{Equation 2.11}$$

where $\lambda = \frac{r_t \omega_t}{v_{wind}}$ is the tip speed ratio, x, c_1 to c_6 are constants that depend on the turbine, $\beta[rad]$ is the pitch angle.

The constants and functions are the following, and were extracted from [HK12; RUT; RUT14]:

$$c_1 = 0.5176; \ c_2 = 116; c_3 = 0.4; \ c_4 = 0; \ x = 0; \ c_5 = 5; \ c_6 = 21; c_7 = 0.08; \ c_8 = 0.035; \ c_9 = 0.0068$$

$$f(\lambda, \beta) = ((1/(\lambda + c_7 \beta)) - (c_8/((\beta^3) + 1)))$$

$$c_p = c_1(c_2 f - c_3 \beta - c_4(\beta^x) - c_5) \ exp(-c_6 f) + c_9 \lambda)$$

Plotting the mentioned function defined in Equation 2.10 for *cp* in MATLAB we get the following surface:

Chair for Wind Power Drives
Univ.-Prof. Dr.-Ing. Georg Jacobs

16
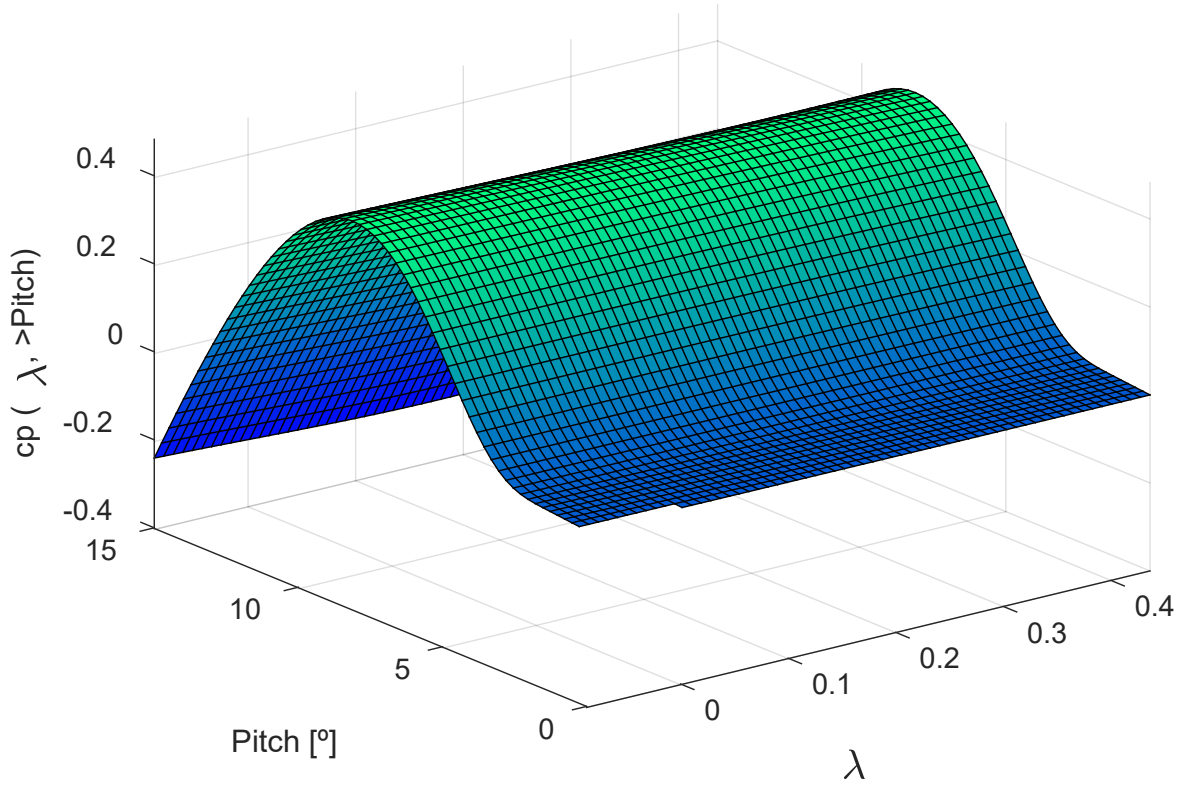
Figure 2.18: *cp* as a function of λ and pitch angle.

Assuming the following hypothesis [DMS15]:

$$\frac{d}{dt}\tilde{v}_{wind}(\tilde{x},t) = 0 \quad \frac{d}{dt}\rho(\tilde{x},t,T,p,\dots) = 0$$

Equation 2.12

where t [s] is time, $\tilde{v}_{wind}$ is the wind speed, $\tilde{x}$[m] is the position, T [Nm] is the temperature and p[Pa] is the pressure.

The rotor torque T_m and the rotor mechanical power P_m can be calculated using the following equations [LCK11; DMS15] :

$$T_m(v_{wind},\beta,\lambda) = \frac{1}{2}\rho\pi r_t^{3}v_{wind}^{2}\frac{c_p(\lambda,\beta)}{\lambda}$$

Equation 2.13

$$P_m = T_m\omega_m$$

Equation 2.14

where ω_m is the rotational speed at the low-speed shaft.

Including the following definition in Equation 2.12:

$$c_q := \frac{c_p(\lambda,\beta)}{\lambda} = \frac{r_t\omega_t}{v_{wind}}$$

we obtain:

$$T_m = T_m(v_{wind},\beta,\lambda) = \frac{1}{2}\rho\pi r_t^{3}v_{wind}^{2}\frac{c_p(\lambda,\beta)}{\lambda} =$$

$$\frac{1}{2}\rho\pi r_t^{3}v_{wind}^{3}\frac{c_p(\lambda,\beta)}{\omega r_t} = \frac{1}{2}\rho\pi r_t^{2}v_{wind}^{3}\frac{c_p(\lambda,\beta)}{\omega} = \frac{1}{2}\rho\pi r_t^{3}v_{wind}^{2}c_q(\lambda,\beta)$$

Equation 2.15

Chair for Wind Power Drives
Univ.-Prof. Dr.-Ing. Georg Jacobs

17

where ρ is the density of the air and $c_q(\lambda, \beta)$ is the torque coefficient.

2.2.4. Drive train model (based on the model in [Gam17]).

This system transfers the mechanical torque of the rotor to electrical energy. To build this model there are different possibilities. The rotor can be modeled by a single mass, but also by a two or three mass representation, as shown in Figure 2.19 [Gam17]. In this work, a three-mass representation will be explained. In the rotation system, there are different subsystems with specific characteristics [Gam17]: high speed shaft, main shaft, gearbox, rotor hub with three blades and generator [Gam17]. The rotor, generator and gearbox are each modelled with a single mass [Gam17]. The mass of the main shaft is allocated to the rotor and the mass of the high speed shaft is allocated to the generator [Gam17]. In addition, it is always considered that all components from each side of the transmission have respectively the same corresponding speed [Gam17].

The following equations are extracted from [Gam17] and describe the dynamic of the drive train as a three-mass oscillator. They will be useful when creating the new simulated controller, but they will be simplified in a two-mass oscillator (see Equation 4.1).

$$\sum \widetilde{T_z} = J \frac{d\widetilde{\omega_z}}{dt}$$

$$J_e = J_{xl} + n_x{}^2 J_{xh}$$

$$B_e = (B_{xl} + D_{lss)} + n_x{}^2(B_{xh} + D_{hss})$$

Rotor and rotor shaft (mass=0):

$$\boldsymbol{\widetilde{T_r} - B_r\widetilde{\omega_r} - (D_{lss})\widetilde{\omega_r} - (K_{lss})\widetilde{\theta_r} + \left(\frac{K_{lss}}{n_x}\right)\widetilde{\theta_{xh}} + \left(\frac{D_{lss}}{n_x}\right)\widetilde{\omega_{xh}} = J_r\widetilde{\omega_r}} \qquad \text{Equation 2.16}$$

Gearbox:

$$\boldsymbol{-B_e\widetilde{\omega_{xh}} + (n_x D_{lss})\widetilde{\omega_r} + (n_x{}^2 D_{hss})\widetilde{\omega_g} + (K_{lss})(n_x\widetilde{\theta_r} - \widetilde{\theta_{xh}}) - (n_x{}^2 K_{lss})(\widetilde{\theta_{xh}} - \widetilde{\theta_g}) =}$$
$$\boldsymbol{J_e\widetilde{\omega_{xh}}} \qquad\qquad \text{Equation 2.17}$$

Generator and generator shaft (mass=0):

$$\boldsymbol{\text{-}\widetilde{T_g} - (D_{hss} + B_g)\widetilde{\omega_g} + D_{hss}\widetilde{\omega_{xh}} - K_{hss}(\widetilde{\theta_{xh}} - \widetilde{\theta_g}) = J_g\widetilde{\omega_g}} \qquad \text{Equation 2.18}$$

where J, B, D, K and n are the moments of inertia, viscous coefficient, damping coefficient, stiffness and gear rate [Gam17]. The variables ω, Θ and Tr correspond to the speed, the angle of rotation and the rotor torque[Gam17]. Sub-indexes $r, g, a, e, x, xl, xh, lss$ and hss correspond to: *rotor, generator, equivalent, gearbox*, and *low-speed side of the gearbox, high-speed side of the gearbox, low-speed shaft and high-speed shaft* [Gam17].

Chair for Wind Power Drives
Univ.-Prof. Dr.-Ing. Georg Jacobs

18
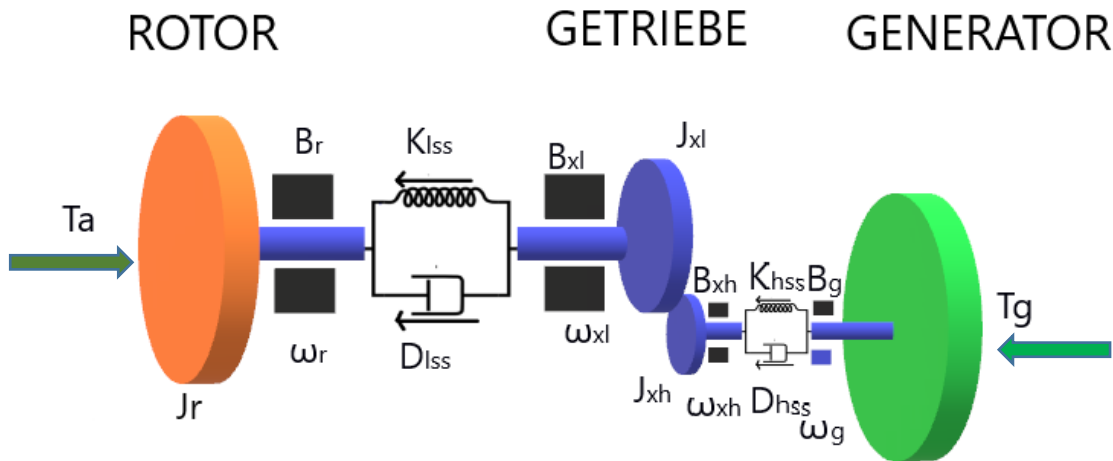
Figure 2.19: Drive train model, Source: Adaptation of [Gam17].

2.2.5. Generator model.

V52 turbine has a DFIG (Doubly-Fed Induction Generator) asynchronous generator with a maximum rotor speed of 1620 rpm/min [WIN]. The DFIG generator is a variable speed induction machine [LA07] and consists of a rotor-wound induction generator and a AC/DC/AC IGBT-based PWM converter [MAT18]. With the DFIG technology, it is possible to gain maximum wind energy at low wind speeds, optimize speed and achieve minimal mechanical loads on the turbine during gusts [WIN].

The AC/DC/AC converter shown in Figure 2.20 consists of RSC (rotor-side converter) and GSC (grid-side converter) connected back-to-back [FY10]. Between the two AC/DC converters there is a *Dc-link* capacitor, so that the voltage change in the *Dc-link* is low [FY10]. The target RSC is to control the torque or speed in the generator, and the GCS goal is to keep *Dc-link* voltage constant [FY10]. RSC operates at variable frequency but GCS at grid frequency [FY10].
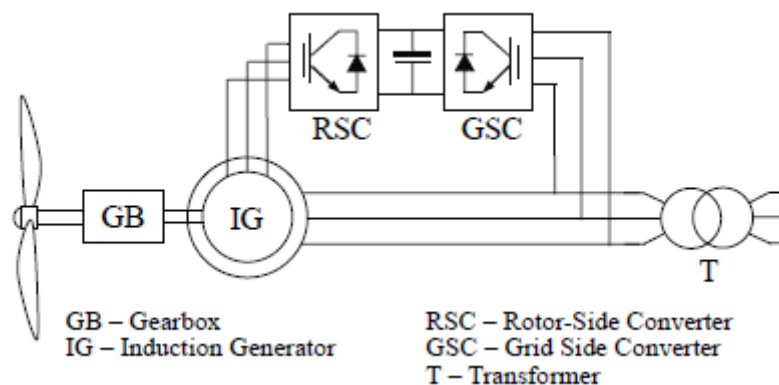
Figure 2.20: Electrical scheme of the DIFG-generator, Source: [FY10].

2.2.6. Star-Delta Switch.

Chair for Wind Power Drives
Univ.-Prof. Dr.-Ing. Georg Jacobs

19

The goal of this strategy is to improve the voltage control of the generator [FSK14]. In variable speed turbines, like V52, star-delta switching provides a way to adjust the generator´s voltage output [FSK14]. Both connections are seen in Figure 2. 21.
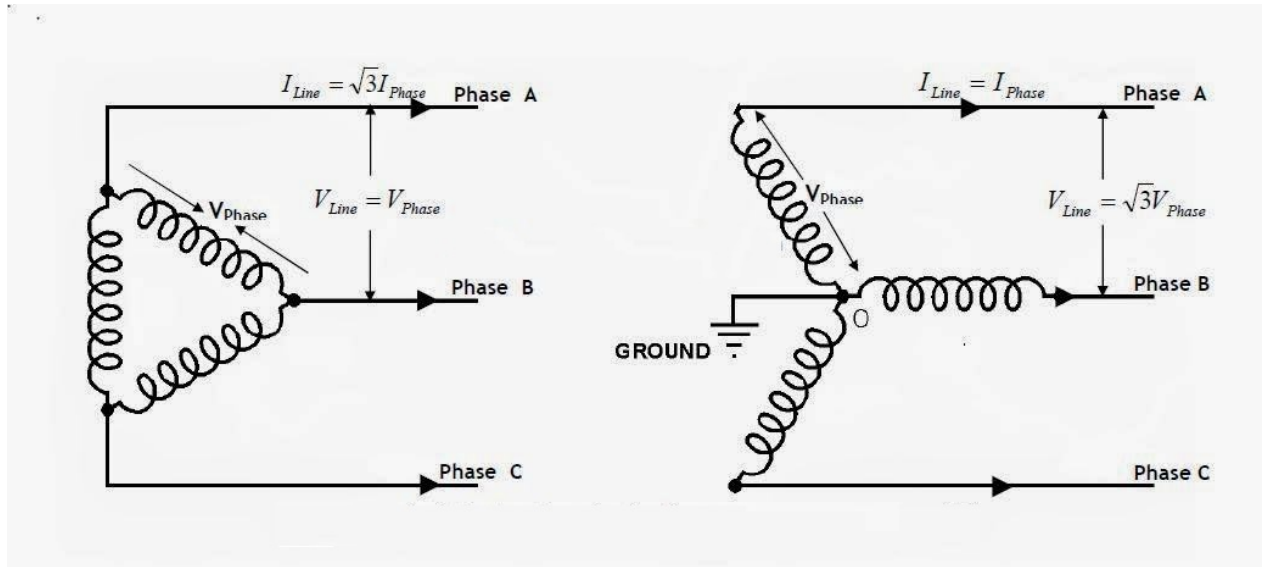
Figure 2. 21: Star (right) and delta (left) connection schemes with coils. Source: [Ele16].

In delta connection, the generator´s voltage is $\sqrt{3}$ times bigger than in star circuit [FSK14]. Therefore, the generator torque and its correspondent power in star connection are one third of the generator torque and power in delta connection [FSK14]. V52-turbine contains the star-delta switch electrical scheme shown in Figure 2.22:
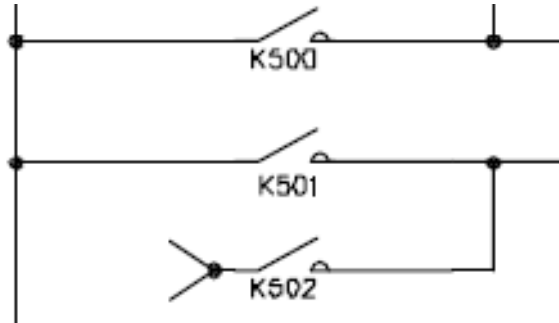
Figure 2.22: Electrical scheme of the V52- DIFG-generator's star-delta switch, Source: [VESEL04].

Chair for Wind Power Drives
Univ.-Prof. Dr.-Ing. Georg Jacobs

20

The switches K501 and K502 are responsible for the delta and star connection respectively [VESEL04; VES04].

Further information about how and why the controller switches between these both connections is provided in the documentation [VESEL04; VES04].

This information was summed up in Figure 2.23 and can be interpreted by means of the information on the right. Figure 2.23 describes the star-delta switch strategy as a Moore machine. It will be useful in Chapter 3 to develop the star-delta switch strategy in Simulink.

P="Power"; $\frac{du}{dt}$ ="Acceleration of the wind speed".

SSD1= "first phase of the Star-Delta switch"

SSD2= "second phase of theStar-Delta switch".

SDS1= "first phase of the Delta-Star switch".

SDS2= "second phase Delta-Star switch".

S&C= "synchronize & connect".

Last P value="Controller saves last power value".

FERTIG= "Connection achieved".

Gen_rpm="high-speed shaft rotation speed"

Gen_rpm="high-speed shaft mirotation speed"
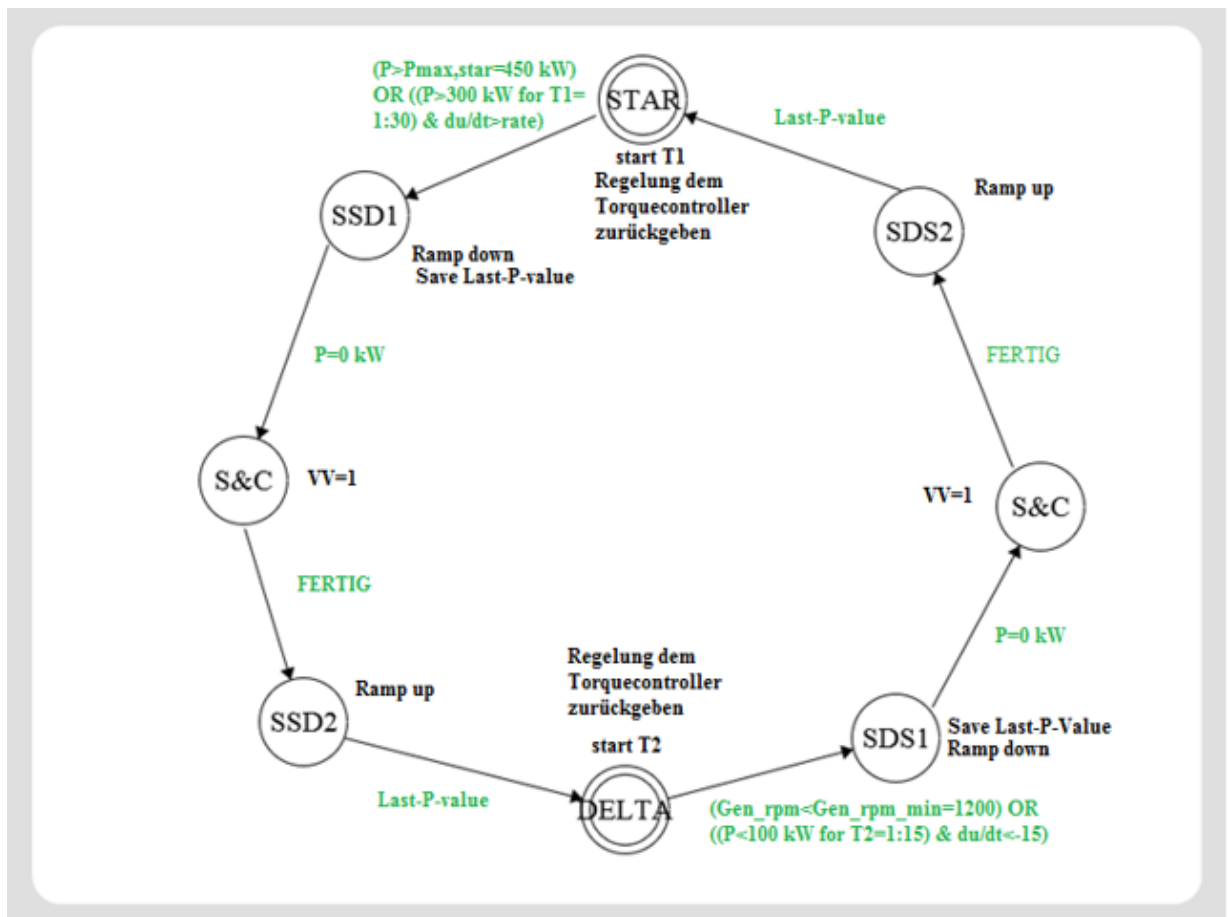
Figure 2.23: Star-delta switch representation for V52-turbine.

This behavior will be reproduced in Simulink in Chapter 3.

Chair for Wind Power Drives
Univ.-Prof. Dr.-Ing. Georg Jacobs

21

2.3   Multi-Body Simulation (MBS) and MATLAB-SIMPACK Co-simulation (MSC).

The experimental measurements taken in the V52-testbench will be used to run the co-simulation MATLAB-SIMPACK needed for the development and implementation of a new simulated controller (NSC).

Simpack is a multi-body simulation software [Bi15], which uses numerical technics based on analytical methods to study interactions between physical bodies [Bi15]. It is used is widely extended in the industry and research institutes [Bi15]. With a focus on wind energy, it's an appropriate tool to study the overall dynamics of a wind turbine [Bi15].

At CWD a Simpack model of the V52-testbench (V52-SM) was developed. This model contains both rigid and elastic bodies and aims to reproduce the real plant [Bi15]. It contains a total of 90 bodies with 306 states at position and velocity level and 90 force elements [Bi15].

The closed-loop behavior of the model requires a controller which works parallel with it. This controller will be closely described as well as tested in the Chapter 3.

Although there are already some implemented control elements in the V52-SM, a new controller is necessary to better reproduce the real plant operation strategy. The new simulated controller (NSC) will be developed in *Simulink* and will run in co-simulation with the V52-SM.

Chair for Wind Power Drives
Univ.-Prof. Dr.-Ing. Georg Jacobs

22

3. Simulations and understanding of the existing simulated controller (ECS).

This chapter goes deeper in the understanding of the ESC. For that, in subsections 3.1 and 3.2 the torque and pitch regulation respectively will be described by analyzing its dynamic response.
The existing simulated controller (ESC) is composed of two important parts: the torque control and the pitch control, as seen in Figure 3.2.

3.1 Torque regulation.

The blocks referring torque regulation get the measurements of the rotor shaft and generator drive shaft as input and generate the desired generator torque as output. They are situated on the upper part of the controller. There are two different blocks conforming the torque regulation: In the first block (*Torque Control*- subsection 3.1), the measured rotational speed is converted into the desired electrical torque. We distinguish various sub-blocks: *Generator characteristics*, *Speed Control PID* and *Control Damping*. In *Generator characteristics*, there is a *Speed/Torque Lookup Table* that converts the high-speed shaft rotational speed into electrical torque. *Speeds Control PID* consists of a PID controller in parallel, *and Active Drive Train Damping* contains a PID controller. In series, we find the *Torque Actuator* block (subsection 3.2). In subsections 3.3 and 3.4 a tower and star-delta switch model respectively will be added to the controller's operation strategy.

3.1.1. Torque control.

This block is responsible for calculating the generator torque by means of the measurements and contains some subblocks:

  ✓ *Generator characteristics:* This subblocks gets a rotational speed reference and outputs the correspondent generator torque, according to the characteristic shown in (see Figure 3. 1). This value will be the input generator torque reference for the next subblock.
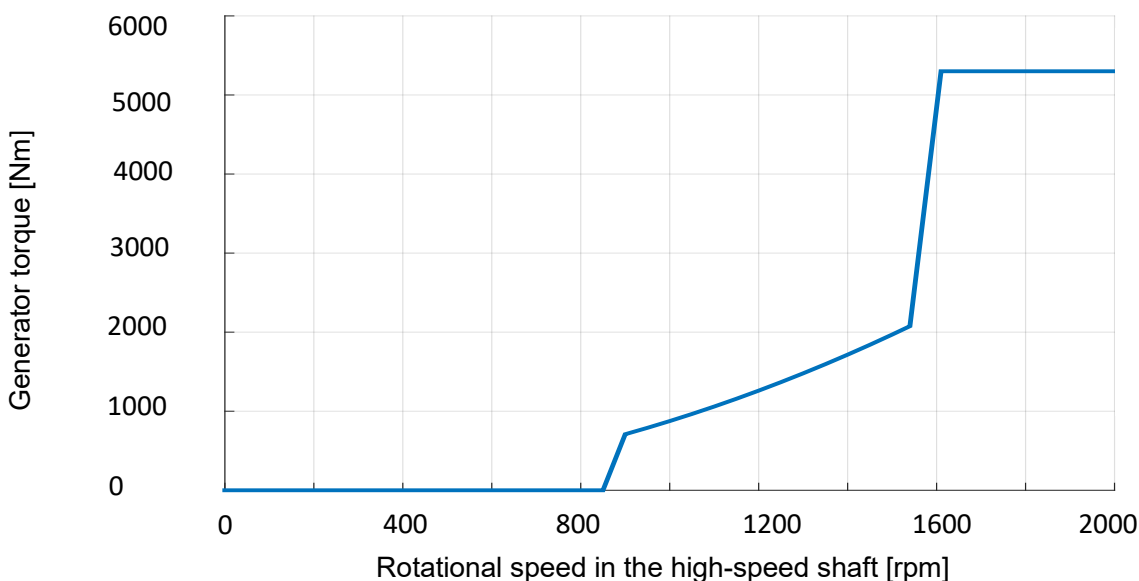
Figure 3.1: Generator characteristics on the ESC, Source: [CWDECS].

Chair for Wind Power Drives
Univ.-Prof. Dr.-Ing. Georg Jacobs

23
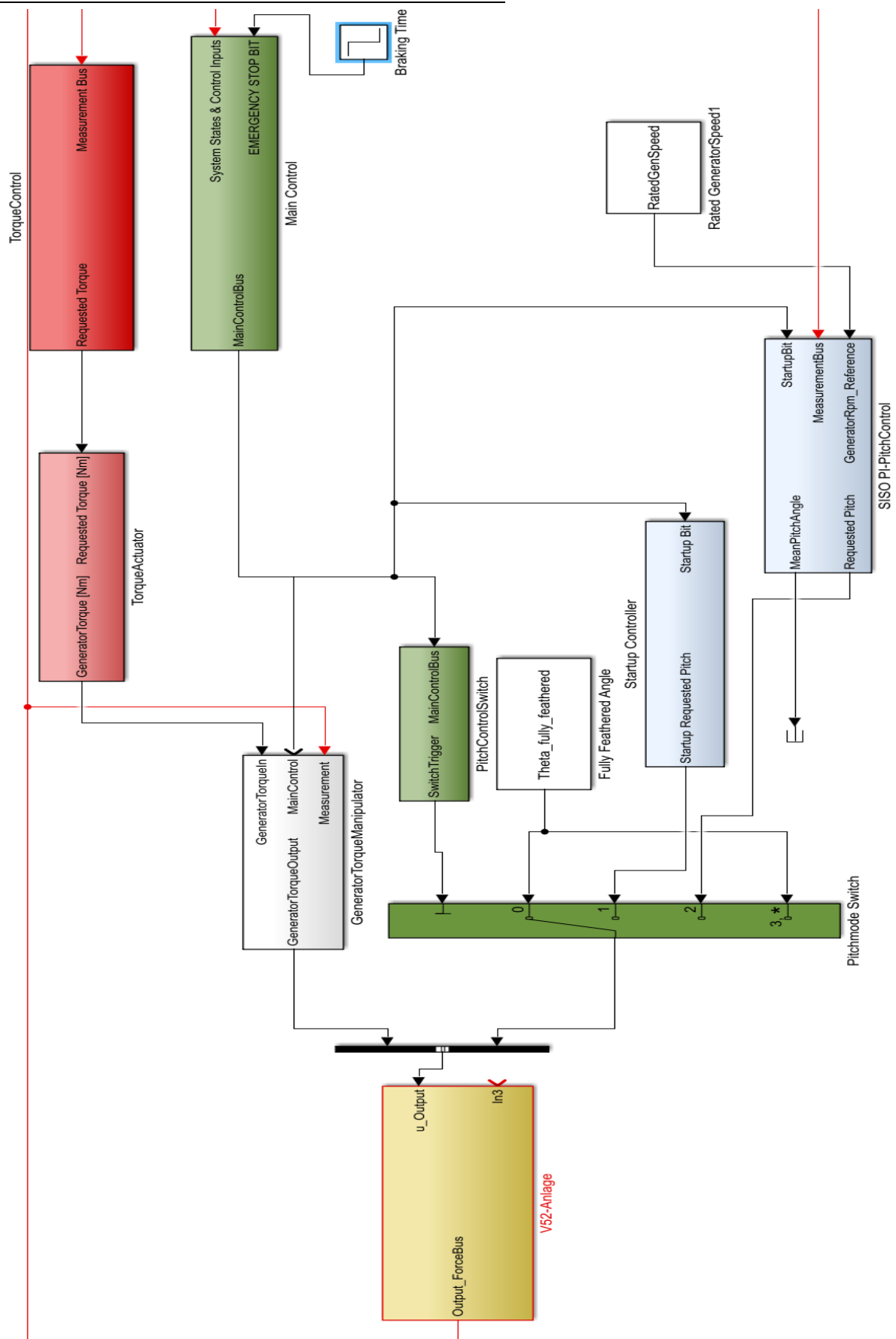
Figure 3.2:   Existing simulated controller (ESC), Source: [CWDECS].

Chair for Wind Power Drives
Univ.-Prof. Dr.-Ing. Georg Jacobs

24

Furthermore, another generator characteristics, seen in Figure 3.3, was implemented with the information from the V52-documentation [VES11], in order to validate the existing one. The V52 documentation provides with the tables shown in Figure 3.11, Figure 3.12 and Figure 3.13. These data was used to extract this generator characterisitcs.
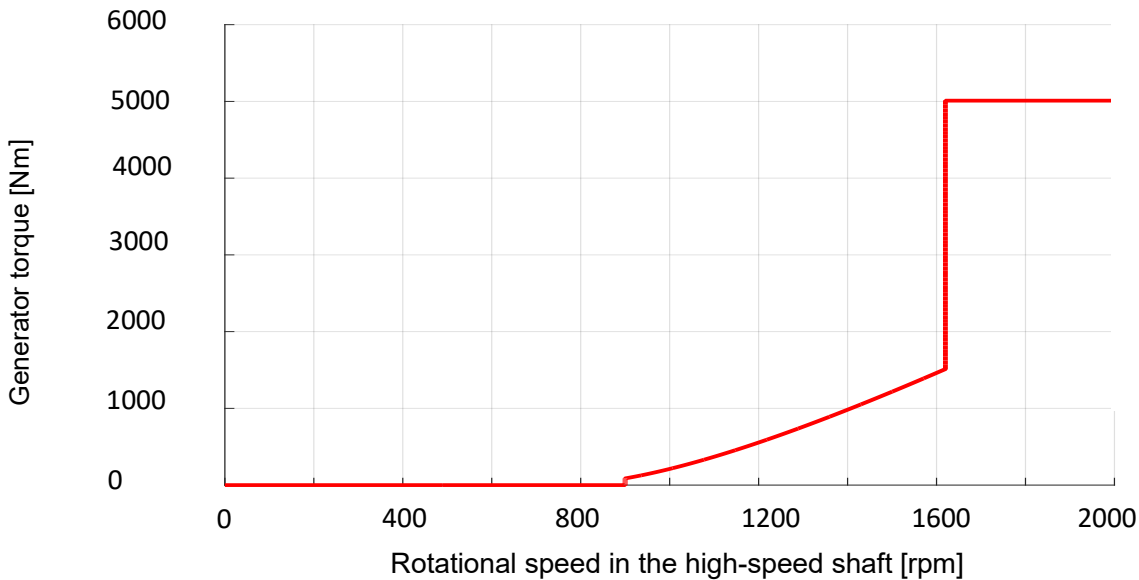
Figure 3.3:   Generator characteristics implemented by means of the V52- documentation.

The procedure followed to extract this curve from the information in the V52 documentation can be found in Appendix 2.

It is possible to see that the existing *Generator characteristic* reproduces quite well what the documentation specifies.

✓   *Speed Control PID*

The control strategy is a parallel PID controller (see Figure 3.4), with a rotational speed reference of 1620 rpm (rated speed in the low-speed shaft) and the measured rotational speed signal as feedback. The purpose of the controller is to produce a generator torque signal out of the error between the rated speed (which is 1620 rpm,see Figure 3.4) and the measured speed.

Chair for Wind Power Drives
Univ.-Prof. Dr.-Ing. Georg Jacobs

25
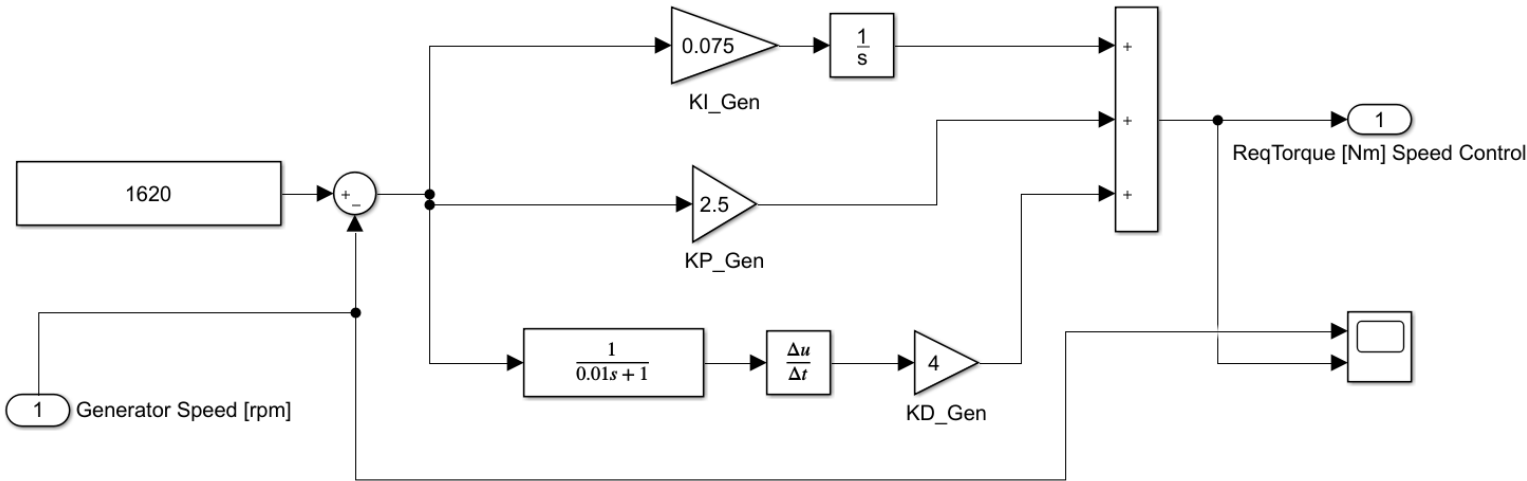
Figure 3.4:   PID Torque control scheme, Source: [CWDECS].

Figure 3.5 shows the response of the *Speed Control PID* block in Simulink. It is relevant to mention that when the step function goes up from 0 to 2.5 rad/s, there is a peak in the torque signal.
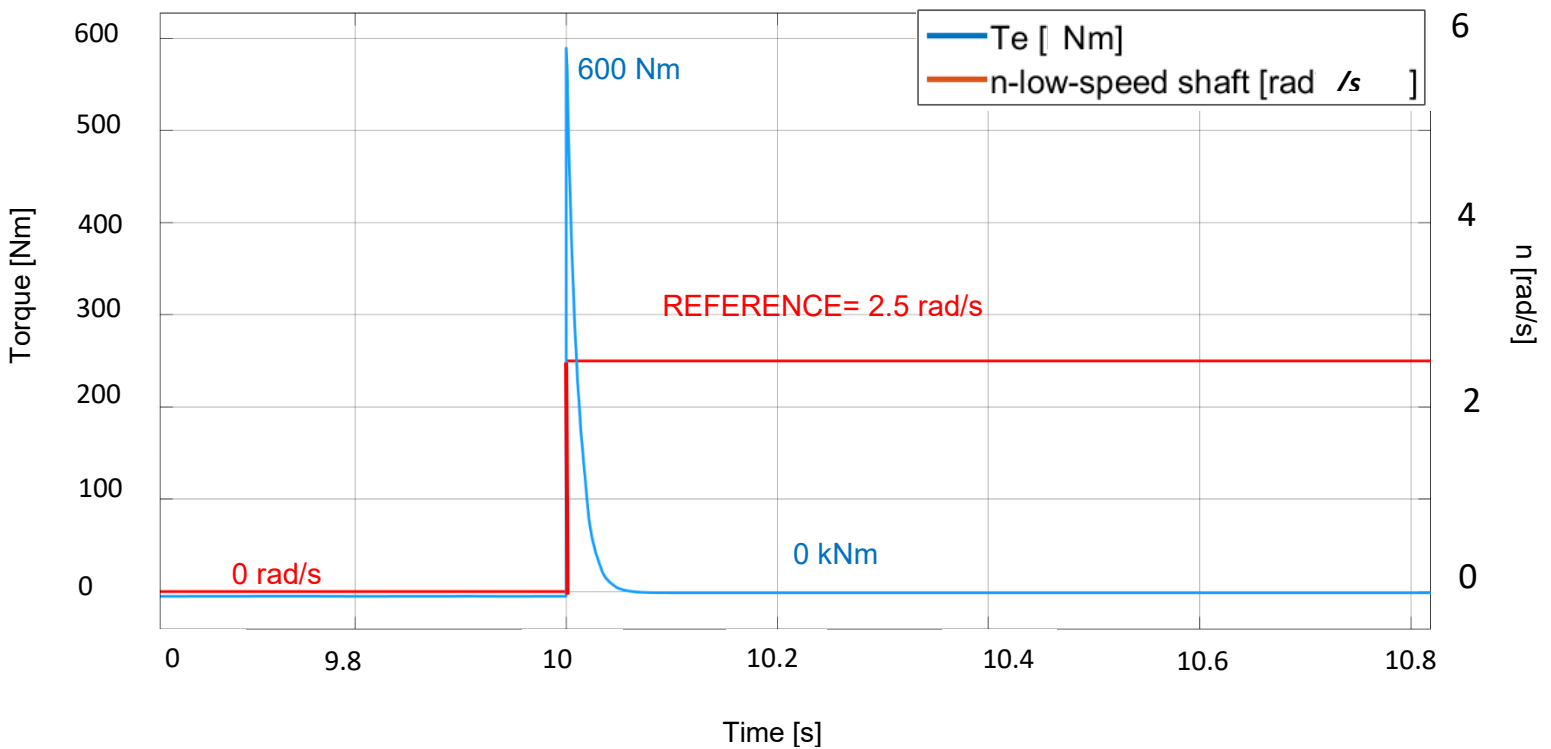
Figure 3.5:   PID Torque control response (blue signal) to a step reference of 2.5 rad/s of low-speed shaft rotational speed (red signal), Source: [CWDECS].

Chair for Wind Power Drives
Univ.-Prof. Dr.-Ing. Georg Jacobs

26

3.1.2. Torque actuator.

This block models the *Torque Actuator* through an integrator. This actuator corresponds to the following differential equation (Equation 3.1):

$$\dot{T}_e^{measured} = -K_1 T_e^{measured} + T_e^{requested}$$
Equation 3.1

where $T_e^{requested}$ is the requested torque in the generator and $T_e^{measured}$ is the measured torque in the generator.

The following scheme describes the differential Equation 3.1 through a torque actuator feedback control:
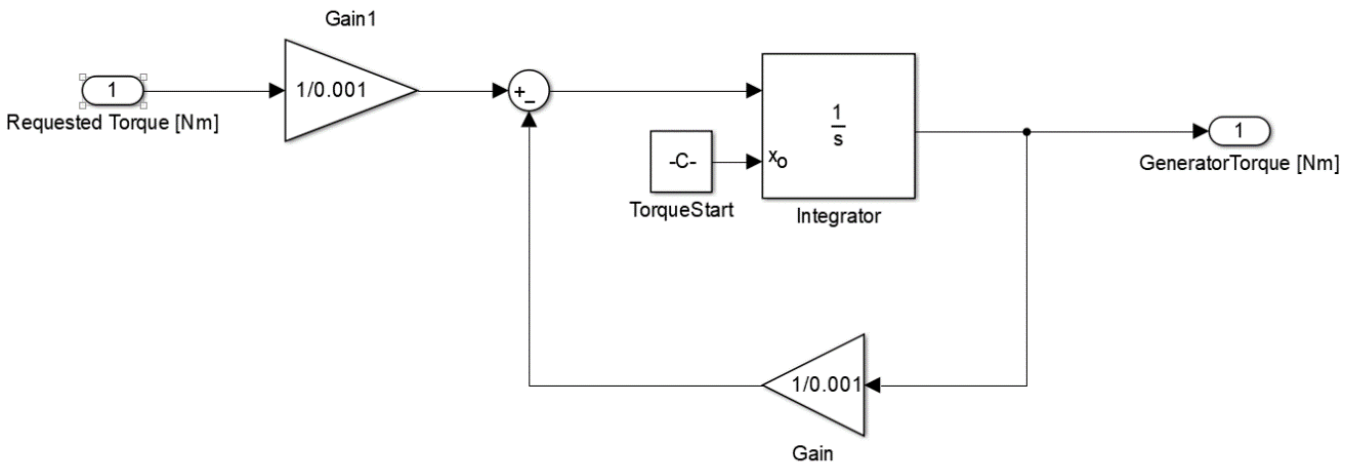
Figure 3.6: Torque Actuator in the ESC, Source: [CWDECS].

The response of this block to a step input function of 5000 Nm is:
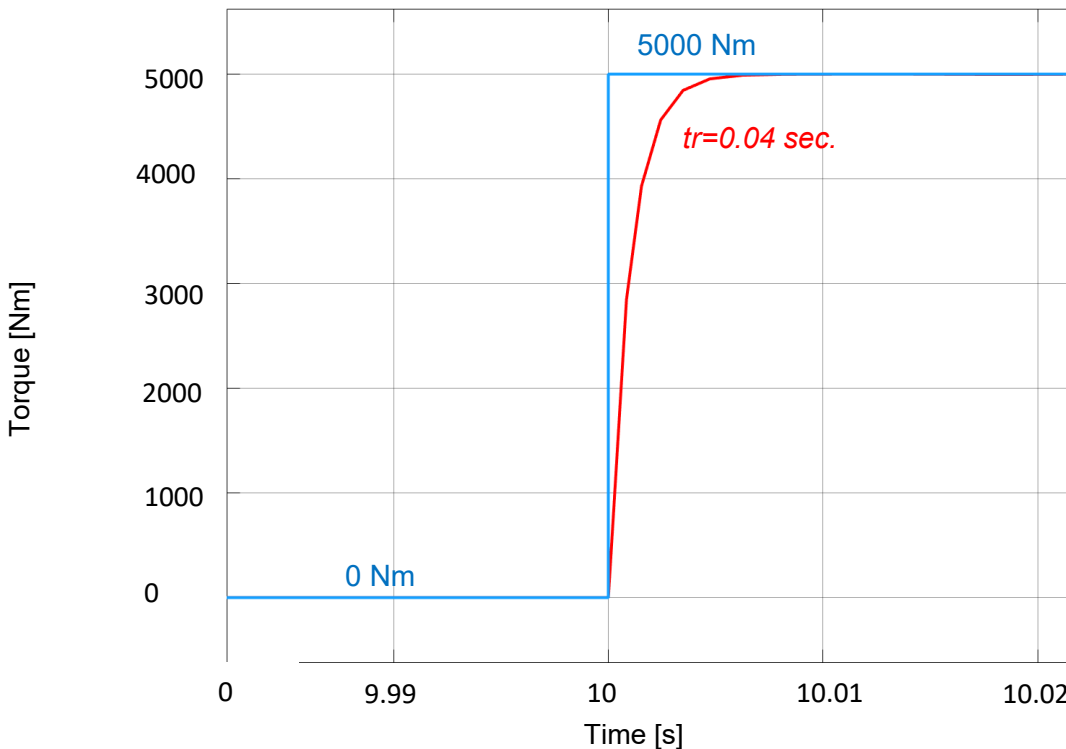
Figure 3.7: Torque Actuator response in the ESC, Source: [CWDECS].

Chair for Wind Power Drives
Univ.-Prof. Dr.-Ing. Georg Jacobs

27

where the measure response time was tr=0.04 sec.

Chair for Wind Power Drives
Univ.-Prof. Dr.-Ing. Georg Jacobs

28

3.2 Pitch regulation.

Pitch servomotors are modelled in the ESC through the following control loop. The main purpose of this control scheme is to reproduce the real dynamic response of the pitch servomotors.
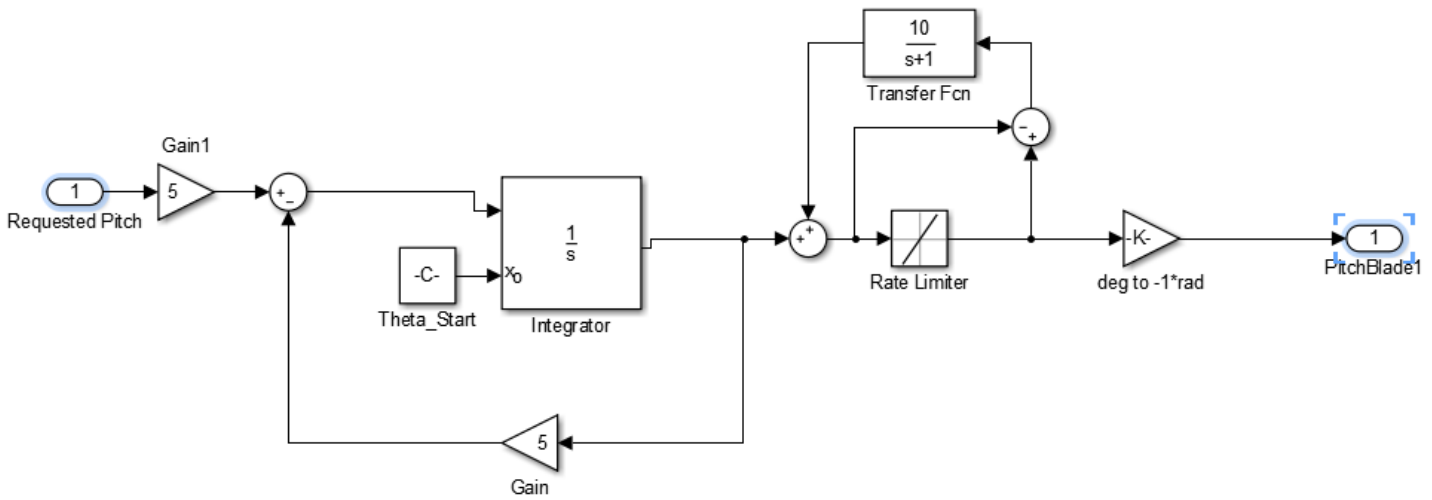
Figure 3.8:   Pitch Actuator in ESC, Source: [CWDECS].

where the specified time constant mentioned in Chapter 1 is τ =5 sec.

Figure 3. 9 shows some of the signals in the control loop. The pink signal shows the output pitch angle, which reaches 0º in a time of tr=0.5973 sec.

Pitch angle actuator response time $t_r = 0.5973$ sec.
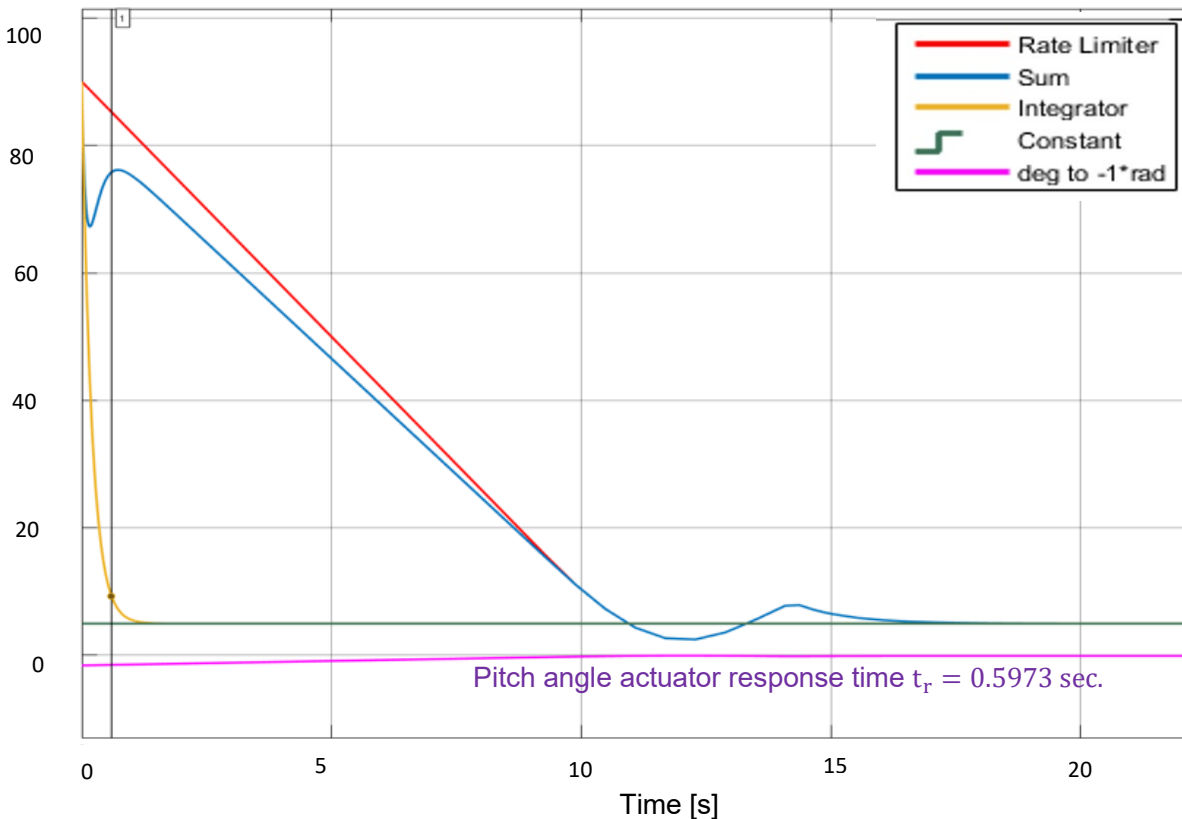
Figure 3. 9:   Pitch Actuator response in ESC, Source: [CWDECS].

Chair for Wind Power Drives
Univ.-Prof. Dr.-Ing. Georg Jacobs

29

Since the objective of the thesis focuses on the generator torque control, this controller (ESC) was arranged in such a way that the inputs are the rotational speed in the low and high-speed shaft and the output is only the desired electrical torque in the generator.

OUTPUT: Electrical Torque

INPUTS: Speeds in low and high-speed shaft.

TorqueControl

GeneratorTorque [Nm]   Requested Torque [Nm]   ◄   Requested Torque   Measurement Bus   ◄   1
In1

TorqueActuator

GeneratorTorqueIn

GeneratorTorqueOutput   MainControl   ◄   MainControlBus   System States & Control Inputs   ◄

Measurement

GeneratorTorqueManipulator   Main Control

Out1
1
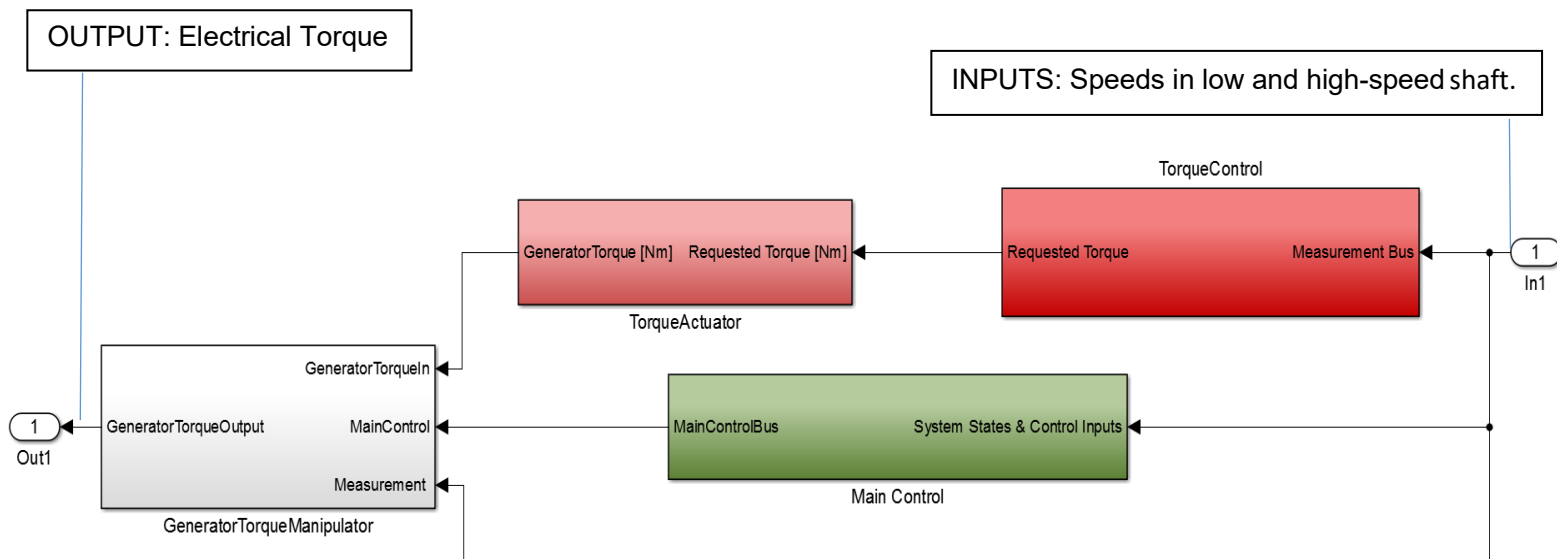
Figure 3.10: Arranged ESC, Source: [CWDECS].

At the beginning of the thesis, some simulations were ran without the V52-SM in order to test the ESC. To do so, the pitch, electrical torque and power characteristic (dependence on wind speed) were implemented in MATLAB as functions (see Figure 3.11, Figure 3.12 and Figure 3.13). Wind speed was chosen to be 15 m/s.

On the left, we find the implemented characteristics in MATLAB and on the right the characteristic specified in the documentation.

Figure 3.11: Pitch [º] curve (simulated and in V52-documentation [VES11]).

Chair for Wind Power Drives
Univ.-Prof. Dr.-Ing. Georg Jacobs

30
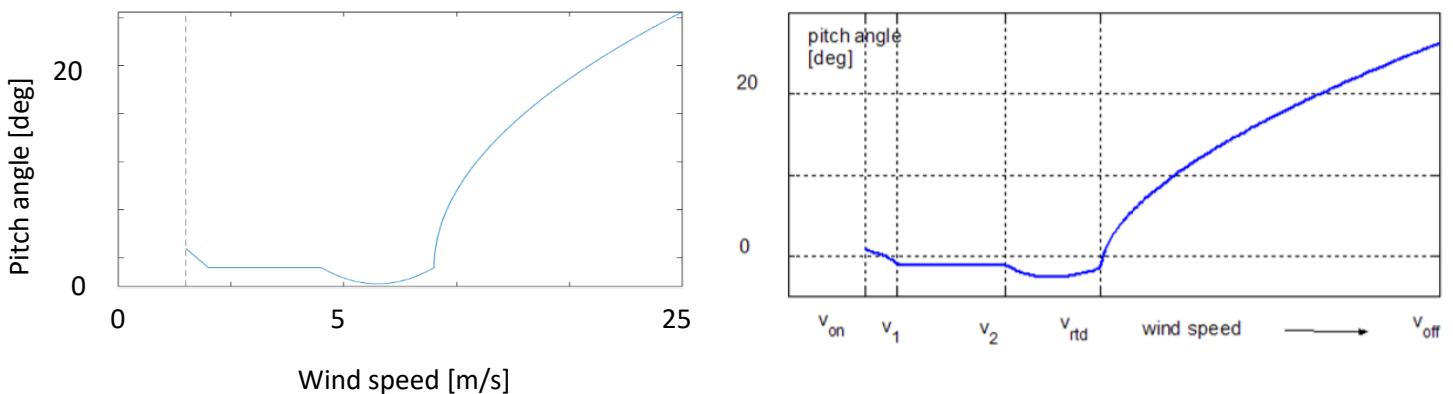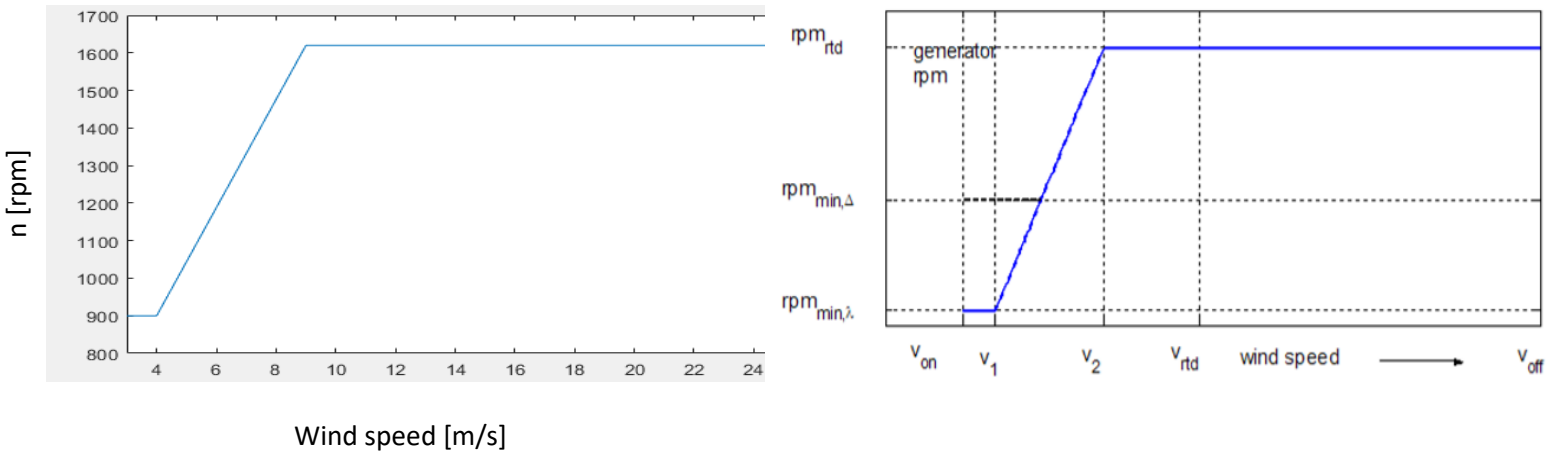
Figure 3.12: High-speed shaft rotational speed [rpm] characteristic curve (simulated and in V52-documentation [VES11]).
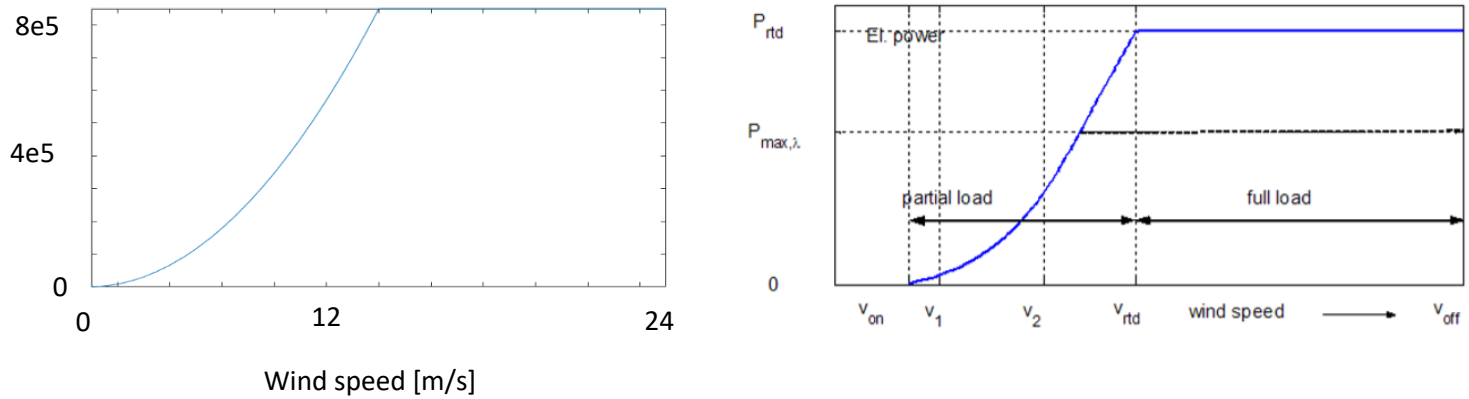
Figure 3.13: Output power [W] characteristic curve (simulated and in V52-documentation [VES11]).

The controller was then simulated giving the following output power for a step input power of 850 kW as seen in Figure 3.14.

Chair for Wind Power Drives
Univ.-Prof. Dr.-Ing. Georg Jacobs

31
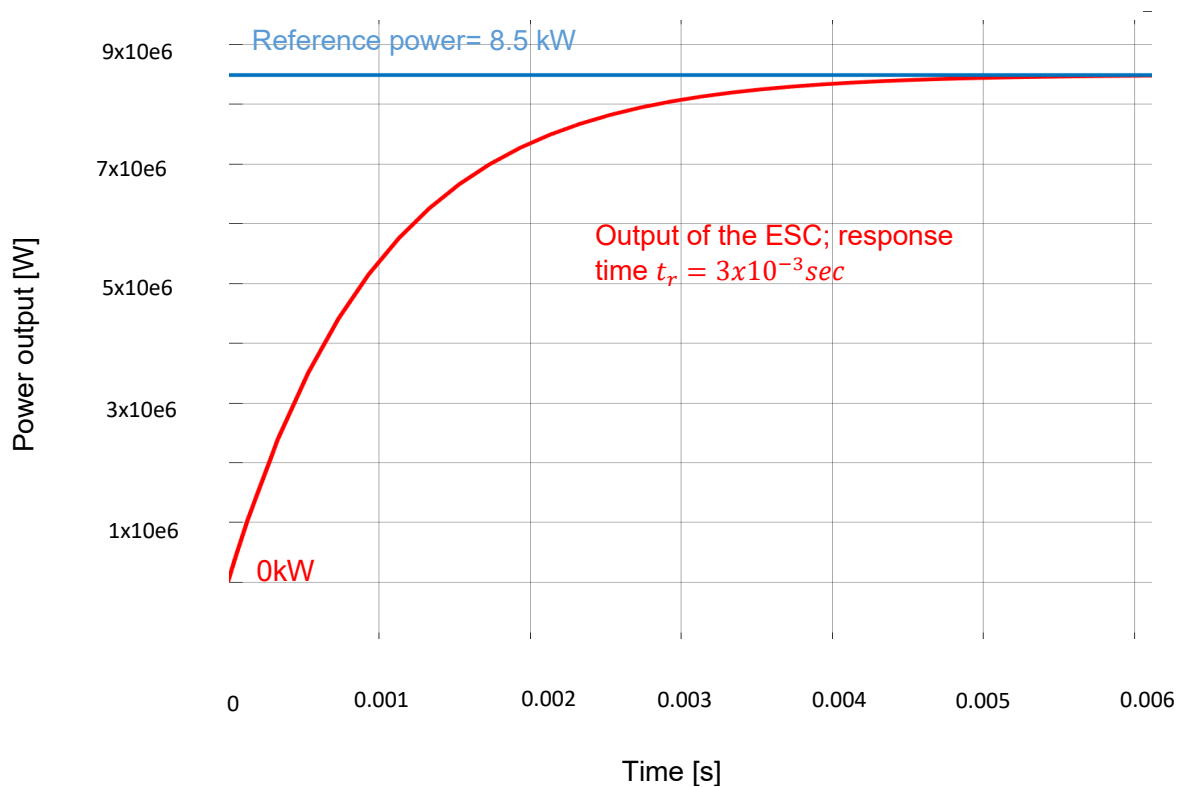
Figure 3.14: Output power [kW] (simulated), Source: [CWDECS].

3.3 Star-delta switch model.

Furthermore, a star-delta switch strategy was implemented in the ESC in order to reproduce the real behavior of the controller. The strategy was modelled and simulated using Simulink using *Logic control*.
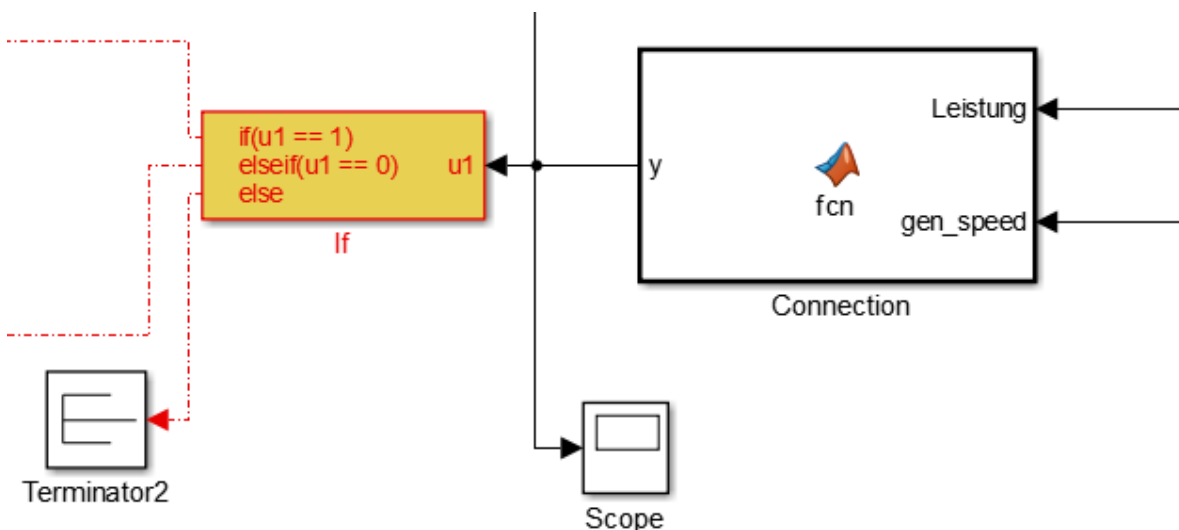
Figure 3. 15: Implemented logic for the star-delta switch.

Figure 3. 15 shows how the system decides which connection is needed at each moment, after the block *Connection* calculates the output signal *y.* This signal will determine which connection is needed,

Chair for Wind Power Drives
Univ.-Prof. Dr.-Ing. Georg Jacobs

32

according to the measured power and rotational speed in the generator. In the moment that the output *y* = *u1* = *1*, the system will switch automatically from star connection to delta connection (Star-Delta Switch Subsystem). If *y* = *u1* = *0*, the system will switch automatically from delta connection to star connection (Delta-Star Switch Subsystem). This decision is made by an *If block*.

Then this signal is inputted in two blocks, one for each connection (star and delta), as shown inFigure 3.16. Depending on the *If block* output, one of the blocks in Figure 3.16 will be activated (one of the *Case* blocks shown in Figure 3.16).
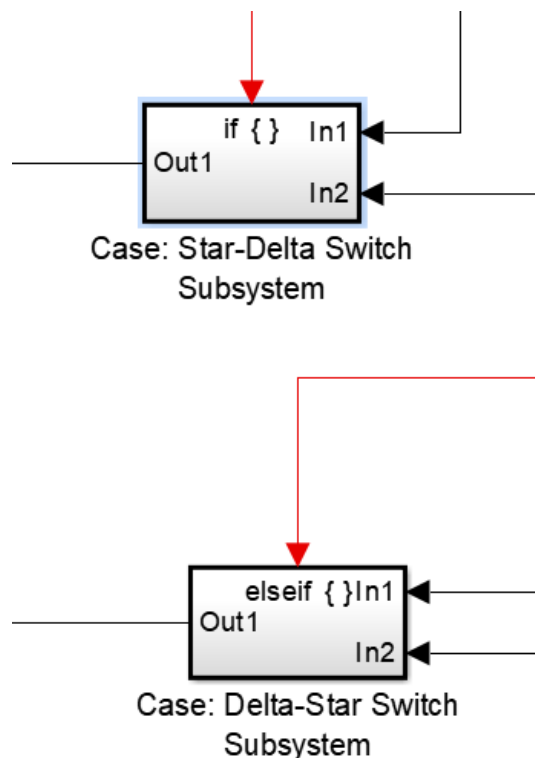
Figure 3.16: Block diagram for the star-delta switch connection

The *Case* blocks referred in Figure 3.16 take as input not only the mentioned u1 signal, but also the measured generated power (*Leistung*), a digital clock and a signal that contains the derivative of the wind speed (*Speed_rate*). Once the type of connection is selected, further specifications determine if the disconnection and the posterior connection will be carried out or not. This will be checked by the block *Calculator,* as seen in Figure 3.17. The clock will provide the time reference necessary to check if the power exceeds some limits within a period specified in the documentation, which depends on the connection. The *Speed_rate* signal and the output power also influence the type of connection. The output signal will be terminated if some specifications in the block *Calculator* (Figure 3.17) are not fulfilled. If these are fulfilled, then the power will be ramped down, the connection will be made and after that, the power will be ramped up again. This will be made by block titled *Ramp down and up* (Figure 3.17).

Chair for Wind Power Drives
Univ.-Prof. Dr.-Ing. Georg Jacobs

33
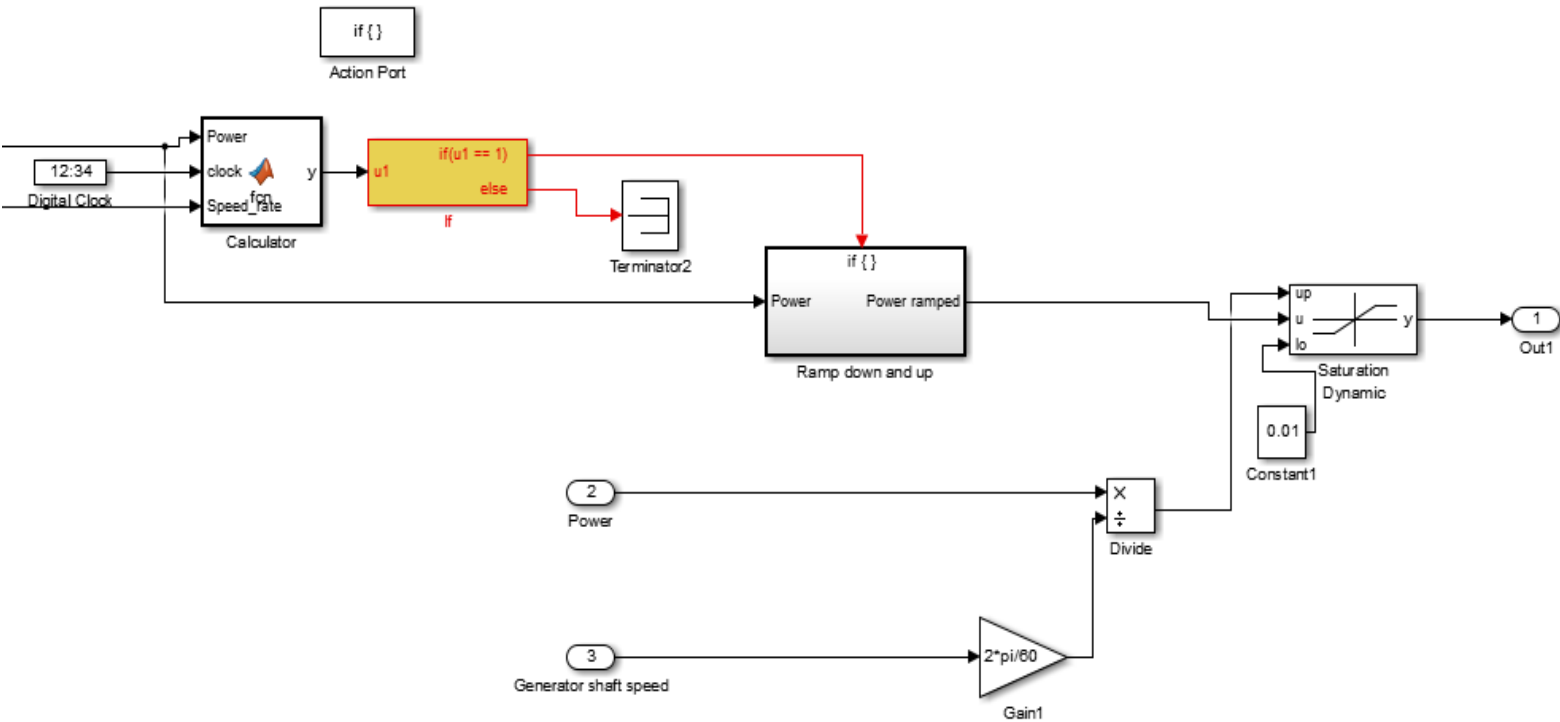
Figure 3.17: Scheme for ramping down and up power output.

The code needed to run the simulation can be found in Appendix 3.

The output power generated by the ECS with the star-delta strategy for a step reference of 850 kW is represented in Figure 3.18. It can be seen, that the controller ramps the power down 15 sec. after the start up. That happens because the system must be initialized in star connection, and the specifications required to switch from star to delta were fulfilled during this whole time period. Once the power reaches 0 kW, the controller will ramp it up again until it reaches the reference power (in this case 850 kW).
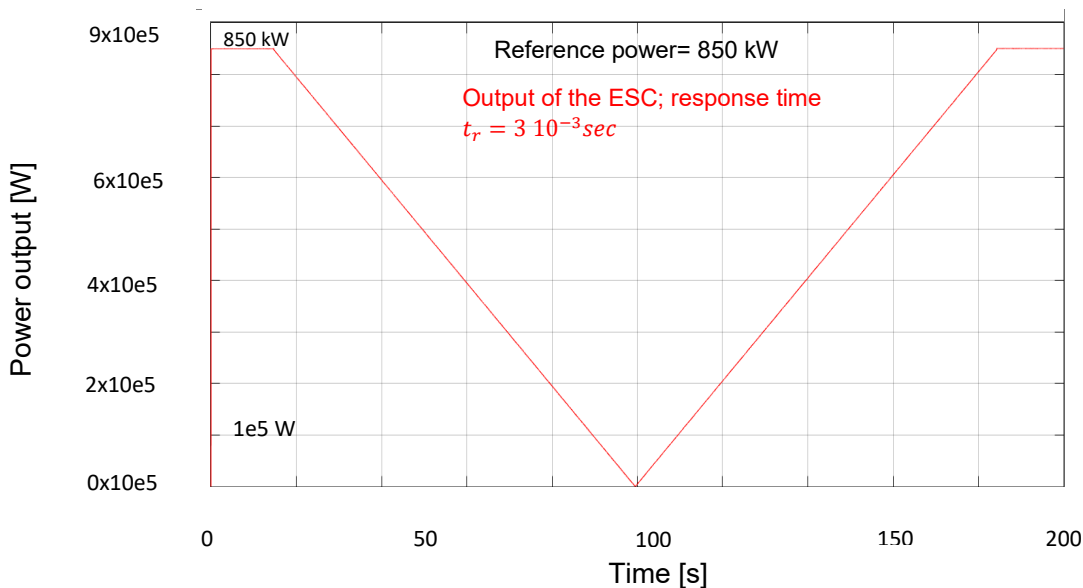
Figure 3.18: Output of the ESC with the star-delta switch strategy.

Chair for Wind Power Drives
Univ.-Prof. Dr.-Ing. Georg Jacobs

34

In these terms, the output power reproduces in a simplified way the information specified in the documentation, although it was nowhere specified how many seconds does the ramp period last. This information was summarized in Figure 2.23 and it is also included in Appendix 3. Nevertheless, in Chapter 4 it will be seen that the behavior described in the documentation and used to implement this strategy doesn't correspond to the real star-delta switch observed in the real test-bench.

Chair for Wind Power Drives
Univ.-Prof. Dr.-Ing. Georg Jacobs

35

4. Analysis of the measured data obtained in the V52-testbench.

The existent data used in the thesis come from the tests made during July and August of 2018. It contains around 8 hours of measurement data. These data contains measurements of the mechanical torque in the low-speed shaft, generator torque, current in every coil in the stator, rotational speed in the low-speed shaft, acceleration in some points of the gearbox and also the behaviour of the star-delta switches. A treatment and analysis of the data was done in the thesis. The sampling frequency was 2000 Hz for mechanical torque in the low-speed shaft, current and voltage in every coil in the stator, rotational speed in the low-speed shaft, acceleration in some points of the gearbox and 6000 Hz for the star-delta switches. Furthermore, times and frequencies of sampling where adjusted, since there was some random delays and inaccuracies in the measurements of the *Star-delta switches*.

Some examples of the treatment of the measurement data carried out are the following plots (*Drehzahl*=$n_{measures}$, *Delta*=Delta Switch contactor, *Star*= Star Switch contactor, *Me*=T_e, *Mm-abtriebswelle*=Torque in the high-speed shaft, *P-el*=Electrical output power):
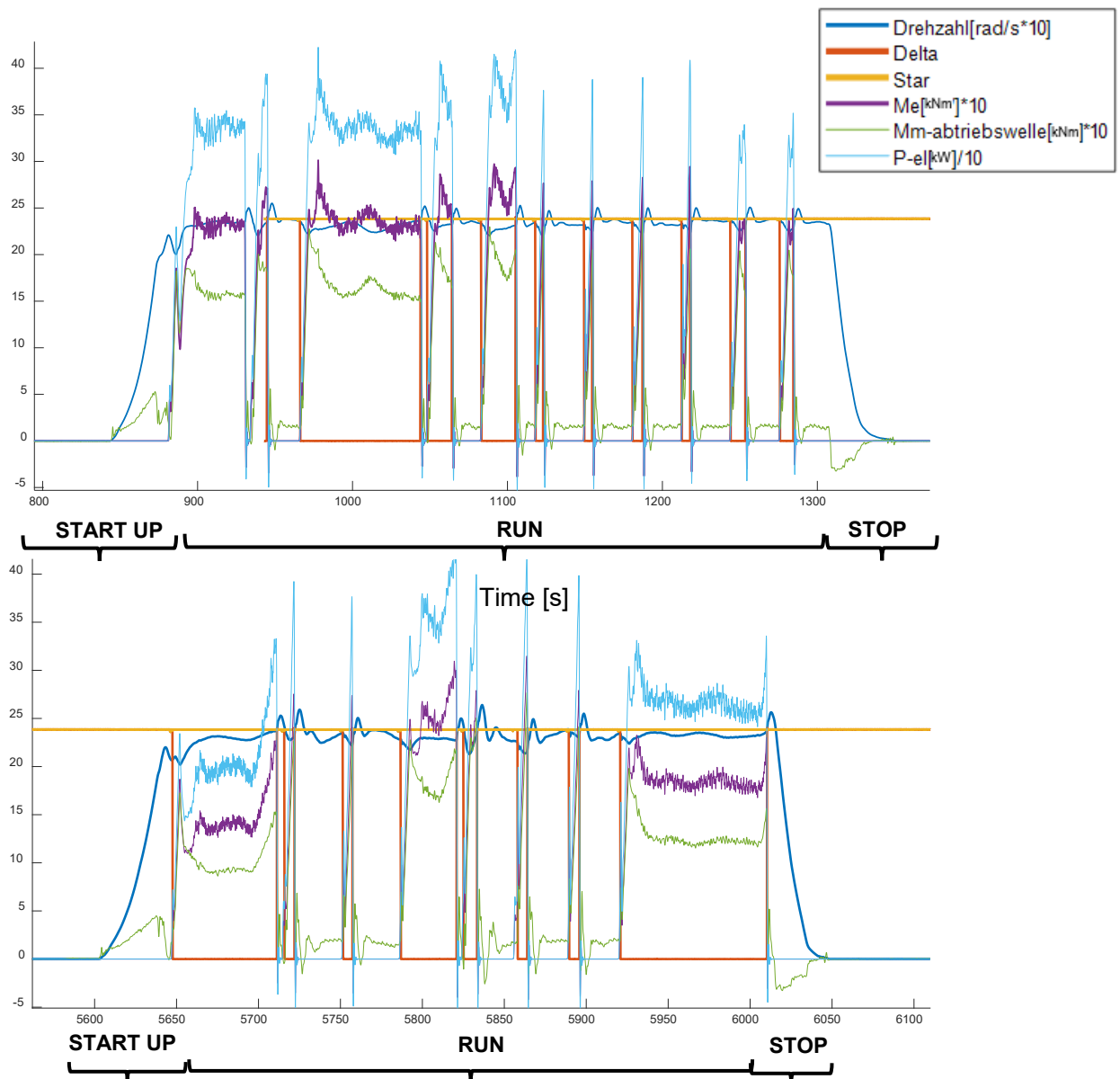
Figure 4.1: Measurement data, Source: [CWD18].

Chair for Wind Power Drives
Univ.-Prof. Dr.-Ing. Georg Jacobs

36

In Figure 4.1 the most important magnitudes that could play a role in the design of the controller are plotted together, so that they can be analysed and the relationship between them can be investigated.

Three operation periods are distinguished in Figure 4.1. These are: start up, run and stop. During the start-up and stop periods, there is no power production (no T_e), so the difference between both generator and mechanical torques is positive enough to create an acceleration (in accordance with Equation 4.1) that takes the rotational speed up to a value near to the rated rotational speed (see Figure 4.1, START UP). When the rotational speed reaches a certain level, and the torque in the high-speed shaft increases significantly rapid and up to a higher value, the run period begins.

Simultaneously with the beginning of the run period, the delta or/and star switches (one for each phase, then 3 in total for each connection) close, as seen in Figure 4.1.The switches have either a certain up-value (logic 1), meaning that they are opened and no power production is possible, or a down-value (logic 0), meaning that they are closed and power production is permitted. In Figure 4.1 the values were adjusted to fit the scale of the rotational speed curve. When a switch has a value of logic 0, then there is generated power (generator torque T_e is produced), and vice versa. That the switches change from open to close when the torque in the high-speed shaft increases rapidly is an important conclusion which could be useful when designing the new simulated controller (NSC).

In a certain moment during the run operation, it can be seen, that T_e is higher than the torque in the high-speed shaft, and for that reason the rotational speed does not increase anymore and remains constant. When the torque in the high-speed shaft decreases, the correspondent switches to the current connection open and no more power is produced, so T_e goes back to zero.

During the remaining periods of the run operation, the rotational speed will be held almost constant by intermittent rapid increases of the torque in the high-speed shaft. Figure 4.2 shows some rotational-speed behaviors that don't match the one explained. It is also important to remark, that during the operation test the rated rotational speed (1620 rpm) and power (850 kW) were never reached.

In Chapter 5, it will be intended that the controller reproduces the behavior explained before.

More conclusions were extracted from the measured data. As shown in Figure 4.3, a proportionality exists between the difference of the torques acting on the high-speed shaft and the angular acceleration in the periods in which there is no electrical power output (start up and stop). When power is produced, the equation seems not to describe the behavior of the testbench, since, as seen in Equation 4.1 (extracted from [SHY16]), although the difference of the torques is negative, the angular acceleration is mainly positive during this period.

$$T_m^{high-speed\ shaft} - T_e\ [kN] = J\ \frac{dn}{dt}\ [rad/s]$$

Equation 4.1

If we now try to get an approximate value of the inertia J for the start-up and stop periods, we get a value of:

$$J_{measurements} = 250000\ kgm^2$$

which is almost 10000 times bigger than the real value $J_{real} \cong 35\ kgm^2$. This could be explained considering that there are other terms that have an influence on the inertia.

Chair for Wind Power Drives
Univ.-Prof. Dr.-Ing. Georg Jacobs

37
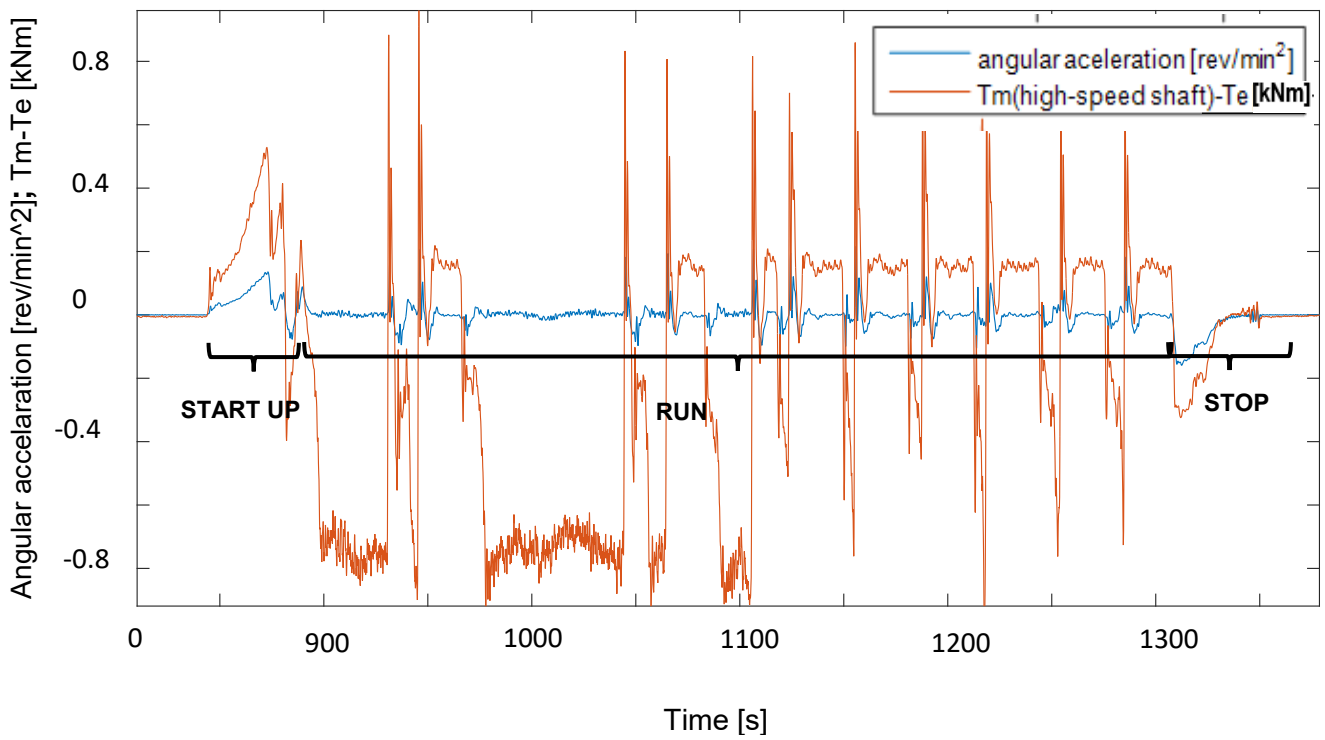
Figure 4.2: Angular acceleration in comparison with the difference of both mechanical and electrical torques in the high- speed shaft.

The code needed to do the analysis and treatment of the measurement data discussed in this chapter can be found in Appendix 4.

Chair for Wind Power Drives
Univ.-Prof. Dr.-Ing. Georg Jacobs

38

5. Implementation of the new simulated controller (NSC).

This chapter contains the procedures followed to design the NSC for both open- and closed-loop simulations (subsections 5.1 and 5.2 respectively).

The following sketch constitutes the co-simulation that will be used to create the new controller (NSC):
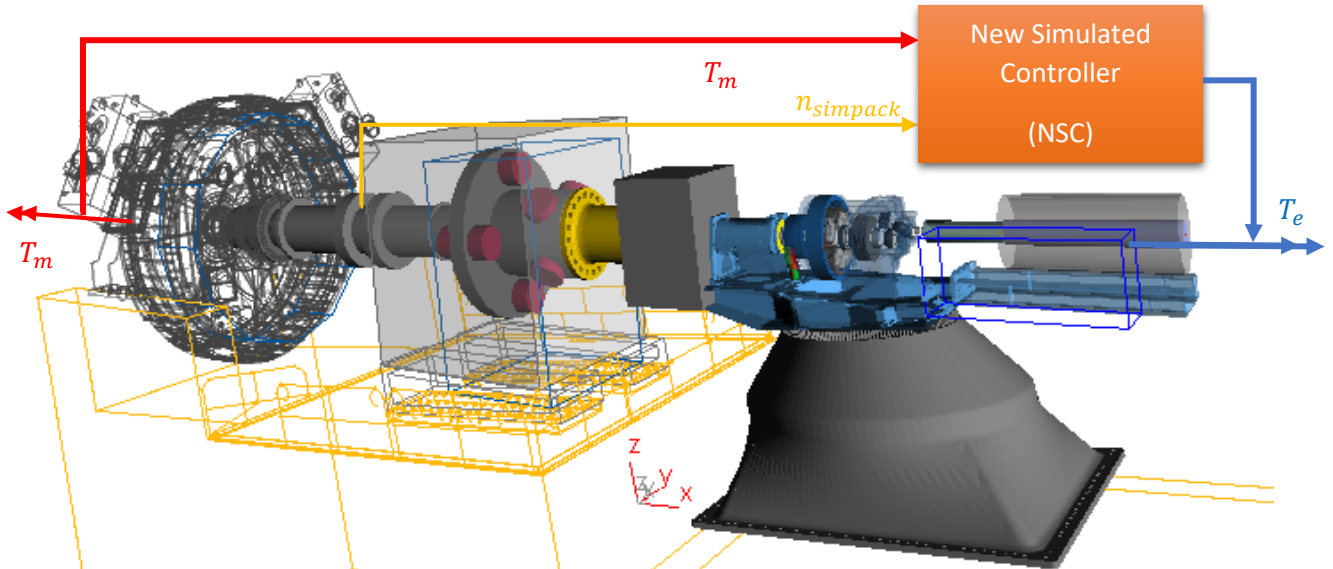
Figure 5.1: V52-Simpack Model (SM) and control scheme strategy, Source: [CWDSIM].

Figure 5.1 shows the V52-Simpack model (V52-SM) used in the thesis. The Simulink-Controller model, which is represented with the orange box (NSC), will run parallel to it. More information about the co-simulation can be found in subsection 2.3.
The co-simulation interface is the following:
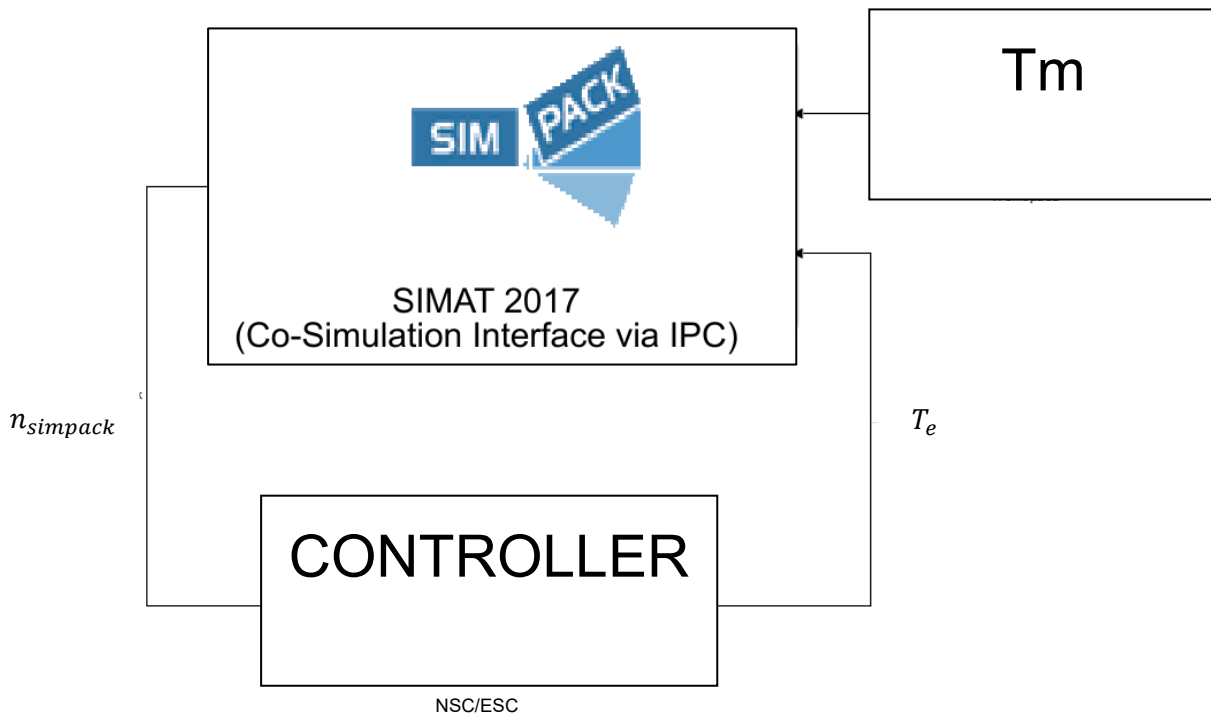
Figure 5.2: Co-simulation MATLAB-SIMPACK, Source: [CWDSIM; CWDECS].

Chair for Wind Power Drives
Univ.-Prof. Dr.-Ing. Georg Jacobs

39

In Figure 5.2 the main block represents the Simpack-model (V52-SM) that was developed in CWD. It contains a model of the V52 test bench. The inputs are the mechanical torque T_m in the low-speed shaft and the electrical torque T_e in the high speed-shaft [Nm].

The output is the rotational speed in the low-speed shaft $n_{simpack}$ [rad/s], which is feedbacked as the controller input. The simulation results will be compared with $n_{measures}$. The controller gets the simulated rotational speed in the low-speed shaft $n_{simpack}$ as input, and outputs the electrical torque in the high-speed shaft.

Firstly, the V52-SM was tested with the ESC. In Figure 5.3 the co-simulation Matlab-Simpack with the ESC is shown. Some gains were added to fit the units (rad/s to rpm). It is relevant also that the generator torque produced by the NSC must be negative (with the opposite sign of the input T_m).
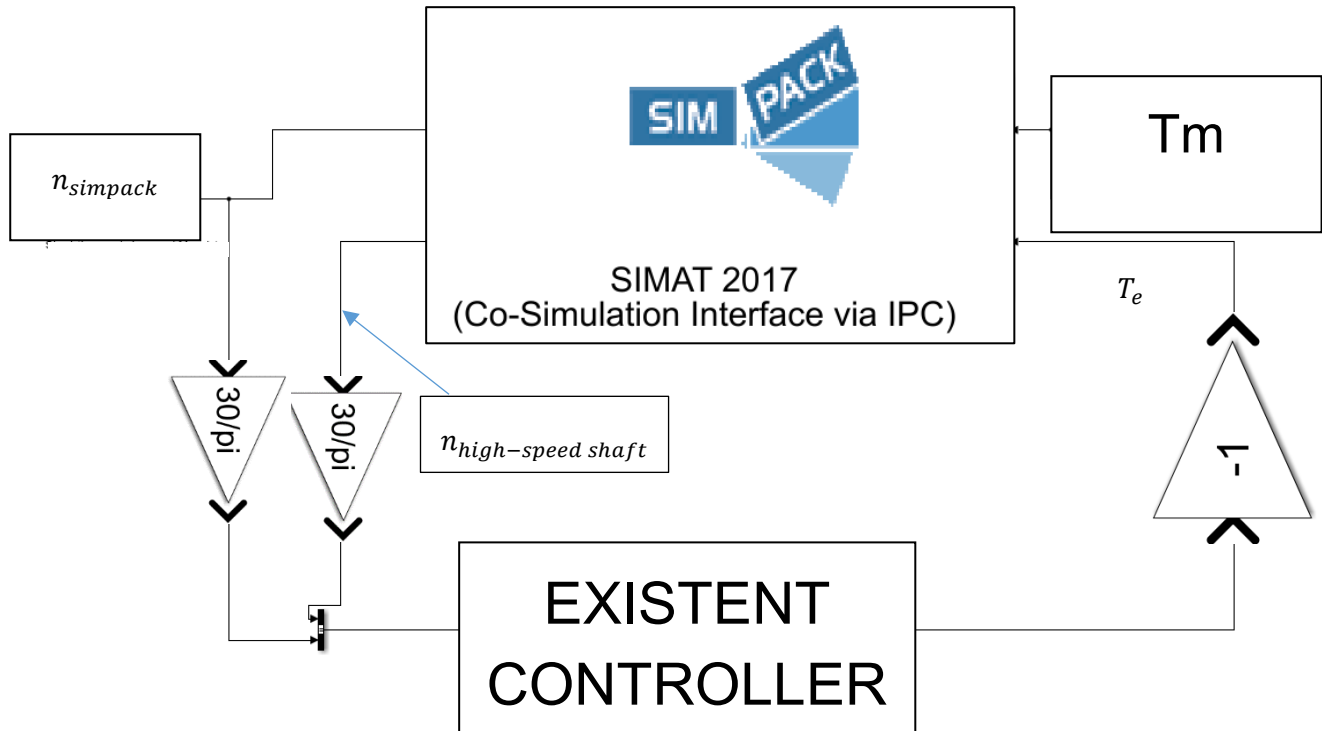
Figure 5.3:   Co-simulation with ESC, Source: [CWDSIM; CWDECS]

The results obtained from this simulation are seen in Figure 5.4. The rotational speed results were quite similar during start up operation (see Figure 4.1), but not satisfactory after it, as seen in Figure 5.4.
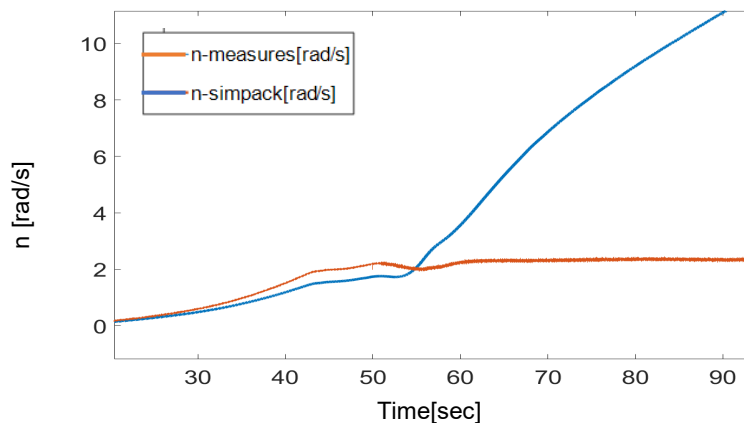
Figure 5.4:   Comparison of $n_{simpack}$ and $n_{measures}$ obained in the co-simulation with ESC.

Chair for Wind Power Drives
Univ.-Prof. Dr.-Ing. Georg Jacobs

40

<u>**Implementation**</u> of the new simulated controller (NSC).

The behavior of the ESC during the simulation was analyzed, in order to know which blocks (described in Chapter 3) are activated and have a contribution on the generated T_e. For that, the signals outputted from the blocks *Speed Control PID* and *Generator characteristics* (see Chapter 3) were analyzed. It was found that the only block that generated a signal different from zero during the simulation was the *Speed Control PID* (described in Chapter 3-Figure 3.4), which contains a PID Controller in parallel. In Figure 5.5 this output is shown. Because of that, the NSC will be chosen to be PID.
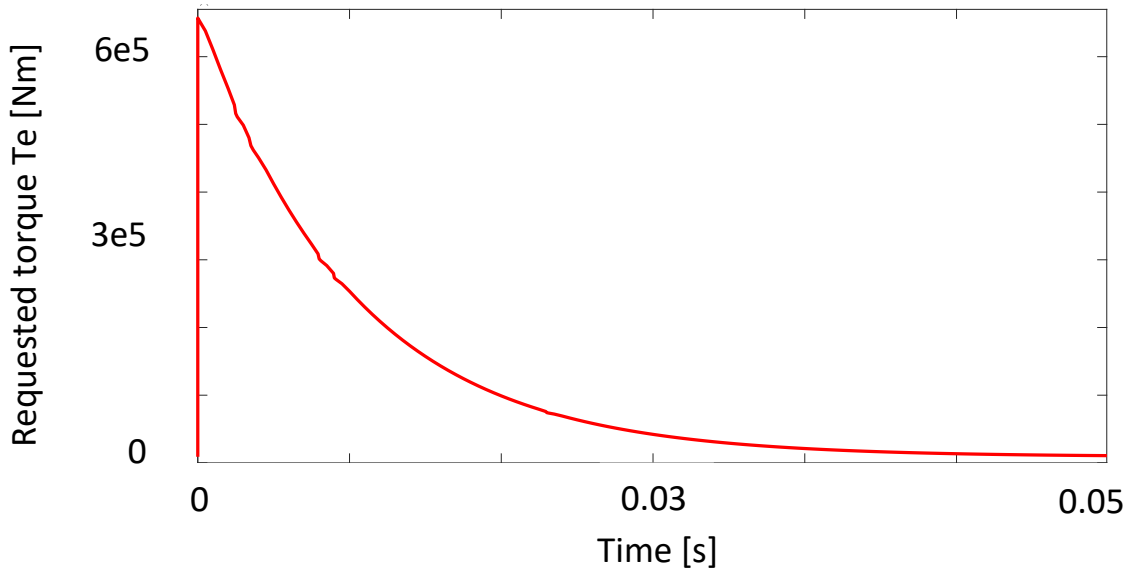
Figure 5.5: T_e signal generated by the *Speed Control PID* block in the ESC simulation.

Secondly, the V52-SM was tested with the electrical torque from the measured data without the ESC. The inputs of the V52-SM were T_m and T_e, and the output $n_{simpack}$ was compared with $n_{measures}$.
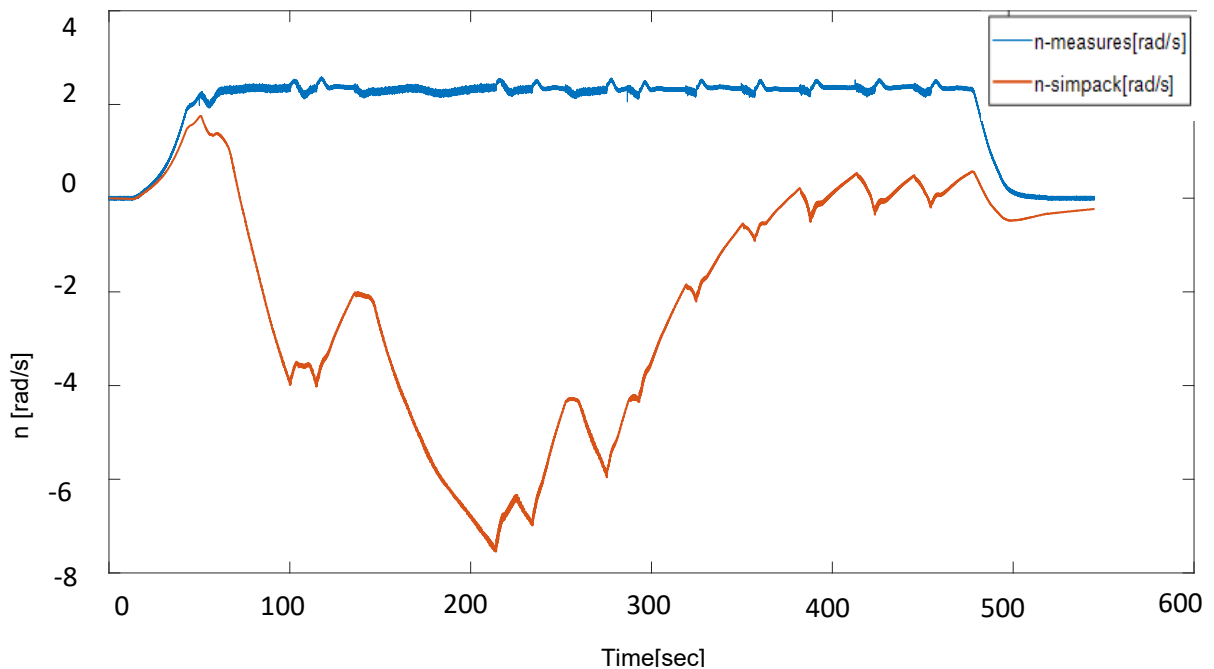
Figure 5.6:   Comparison of $n_{simpack}$ and $n_{measures}$ obtained in the simulation with T_e from measurement. .

Chair for Wind Power Drives
Univ.-Prof. Dr.-Ing. Georg Jacobs

41

Implementation of the new simulated controller (NSC).

Since the V52-SM doesn't reproduce exactly the dynamic of the real testbench (effects like rubbing and operation behavior), the results were very far from the measurement data, as Figure 5.6 shows. It is also possible that the V52-SM has some constructive failures. The **mean-square root error** between the measurement data and the simulated rotational speed $n_{simpack}$ was **23.7860 rad/s**. That means that the appropriate generator torque T_e must be calculated, so that the error between both rotational speeds, $n_{measures}$ and $n_{simpack}$, is minimized. This T_e must produce the measured rotational speed in the low-speed shaft when inputted together with the mechanical torque T_m in the low-speed shaft.

Chair for Wind Power Drives
Univ.-Prof. Dr.-Ing. Georg Jacobs

42

5.1 Open-loop simulation.

Simulation on the bottom of Figure 5.7 will be referred from now on as open-loop simulation, because we are giving a reference rotational speed (low-pass filtered $n_{measures}$; pass-band frequency= 0.2 Hz, stop-band frequency=1 Hz) to the controller, and the V52-SM output $n_{simpack}$ will not be used as feedback to generate T_e, but only compared to the measurement data $n_{measures}$. The closed loop simulation is shown on the top of Figure 5.7.
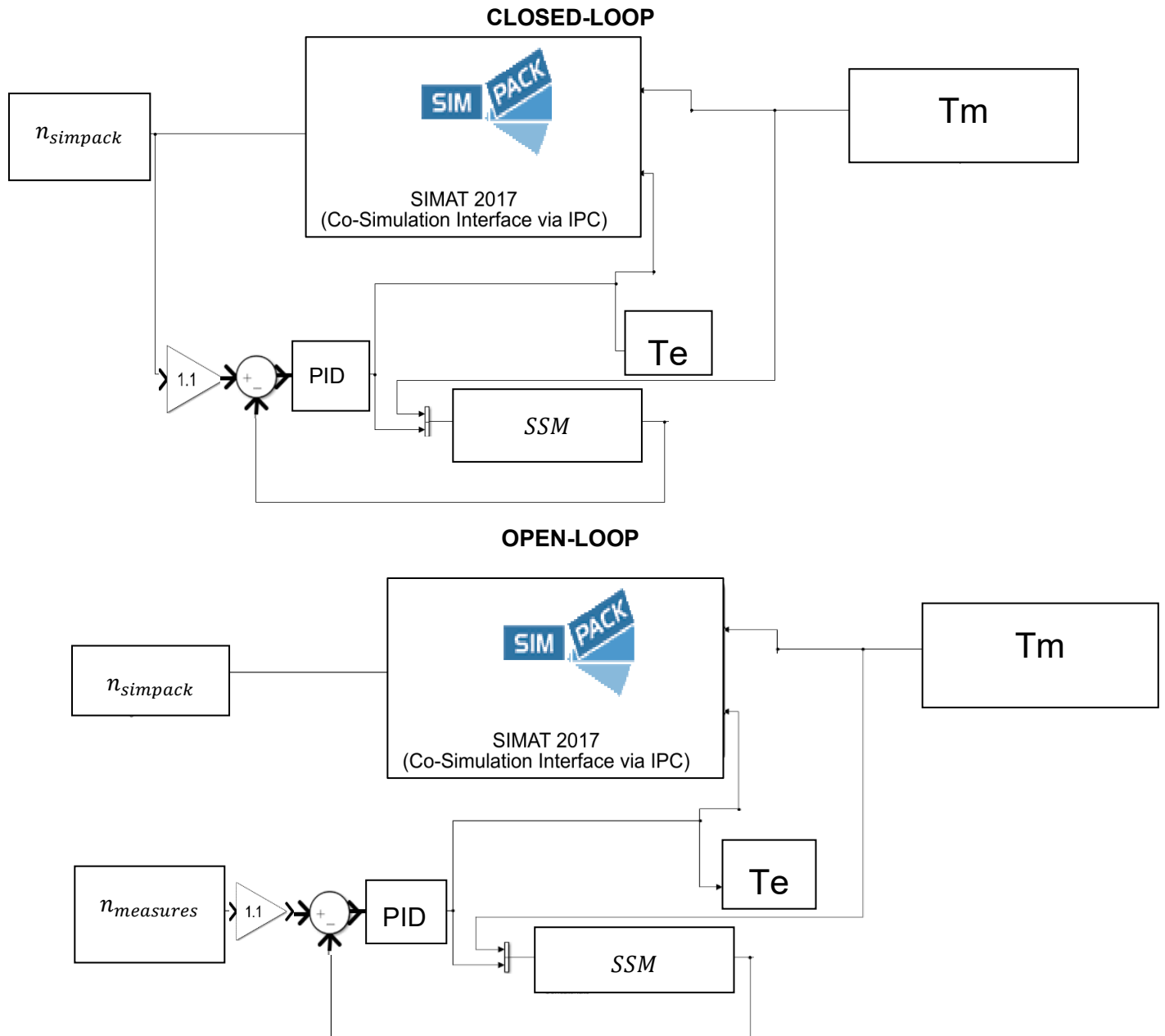
Figure 5.7:   Comparison between open- and closed-loop simulation´s scheme.

A solution to calculate the necessary T_e was implemented by the creation of a continuous state-space model (SSM) (see Figure 5.8) of the V52-SM through the Application Toolbox *System Identification* provided by MATLAB. A discrete state-space model was also created, but later it will be not used since the tuning of the controller for enough little time responses was not possible.
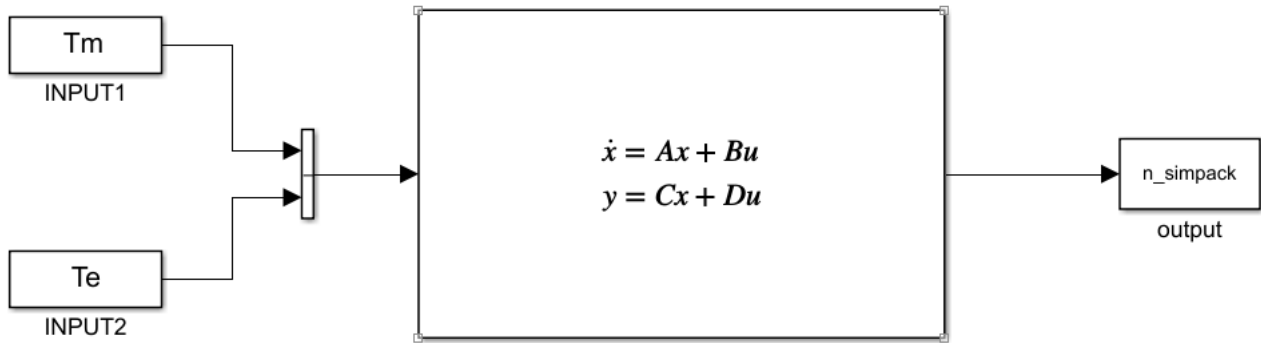
Figure 5.8:   Continuous SSM configuration.

To choose the order of the model, the fitting value between the response of the SSM to the real response of the V52-SM given by the *Application Tool Box* was considered, obtaining a fit of *fit* (1-POLE) =97.57% and *fit* (2-POLES) =76.72%, with the discrete and continuous model respectively. This indicator (*fit*) calculates, through Equation 5.1 (extracted from [MAT]), how well the simulated model response matches the measurement data [MAT]. For that reason, a first order system was chosen, due to its higher fit to the real measurement data.

$$\text{fit} = 100\left(1 - \frac{||y - \widehat{y}||}{||y - \text{mean}(y)||}\right)$$

Equation 5.1

Figure 5.9 and Figure 5.10 show the SSM model output and the real response for both continuous and discrete models respectively.
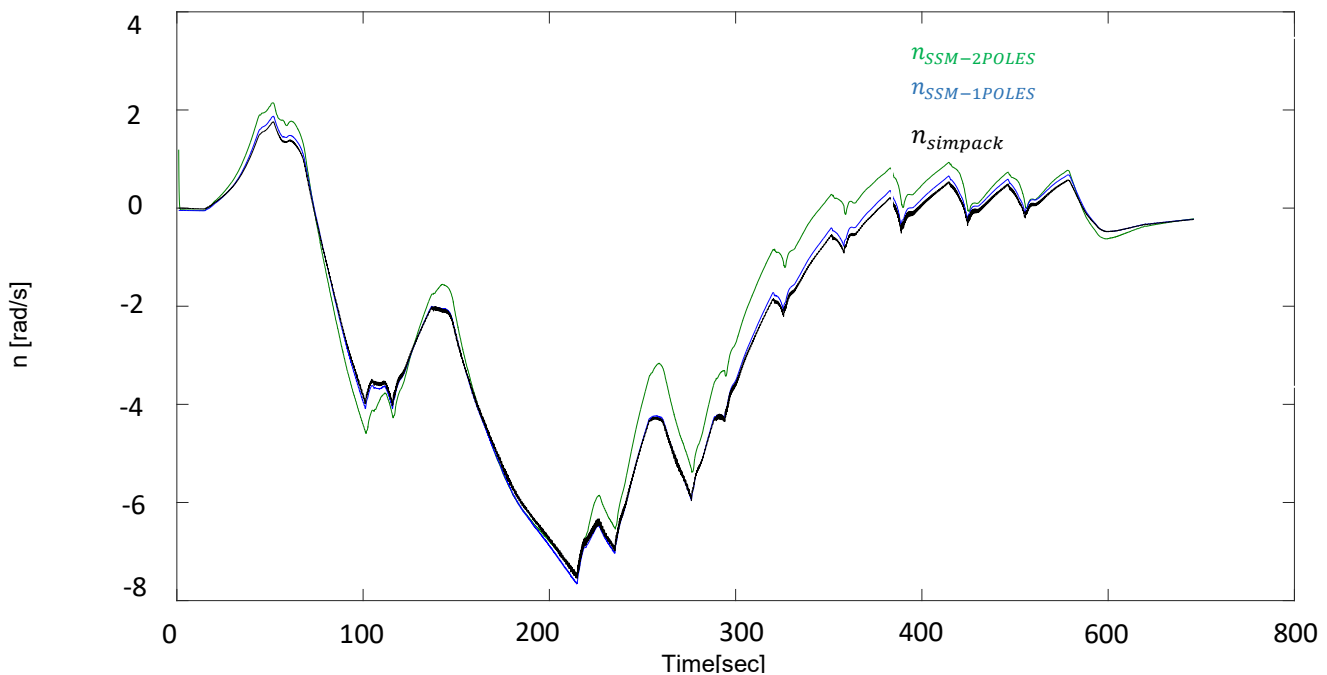
Figure 5.9:   Designed continuous SSM response to measurement data.

Chair for Wind Power Drives
Univ.-Prof. Dr.-Ing. Georg Jacobs

44
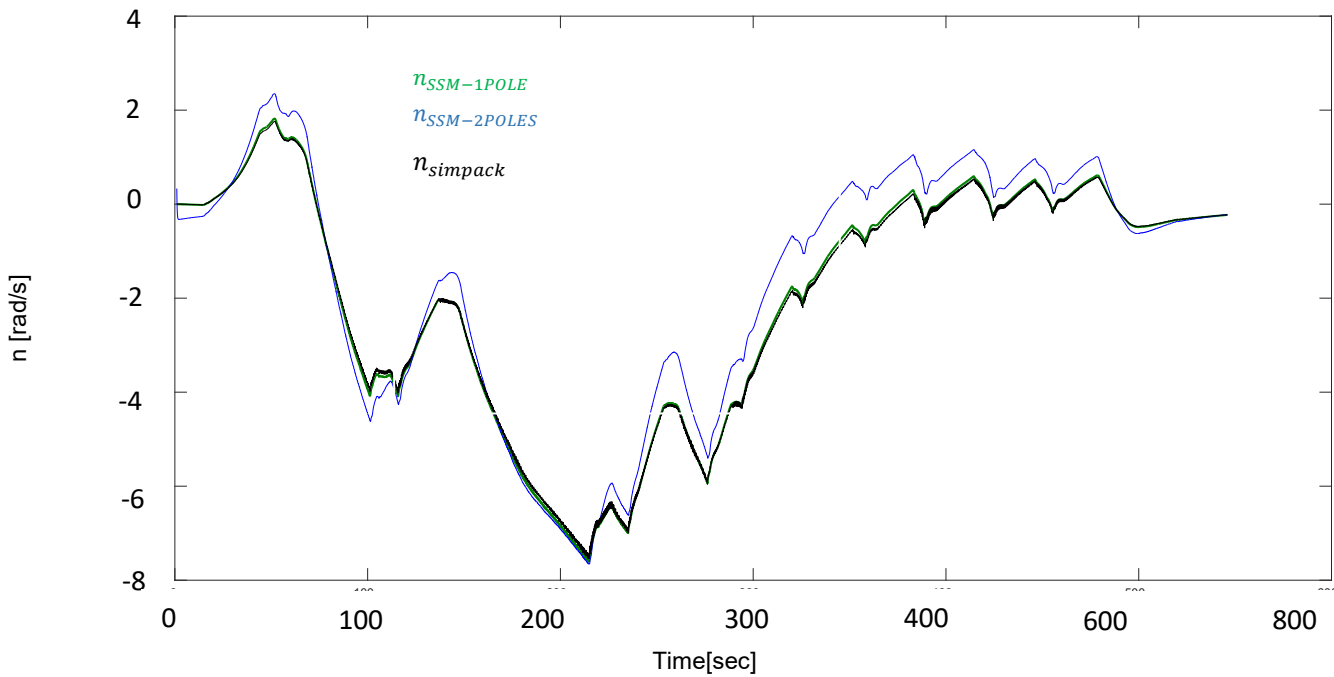
Figure 5.10: Designed discrete SSM response to measurement data.

Suprisingly, in spite of the complicated dynamic of the system, the fitting value between the response of the SSM to the real response of the V52-SM was very high (97.57%), so the dependence of the rotational speed was first-order-linear with some combination of T_e and T_m. Between continuous and discrete SSM, a continuous SSM was chosen, because as it will be later shown, the design of the controller will be easier. The state matrices and characteristics of the model are seen in Figure 5.11:

```
Continuous-time identified state-space model:
    dx/dt = A x(t) + B u(t) + K e(t)
     y(t) = C x(t) + D u(t) + e(t)


A =
              x1
   x1   -0.01925


B =
              u1          u2
   x1   1.737e-09   1.063e-07


C =
           x1
   y1   2444


D =
        u1   u2
   y1    0    0


K =
            y1
   x1   0.05533
```

Figure 5.11: Continuous designed SSM matrices.

Chair for Wind Power Drives
Univ.-Prof. Dr.-Ing. Georg Jacobs

45

The following control loop was used to produce the corrected T_e input signal:
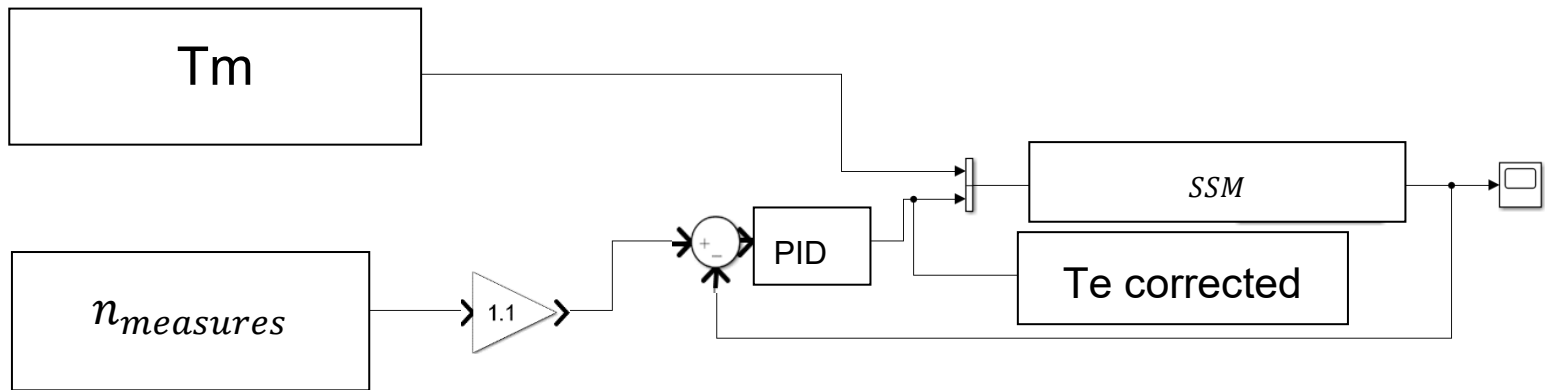
Figure 5.12: Tuned PID Controller operating in the designed control-feedback loop to calculate the corrected T_e.

Figure 5.12 shows the strategy followed to adjust T_e. T_m and $n_{measures}$ are the measurement data inputted into the SSM. $\boldsymbol{n_{measures}}$ **was low-pass filtered** to simplify the simulation and get a soft T_e behavior. A feedback loop control was implemented to adjust the output SSM-rotational speed to the reference value ($n_{measures}$). A PID Controller was chosen and tuned with the Application Toolbox PID Tuning provided by MATLAB, and the step response was adjusted in a way that the controller action (T_e), was as similar as possible to the measured T_e. Figure 5.14 shows the tuned parameters for the PID. A gain of 1.1 was added after the reference $n_{measures}$, according to the simulation results.

For the sake of clarity, the control scheme shown in Figure 5.12 will be named as the new simulated controller (NSC).

Figure 5.13 shows a comparison of the PID action T_e for different response times. Chosen were tr= 0.1 sec. and tr= 0.0005 sec
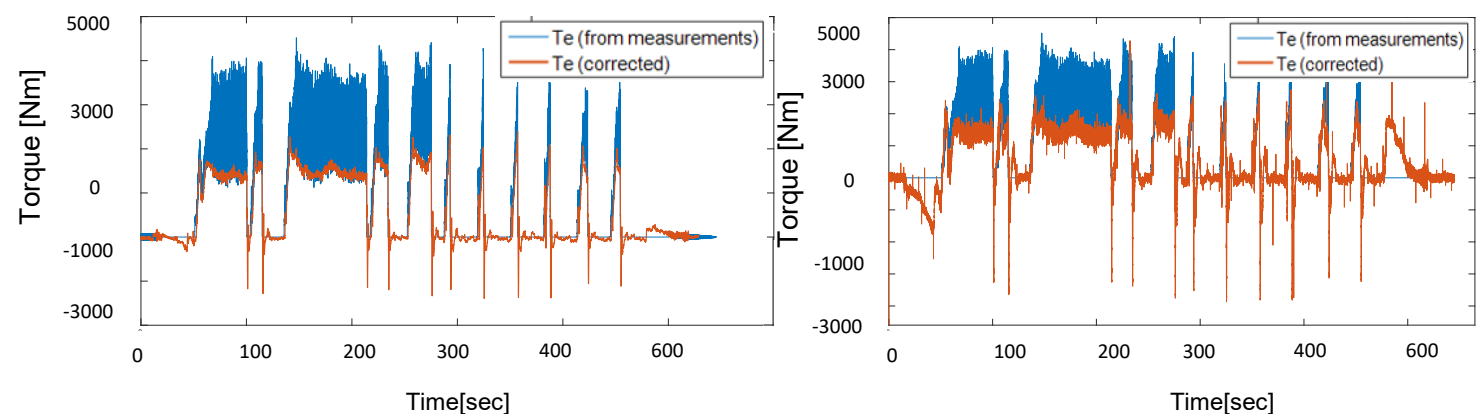
Figure 5.13: Comparison of the PID action *Te* for different response times (tr =0.1 sec. on the left and tr=0.0005 sec. on the right).

Results from the simulation in Figure 5.11 (Figure 5.13) show that the generated T_e is very oscillating for reduced response times like the sampling period (image on the right) and that is far from 0 Nm during the start-up and stop operation (see Chapter 4). Therefore, the PID response time was chosen to be *tr= 0.1 sec* (image on the left).

Chair for Wind Power Drives
Univ.-Prof. Dr.-Ing. Georg Jacobs

46

<u>**Implementation** of the new simulated controller (NSC).</u>

Comparing the corrected T_e with the measured one, it is seen that the corrected T_e follows the inferior part of the measured T_e and also has some peaks during the run operation (see Chapter 4). This is interesting because now we have a controller that can reproduce the behaviour of the real plant, meaning that it produces a T_e that matches globally the dynamic of the measured T_e but at the same times works for the V52-SM.

Controller Parameters

	Tuned	Block
P	73383.776	73383.776
I	259235.825	259235.825
D	696.8206	696.8206
N	72.9365	72.9365

Performance and Robustness

	Tuned	Block
Rise time	0.0907 seconds	0.0907 seconds
Settling time	0.694 seconds	0.694 seconds
Overshoot	10.2 %	10.2 %
Peak	1.1	1.1
Gain margin	Inf dB @ NaN rad/s	Inf dB @ NaN rad/s
Phase margin	90.1 deg @ 20 rad/s	90.1 deg @ 20 rad/s
Closed-loop stability	Stable	Stable

Figure 5.14: Tuned unit step response and tuned PID parameters.

Once the adequate T_e is generated, this torque was used as the corrected input for the Simpack model to produce the desired rotational speed in the low-speed shaft, as shown in Figure 5.15.

Figure 5.15 is also equivalent to the image on the bottom in Figure 5.7, meaning that to produce the signal T_e *corrected* (see Figure 5.7), the simulation in Figure 5.12 must be done before.
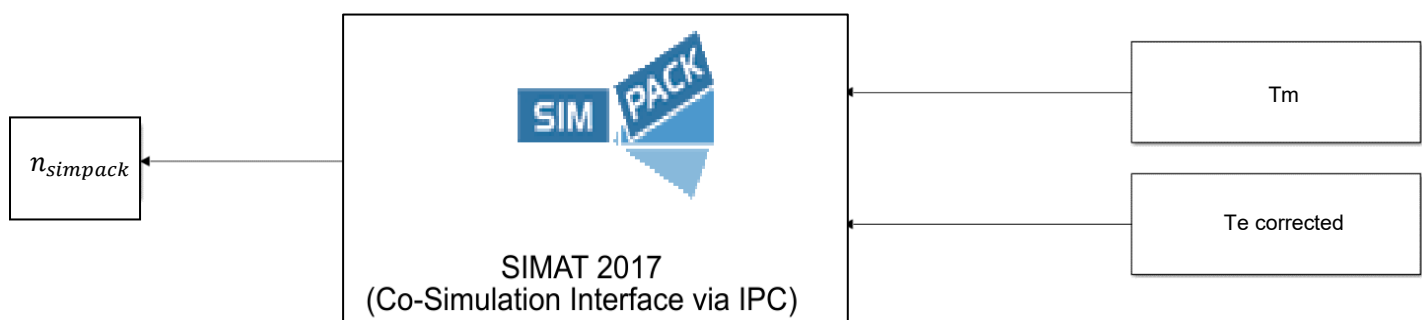
Figure 5.15: Simulation scheme to test the NSC *Te corrected* signal.

Chair for Wind Power Drives
Univ.-Prof. Dr.-Ing. Georg Jacobs

47

Now the open-loop simulation results will be discussed. To estimate the error between the measurement data ($n_{measures}$) and the simulated rotational speed ($n_{simpack}$), the **mean-square root error between both signals** will be calculated. The results of the open-loop simulation for different measurement data are shown in Figure 5.16 to Figure 5.19.
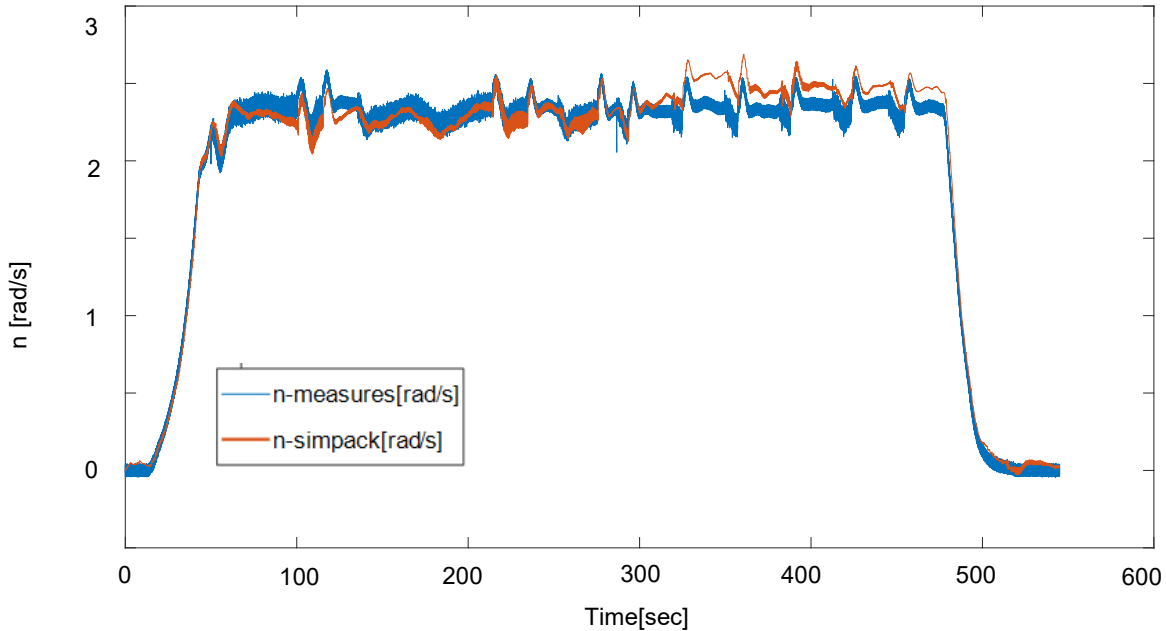
Figure 5.16: Comparison of n-simpack and n-measures obtained in the first test of the open-loop simulation with the corrected electrical torque *Te*.

Although the controller was developed working only with a specific measurement in a time period (600 sec.), the NSC also worked with the rest of the measurement data. Then we conclude that there is no overfitting.

As shown in Figure 5.16, the simulation results were satisfactory (**mean-square root error= 0.0137 rad/s**).The designed control strategy was also tried for another measurements, obtaining also satisfactory results.
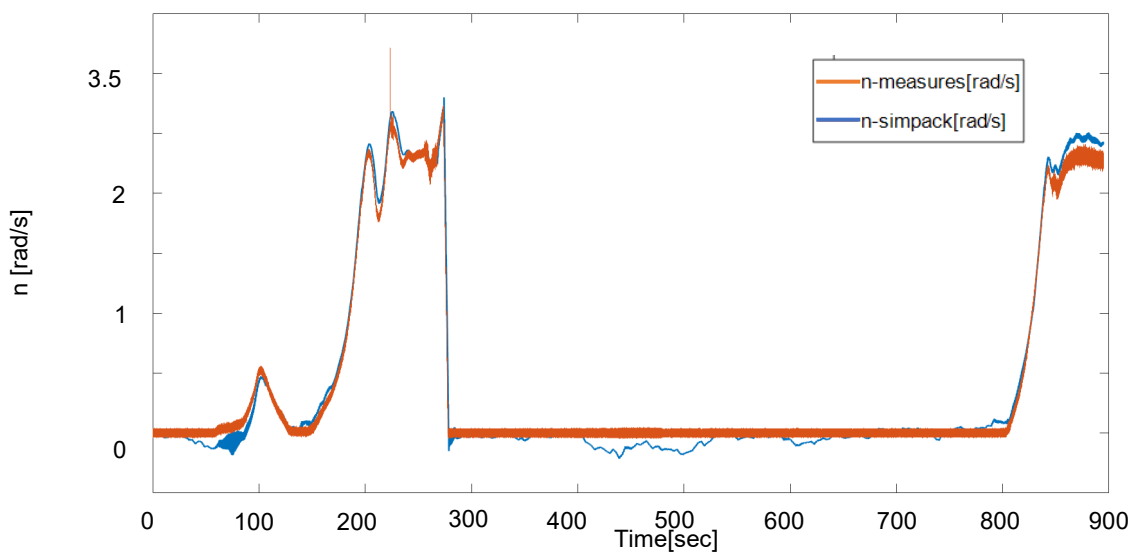
Figure 5.17: Comparison of n-simpack and n-measures obtained in the first part of the second test of the open-loop simulation with the corrected electrical torque Te.

Chair for Wind Power Drives
Univ.-Prof. Dr.-Ing. Georg Jacobs

48

Simulations results in Figure 5.17 have a **mean-square root error= 0.0068 rad/s.**
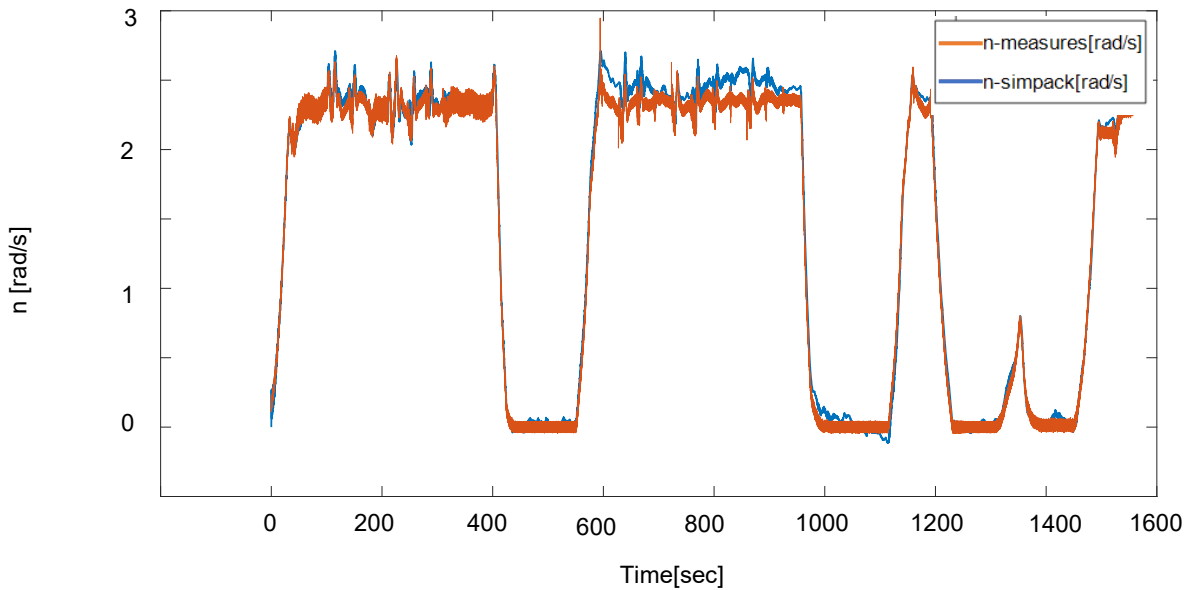
Figure 5.18: Comparison of n-simpack and n-measures obtained in the second part of the second test of the open-loop simulation with the corrected electrical torque Te.

Simulations results in Figure 5.18 have a **mean-square root error= 0.0857 rad/s.**
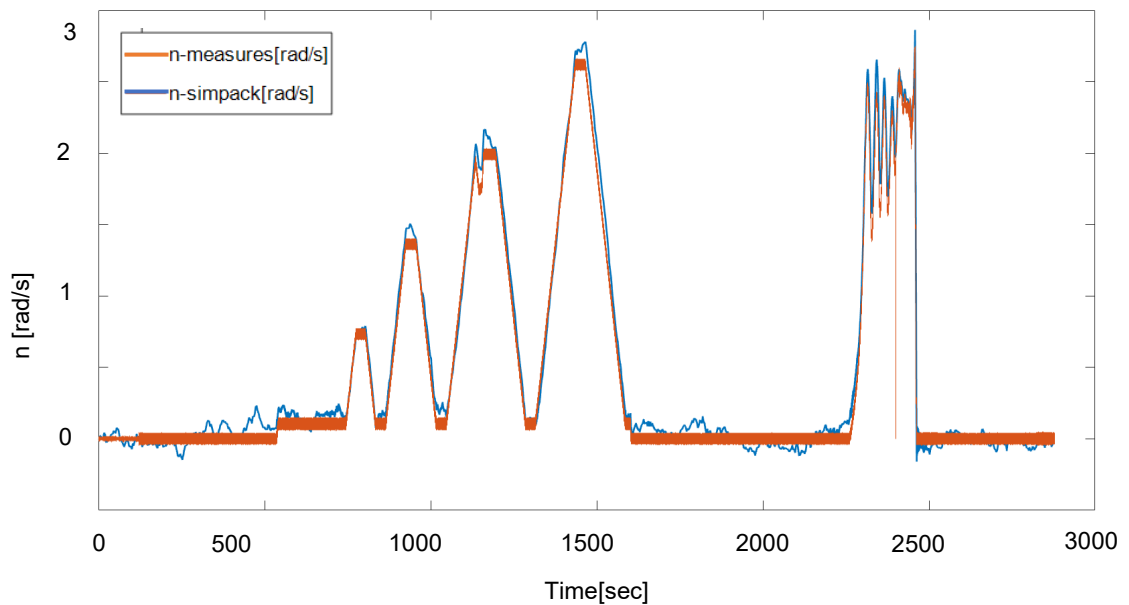
Figure 5.19: Comparison of n-simpack and n-measures obtained in the third test of the open-loop simulation with the corrected electrical torque *Te*.

Simulations results in Figure 5.19 have a **mean-square root error= 0.0067rad/s.**

Chair for Wind Power Drives
Univ.-Prof. Dr.-Ing. Georg Jacobs

49

A total of 6044 seconds (1.68 hours of the V52-testbench operation) were simulated, which validates the designed open-loop NSC for the open-loop control.

If we now observe the errors obtained, we can see that these are between 0.0067 rad/s and 0.0137 rad/s for the first test, second part of the second test and third test, but the error is much higher in the second part of the second test (0.0857 rad/s).

An explanation for this fact tried to be found, but unfortunately it was no reason regarding the dynamic of the controller or the plant that can prove this different error. The only argument found was that, since the second test was divided into two parts (see Figure 5.16 and Figure 5.17), when we run the second part, we don't take into acount the conditions of the last moment simulated in the first part, meaning that the initial conditions for the second part don't correspond the final conditions of the first part.

We conclude then that it is better to run complete tests in the simulation, and not split them into sperated parts.

5.2 Closed-loop simulation.

The next step consists of producing the T_e (generator torque) out of $n_{simpack}$ (rotational speed of the low-speed shaft of the V52-SM), so that the rotational speed reference $n_{measures}$ (rotational speed of the low-speed shaft from measurement data) is not necessary. The closed-loop simulation gave bad results (unstable rotational speed). Several possible solutions were considered: first, a low-pass filter was implemented. This filter should adequate the signal $n_{simpack}$ (a very oscillating signal- see Figure 5.19), and now the input of the controller, to the designed open-loop NSC. This input was before $n_{measures}$, a very smooth filtered signal. This filter is represented by the yellow block in Figure 5.20. It has a pass-band frequency=0.2Hz and a stop-band frequency=1Hz. However, the closed-loop simulation gave also bad results. Even after doing a sensibility analysis by changing the PID parameters, with special emphasis on the derivative part, results were bad (see Figure 5.22).
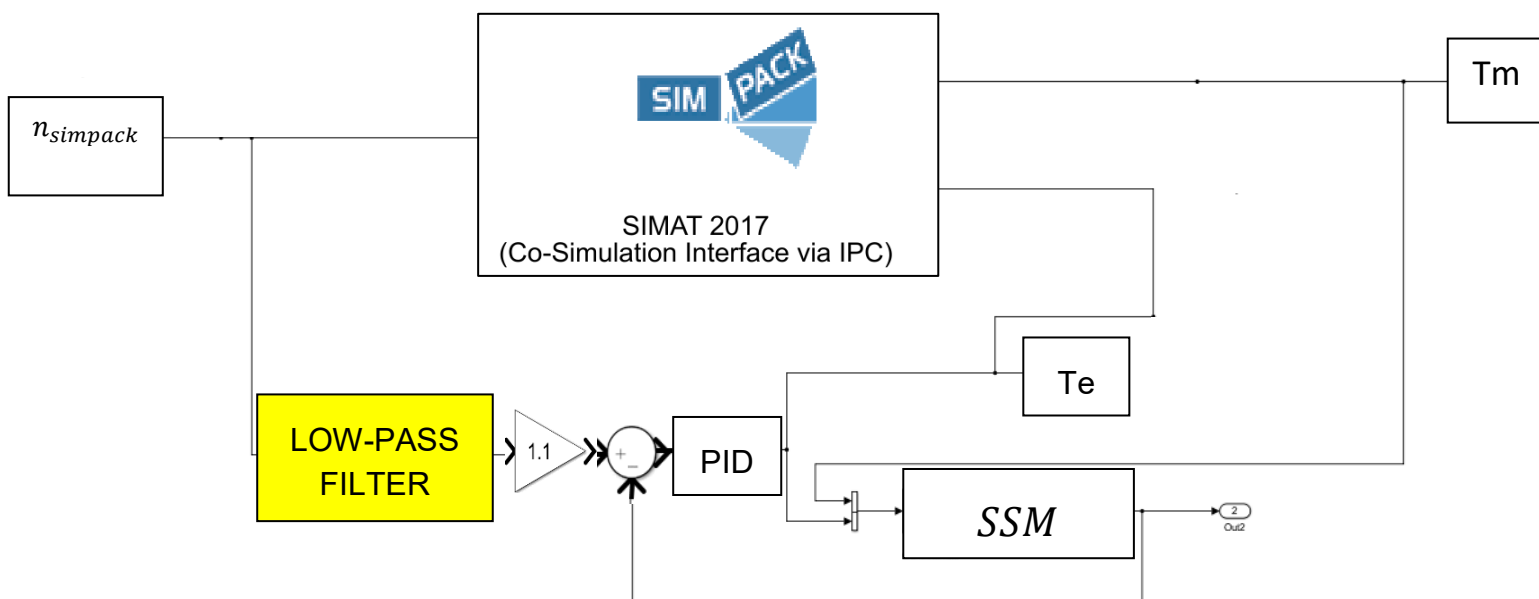
Figure 5.20: Closed-loop simulation with the low-pass filtered $n_{simpack}$ signal.

<u>**Implementation**</u> of the new simulated controller (NSC).

The results of the simulation in Figure 5.20 with the filter and a PID derivative part of *Kd=696.82/10.75* instead of *Kd= 696.82* (best result achieved until that moment) were the following:
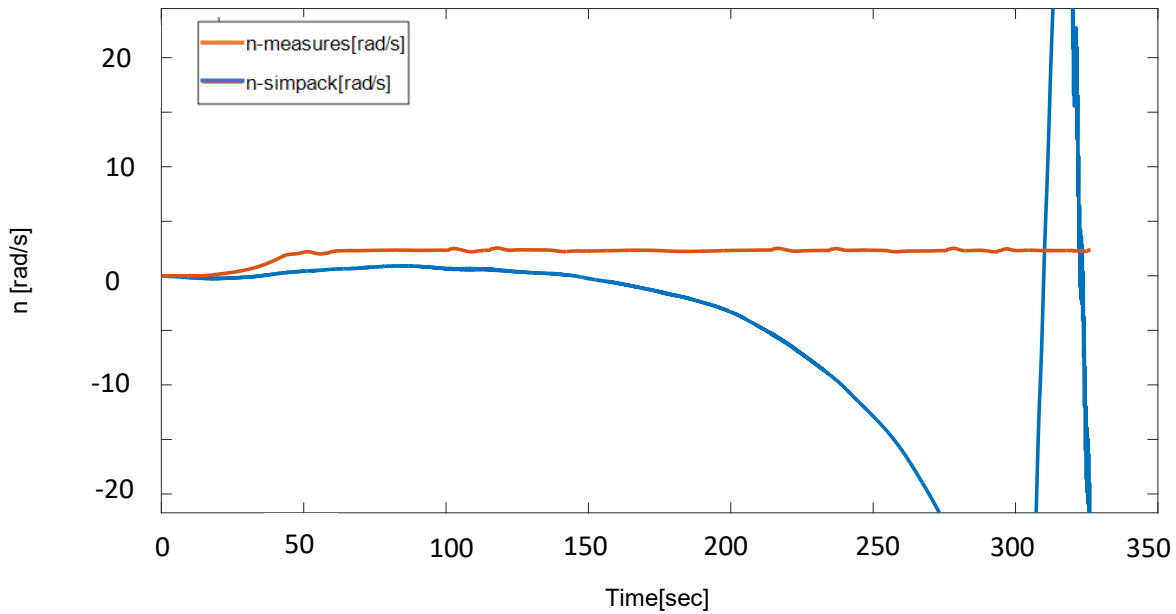
Figure 5.21: Closed-loop simulation results with the low-pass filtered $n_{simpack}$ signal and a corrected PID derivative part.

The PID action (T_e) obtained in the simulation in Figure 5.20, which is the T_e, will be compared with the corrected one (see Figure 5.23). The obtained T_e was the following:
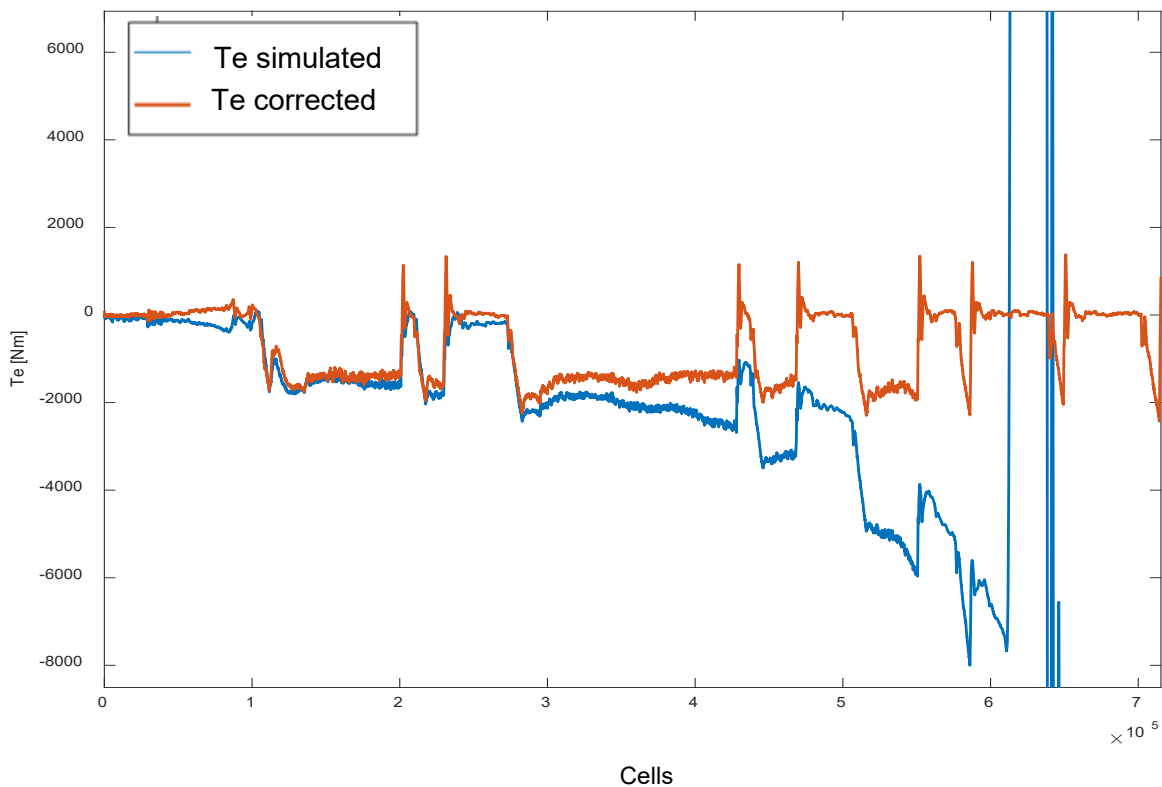
Figure 5.22: T_e obtained in the simulation in Figure 5.20 (blue signal) and the corrected one (red signal). The horizontal axis represents the MATLAB-cells in which the data are sampled with a sampling frequency of 2000 Hz.

Chair for Wind Power Drives
Univ.-Prof. Dr.-Ing. Georg Jacobs

51

<u>**Implementation**</u> of the new simulated controller (NSC).

At the beginning of the simulation (see Figure 5.23), T_e is very similar to the corrected one. Then T_e starts decreasing drastically and $n_{simpack}$ decreases also drastically according to Equation 4.1.

Several possible solutions to the problem were considered. Among them, the possibility to create a look-up table that could describe the relationship between the rotational speed and the generator torque was investigated. This new strategy was developed with help from the research assistant M.Sc. Martin Cardaun.

In this new strategy, a look-up table, shown in Figure 5.24, was created and also a sliding mean was added in order to smooth the signal $n_{simpack}$. The fundamental frequency of the block was first estimated to be 2 Hz.

The look-up table is the following:

LOOK-UP TABLE FOR V52-SM:

T_Gen = [0; 0; 0; 0; 1500; 5010; 5010];

n_T_Gen = [-50; 0; 10; 1400; 1401; 1620; 2000];

The simulation scheme and results are shown in Figure 5.24 and Figure 5.25 respectively.
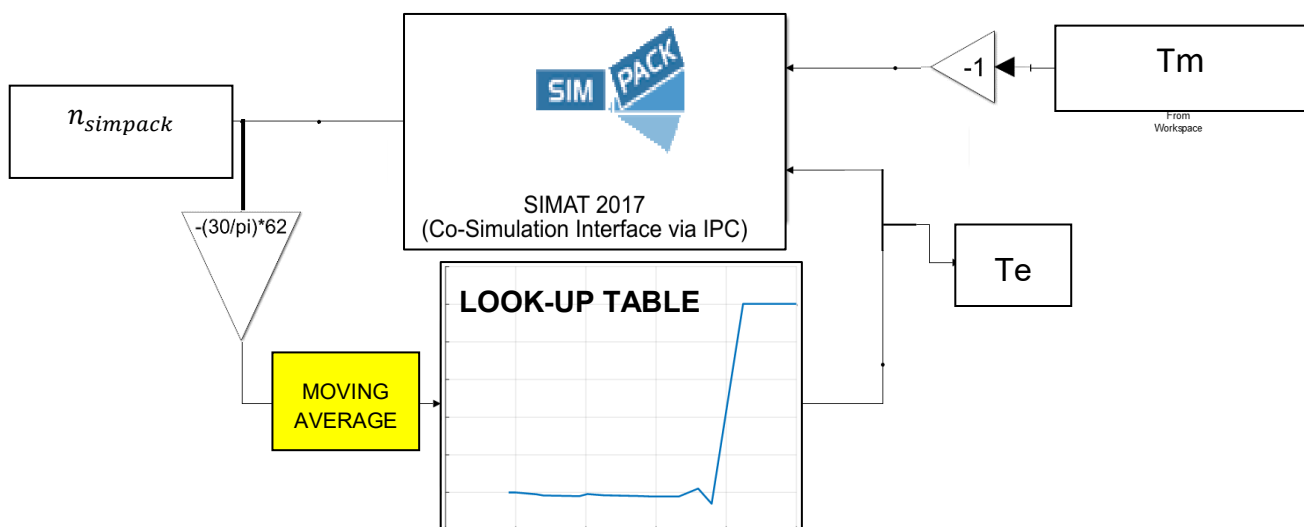
Figure 5.23: Simulation scheme of the closed-loop simulation with the look-up table strategy.

Chair for Wind Power Drives
Univ.-Prof. Dr.-Ing. Georg Jacobs

52
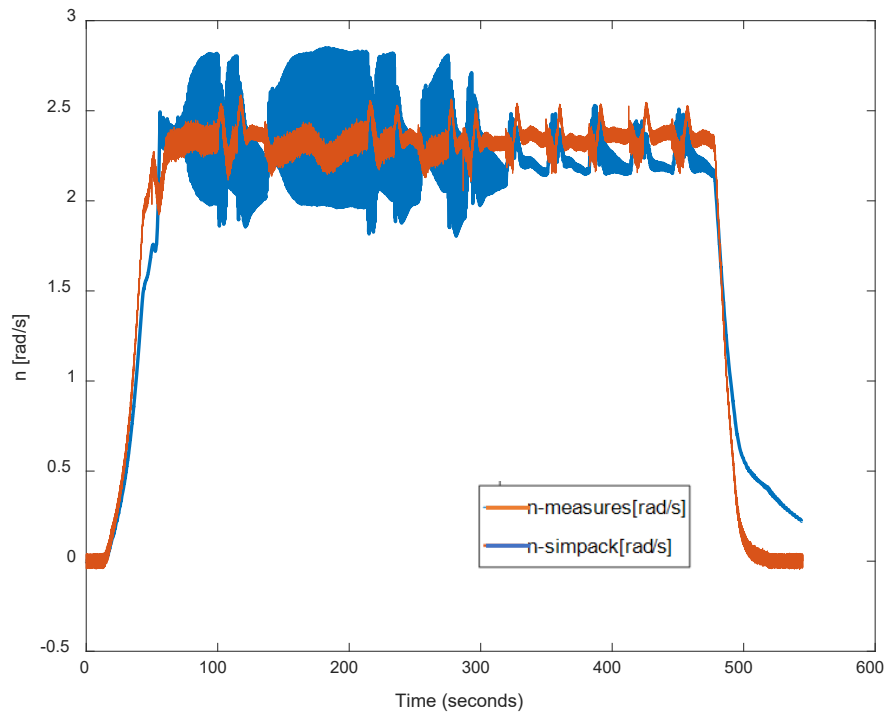
Figure 5.24: Results of the simulation in Figure 5.24.

To get rid of the high frequency oscillation seen in Figure 5.25, the fundamental frequency of the blue signal in Figure 5.25 was measured.

A seen in Figure 5.26, we obtain an oscillation period of 0.3 sec, which corresponds to a frequency of approximately 3 Hz.
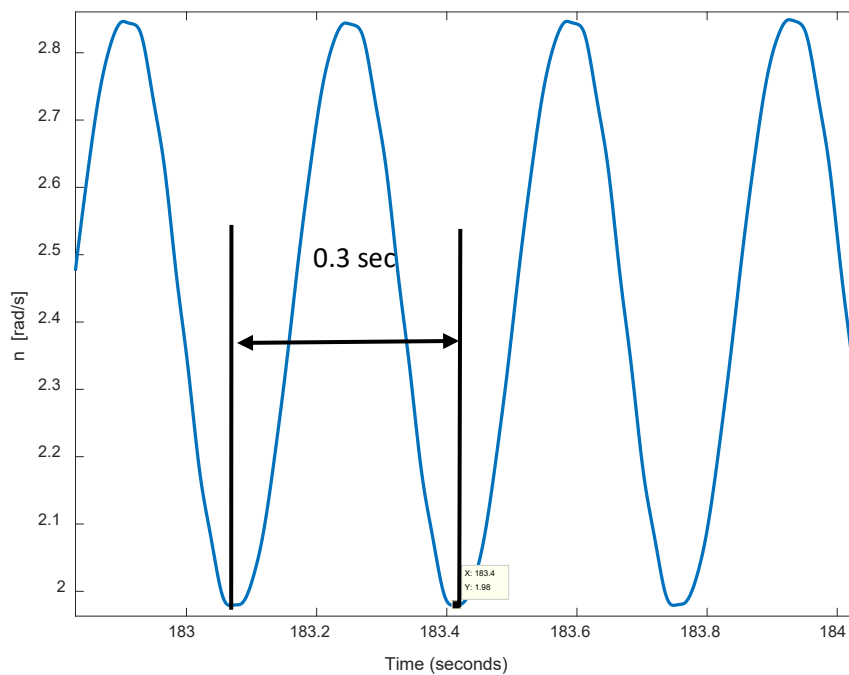
Figure 5.25: High-frequency oscilation in $n_{simpack}$ during the run operation.

Chair for Wind Power Drives
Univ.-Prof. Dr.-Ing. Georg Jacobs

53

Modifying this parameter in the moving average block we observe that the oscillation is considerably reduced (see Figure 5.27).

If we further increase the fundamental frequency, we significantly reduce the high-frequency oscillation. Figure 5.28 shows how this works for a fundamental frequency of 4 Hz.
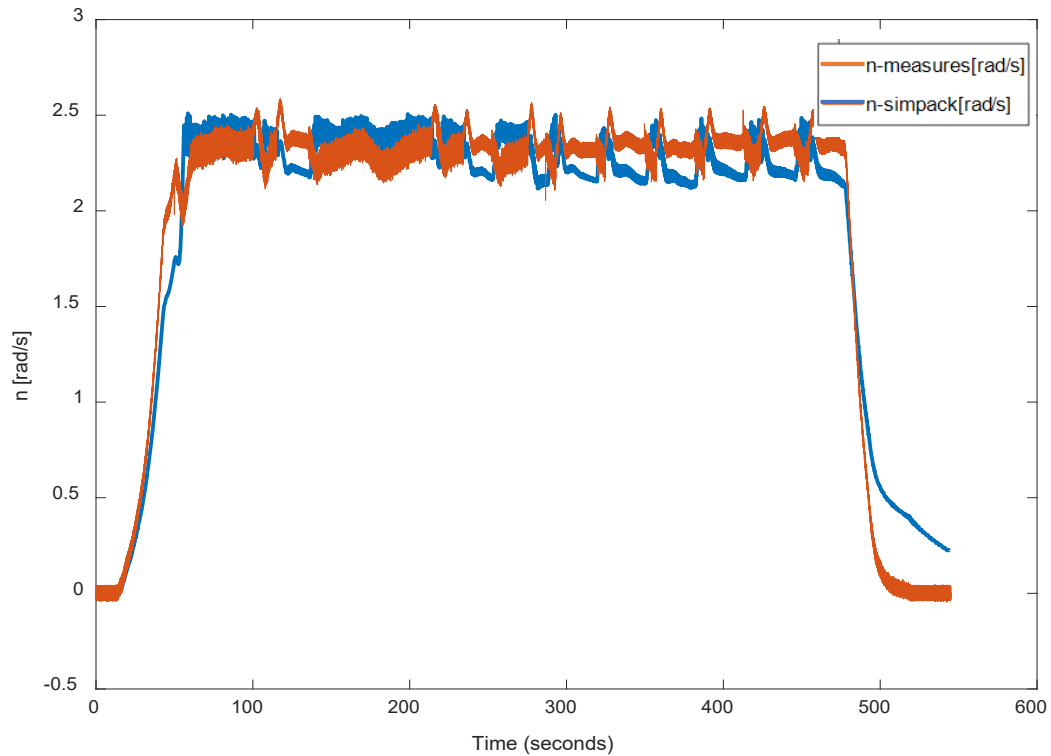
Figure 5.26: Simulation results after changing the moving average fundamental frequency to 3 Hz.
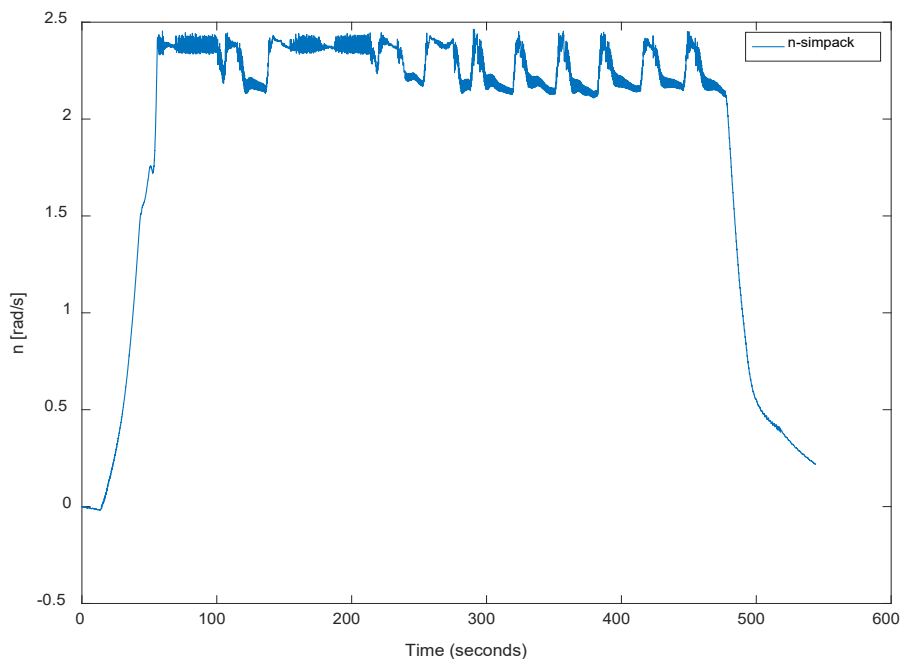
Figure 5.27: Simulation results after changing the moving average fundamental frequency to 4 Hz.

Chair for Wind Power Drives
Univ.-Prof. Dr.-Ing. Georg Jacobs

54

For the results in Figure 5.28, a **mean-square root error= 0.0341 rad/s** was estimated

The new NSC also worked with further measurement data (duration of the simulation=100 sec.), as seen in Figure 5.29 (fundamental frequency of the moving average was chosen to be 4 Hz), obtaining **a mean-square root error=0.0435 rad/s**.
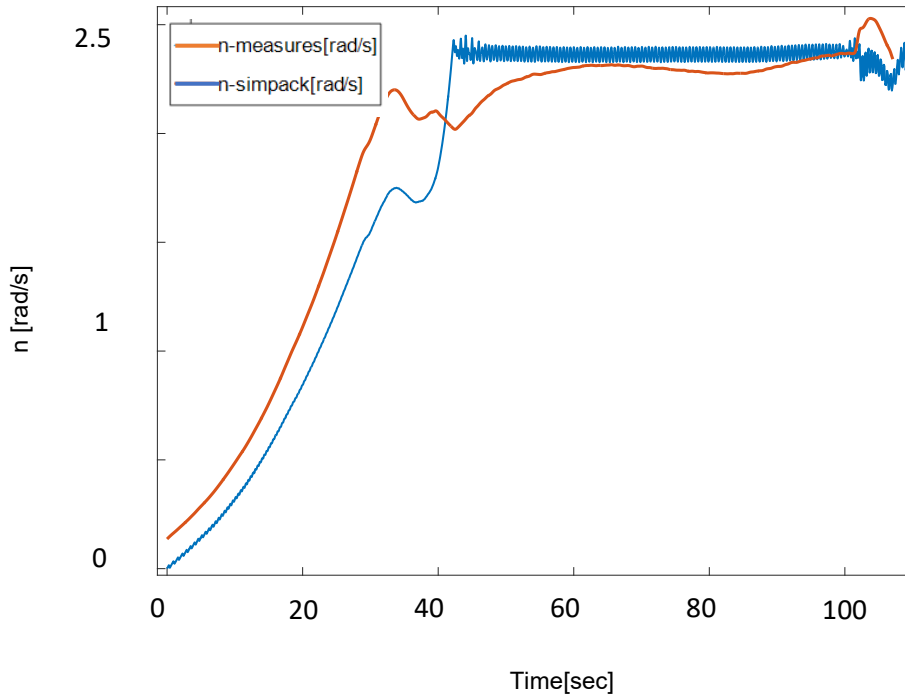
Figure 5.28: Simulation results with further measurement data.

In Figure 5.27 and Figure 5.29 it is possible to see that during start-up and some periods of the run operation $n_{simpack}$ is lower than $n_{measures}$, and during stop operation $n_{simpack}$ is higher than $n_{measures}$. To correct this deviation the look-up table was modified to better fit the measurements. It was necessary to modify the original look-up table, which now describes only the dynamics of the start-up and run operations (see Chapter 4). Another look-up table was created for the stop operation.

It was not possible to represent the behavior of the three operations modes in one look-up table due to incompatibilities between rotational speed and torque (for the same rotational speed we have different torques depending on the operation mode; this fact cannot be considered in a single look-up table).

The process of creation of the mentioned look-up tables is described in Appendix 5.

The created tables are the following:

LOOK-UP TABLE FOR V52-SM FOR START-UP AND RUN OPERATION:

```
T_Gen =    [0;  0; -48.57;-80; -97.58 ;  -101.9+60  ;-124.5+50 ;-
143.3+60;   -155.2+60  ; -165.7+60 ; -188.3+80 ; -103.4+60;
24+80; -300; 5010; 5010];
```

```
n_T_Gen = [-50; 0;  148.3; 197;   453.4  510.7  ; 625.6  ;   733.2
; 887.5    ;959;1162;1204;1300; 1396; 1620; 2000];
```

LOOK-UP TABLE FOR V52-SM FOR STOP OPERATION:

```
T_Gen1 = [0; 2.684; 19.7; 69.01; 133.5; 228; 138.8];
```

```
n_T_Gen1 = [0; 2.684; 19.7; 69.01; 133.5; 228; 1131];
```

In the values above, T_Gen refers to the generator torque, and `n_T_Gen` refers to the rotational speed of the high-speed shaft.

In Figure 5.30, Figure 5.31 and Figure 5.32 the mentioned look-up tables are shown:
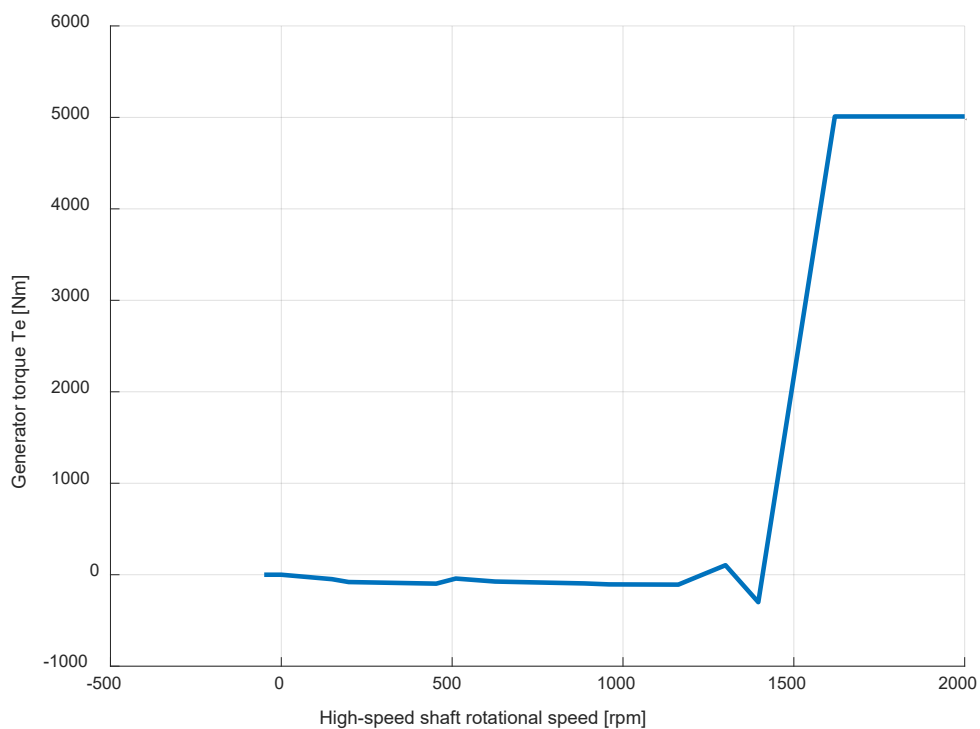
Figure 5.29: Look-up table for the start-up and run operation modes.

Chair for Wind Power Drives
Univ.-Prof. Dr.-Ing. Georg Jacobs

56
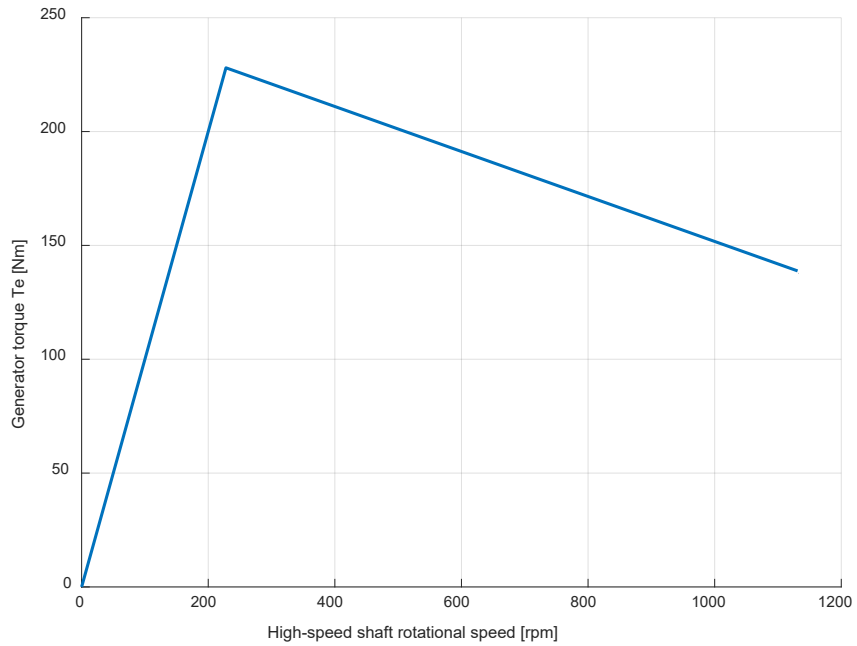
Figure 5.30: Look-up table for the stop operation mode.
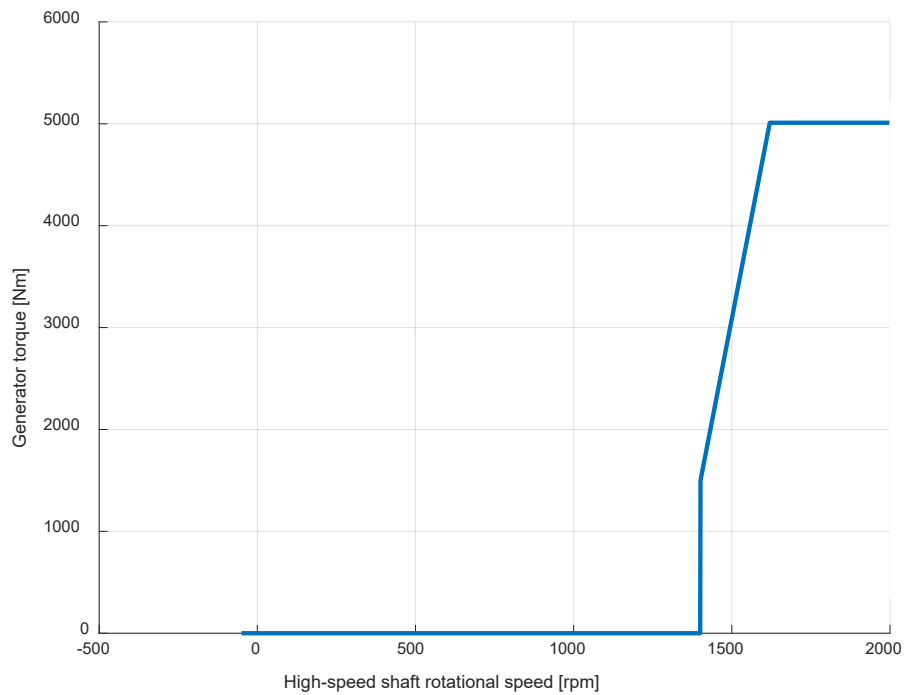
Figure 5.31: Original look-up table.

Figure 5.33 shows the new simulation interface. As there are two look-up tables, depending on the operation mode one or another will be activated. There are two things which characterize and distinguish the stop operation from the other two operations modes: during this period the rotational acceleration (calculated by means of the derivative block) is negative and at the same time the rotational speed falls under a certain value, which in this case was taken as 1000 rpm.

Chair for Wind Power Drives
Univ.-Prof. Dr.-Ing. Georg Jacobs

57

<u>**Implementation**</u> of the new simulated controller (NSC).

The Matlab block (Matlab function- named as F in the blue block in Figure 5.33) will output a positive value, chosen to be 1000 (it does not matter how high this value is, just that is positive) if these conditions are not fulfilled (meaning that we are in start-up or run operation), and will output a negative value, chosen to be -1000 (it does not matter how high this value is, just that is negative), if they are no fulfilled.

A positive output of the Matlab block (Matlab function) will activate the start-up and run operation look-up table, and a negative output will activate the stop operation look-up table (see Figure 5.33).
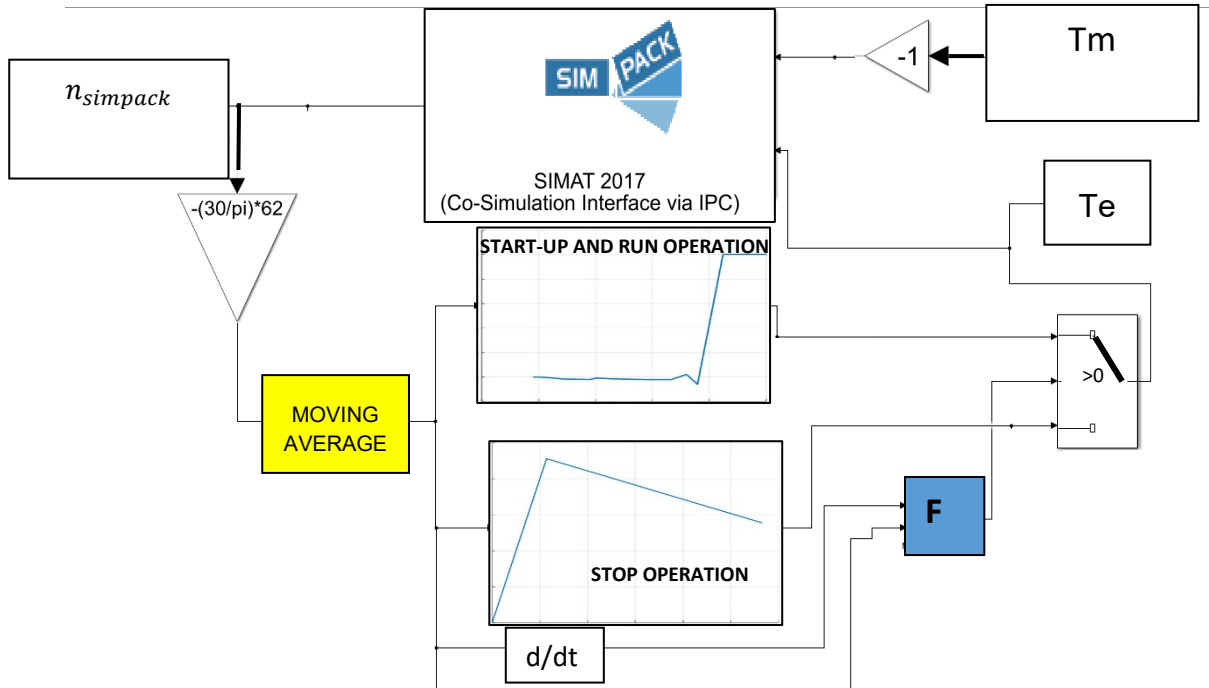
Figure 5.32: New simulation interface with the two look-up tables, the derivative block and the switch.

The results obtained with the simulation in Figure 5.33 are shown in Figure 5.34. It is possible to observe that at the beginning of the run operation, the simulated rotational speed is slightly higher than the measured one, but this is the only way found (and which resulted in better results) to avoid the behavior seen in Figure 5.27 (in which $n_{simpack}$ is under $n_{measures}$ during a greater time in the run operation). Later in the run operation, both signals fit better, as shown in Figure 5.34.

Chair for Wind Power Drives
Univ.-Prof. Dr.-Ing. Georg Jacobs

58
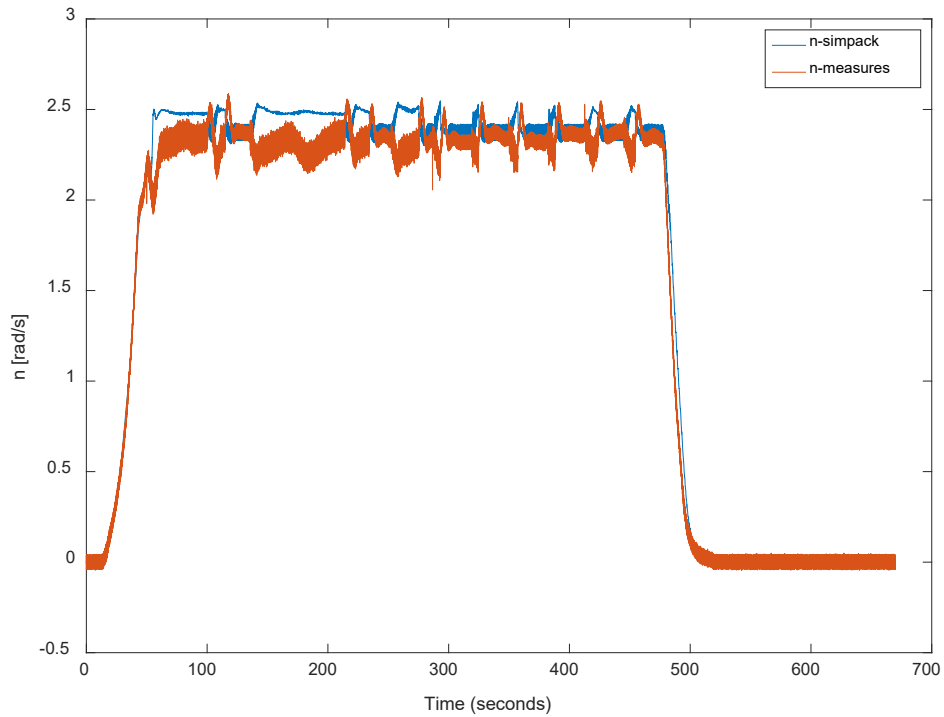
Figure 5.33: Results of the closed-loop simulation with the new strategy with two look-up tables.

A **mean-square root error= 0.0252 rad/s** was estimated, which means that the error was reduced a 26% with respect to the strategy with just one look-up table.

The simulation was run with further measurement data, obtaining also satisfactory results, as show in Figure 5.35.
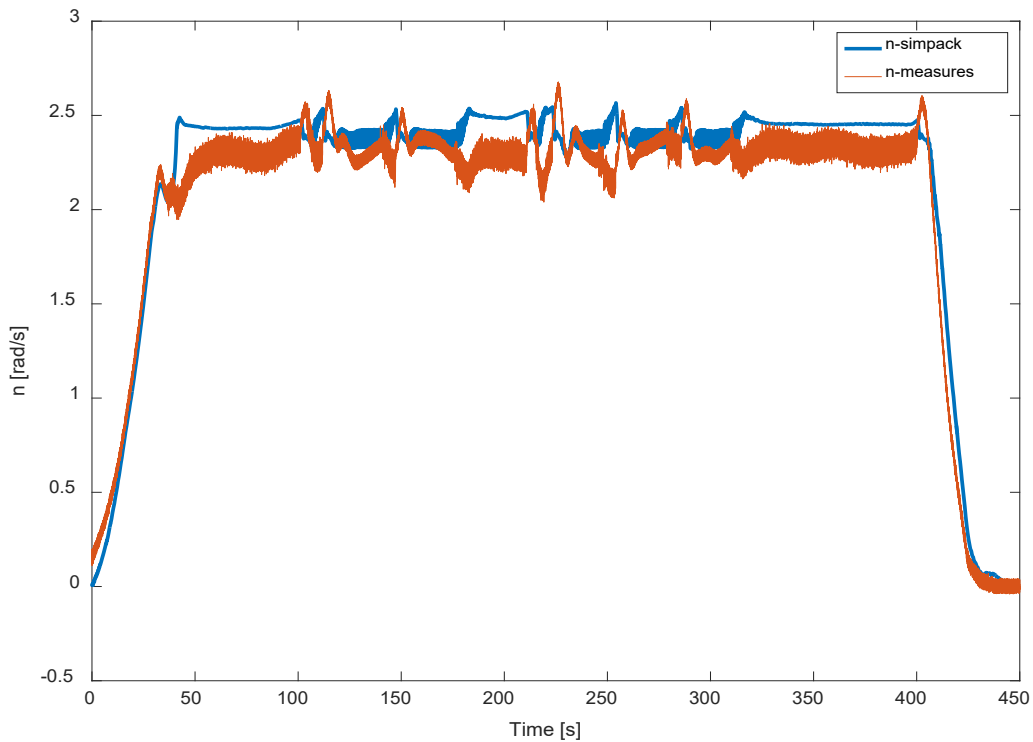
Figure 5.34: Results of the closed-loop simulation with the new strategy with two look-up tables with further measurement data.

Chair for Wind Power Drives
Univ.-Prof. Dr.-Ing. Georg Jacobs

59

<u>**Implementation**</u> of the new simulated controller (NSC).

A **mean-square root error= 0.0270 rad/s** was estimated, which means that the error was reduced a 37.9% with respect to the strategy with just one look-up table. It was concluded then that the use of two look-up tables gives better results than the use of just one.

If we now compare T_e *corrected*, T_e generated by the closed-loop simulation NSC and T_e from the measurement data, we obtain Figure 5.36 and Figure 5.37 respectively.

In Figure 5.36, it is possible to see that T_e *corrected* (see section 5.1) mainly follows T_e generated by the open-loop simulation NSC, excepting the periods in which this last signal is a negative peak and then almost zero. This is the reason why during these periods there is still an error between $n_{measures}$ and $n_{simpack}$.
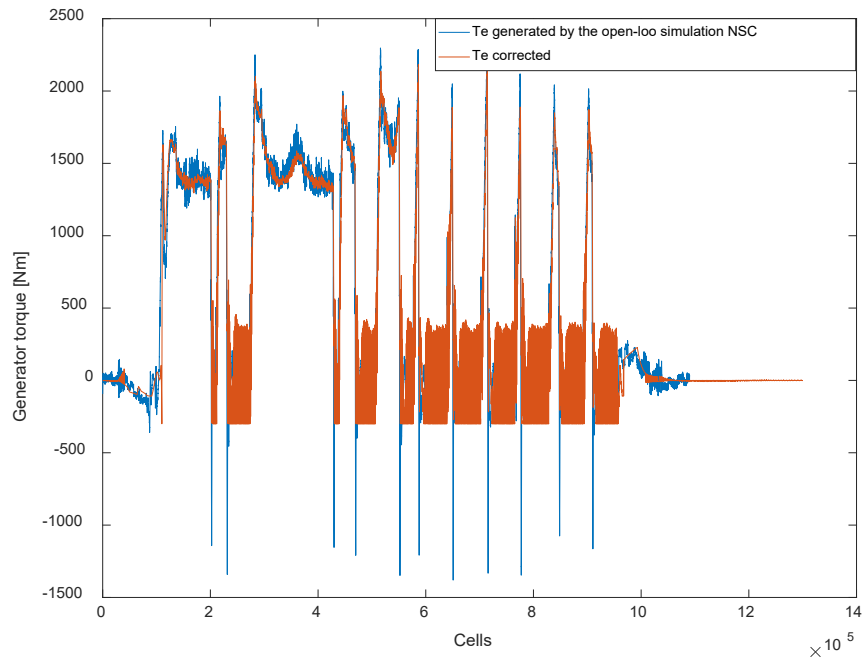
Figure 5.35: Comparison of T_e *corrected* and T_e generated by the closed-loop simulation NSC. The horizontal axis represents the MATLAB-cells in which the data are sampled with a sampling frequency of 2000 Hz.
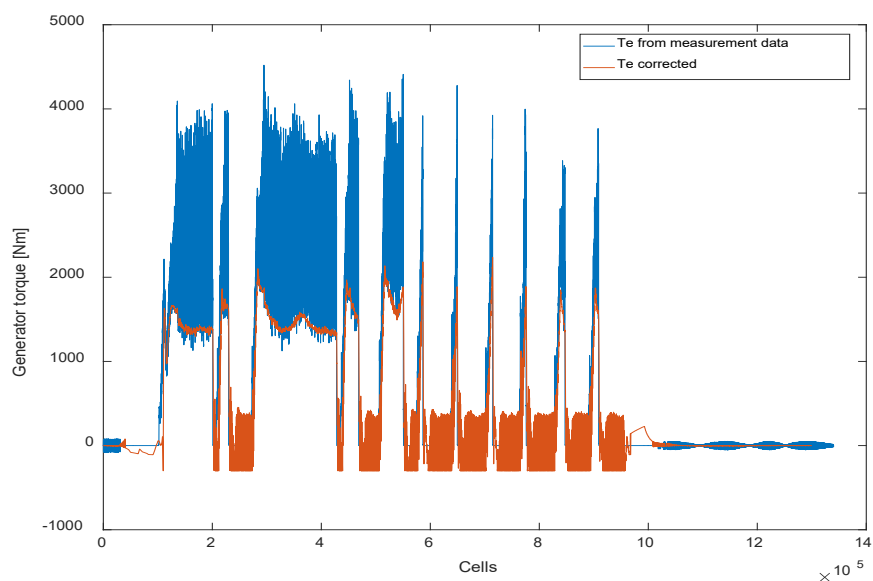
Figure 5.36: Comparison of T_e generated by the closed-loop simulation NSC and T_e from measurement data. The horizontal axis represents the MATLAB-cells in which the data are sampled with a sampling frequency of 2000 Hz.

Chair for Wind Power Drives
Univ.-Prof. Dr.-Ing. Georg Jacobs

60

It is relevant to mention that the behavior of the star-delta switches was not used to develop the closed-loop simulation NSC, as it was planned at the beginning of the thesis (see Chapters 3 and 4), since it was found that it was not necessary to include their behavior.

This last conclusion is confirmed by the fact that, as explained in Appendix 5, during periods of no electrical load in the generator, like start-up and stop operation, the closed-loop simulation NSC actually generates electrical load (T_e *corrected* needed to fit the dynamic of the V52-SM- detailed information in Appendix 5), which does not make sense physically, since both star and delta switches are disconnected and no power production is possible. Therefore, we conclude that the star-delta switch strategy is not relevant for the design of the controller.

Chair for Wind Power Drives
Univ.-Prof. Dr.-Ing. Georg Jacobs

61

6. Sensitivity analysis for the upcoming generator

The objective of this chapter is to determine if the method used to implement the open-loop simulation's NSC is transferable to the upcoming generator on the V52-testbench. The behavior of this new generator will be integrated in the V52-testbench SIMPACK-model by modifying the generator's shaft moment of inertia in the V52-SM.

The purpose of the sensitivity analysis will be to identify which parameters to change when adapting the controller (NSC) to the new generator that CWD will use in the future.

Since the type of generator (3.5 MW and diameter D) is not decided yet by CWD, it is only possible to carry out an estimation of its moment of inertia based on the diameter of the rotor $D = 920\ mm = 0.920\ m$.

The moment of inertia of the rotor will be calculated as if it was a cylinder rotating about its axis, as Equation 6. 3 shows. Considering that the new generator's shaft will have the same length L and material as the current one, the new inertia will be calculated as follows:

$$\rho = \frac{m}{V}\ \left[\frac{kg}{m^3}\right]$$
Equation 6.1

$$V_{existing\ generator} = \pi L \left(\frac{d}{2}\right)^2 [m^3]$$
Equation 6.2

where ρ is density, m is mass, V is the volume, L is the length of the rotor shaft and d is the diameter of the existent generator's rotor.

Considering that,

$$I_{existing\ generator} = 35.7 [\text{kgm}^4];\ L = 1.8\ [\text{m}];\ m_{existing\ generator} = 1250\ [\text{kg}];\ d = 0.34\ [\text{m}].$$

Substituting the values,

$$\rho = \frac{1250}{\pi 1.8 \left(\frac{0.34}{2}\right)^2} = 7648.7381\ \left[\frac{kg}{m^3}\right]$$

$$m_{new\ generator} = \rho V_{new\ generator} = \rho\pi \left(\frac{D}{2}\right)^2 = 7648.7381\pi \left(\frac{0.92}{2}\right)^2 = 5084.58283\ [\text{kg}m^2]$$

The moment of inertia of a cylinder rotating about its axis is:

$$I_{new\ generator} = \frac{1}{2} m_{new\ generator} \left(\frac{D}{2}\right)^2 = \frac{1}{2}\rho V_{new\ generator} \left(\frac{D}{2}\right)^2 = \frac{1}{2}\rho\pi \left(\frac{D}{2}\right)^2 L \left(\frac{D}{2}\right)^2 = \frac{1}{32}\rho\pi L D^4$$

Equation 6.3

Substituting the values,

$$I_{new\ generator} = \frac{1}{32} 7648.7381\pi\ 1.8\ 0.92^4 = 968.308\ [\text{kg}m^2]$$

Chair for Wind Power Drives
Univ.-Prof. Dr.-Ing. Georg Jacobs

62

The non-controlled response when inputting both T_m and T_e from the measurement data is the following (see Figure 6.1):
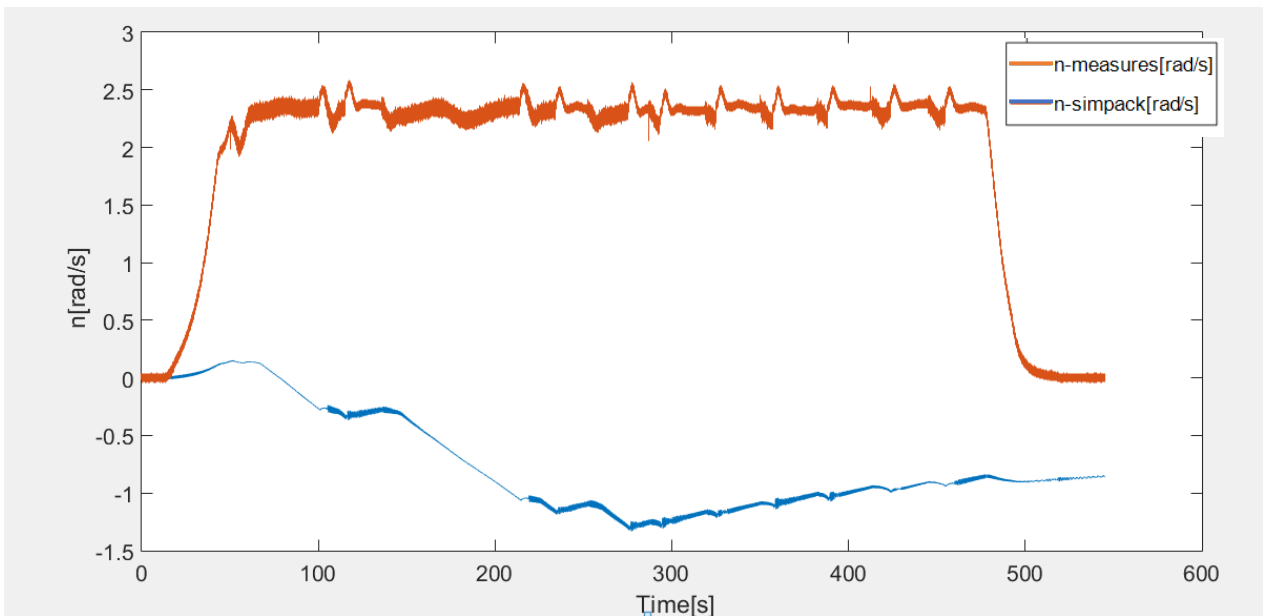
Figure 6.1: Results of co-simulation with the new generator with the measurement data.

The increase of the inertia of the generator has notably reduced the acceleration of the rotor in the V52-SM (in accordance with the inverse proportionality predicted by Equation 4.1), and therefore the rotational speed decreases with respect to the existent generator as well, as seen in Figure 6.2.
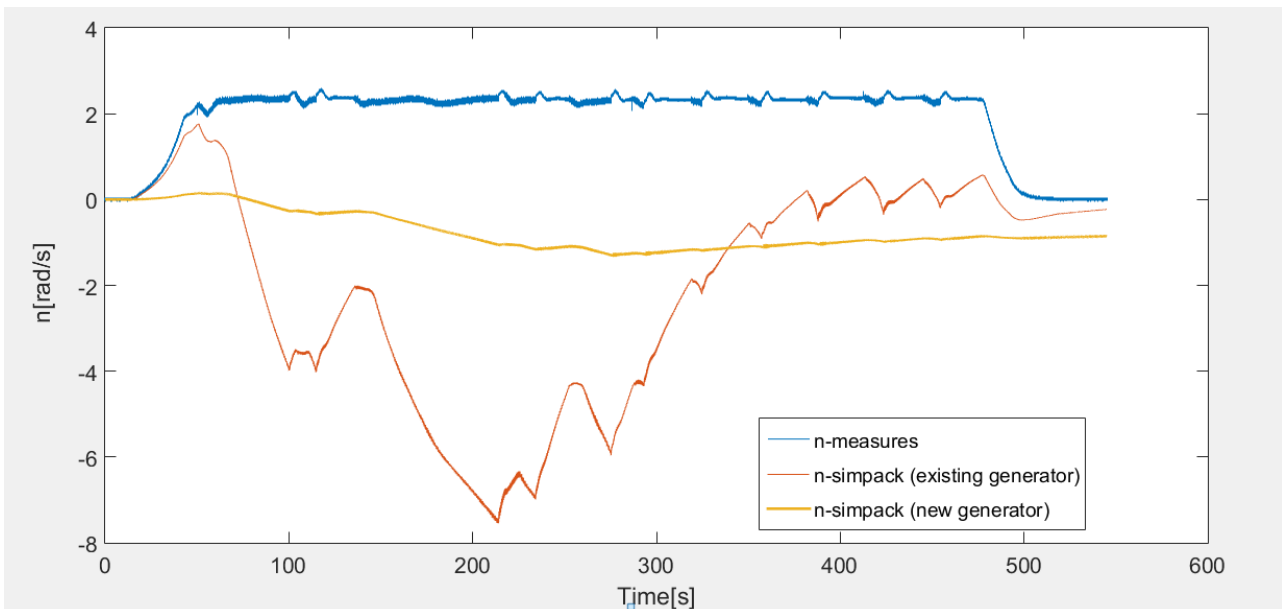
Figure 6.2: Comparison of the results of co-simulation with the measurement data obtained with the existent and the new generator.

Chair for Wind Power Drives
Univ.-Prof. Dr.-Ing. Georg Jacobs

63

The same steps followed to develop the open-loop NSC in Chapter 5 were entirely reproduced by changing the SSM that describes the existent generator for the SSM that describes the new generator. Following the same procedure as the one mentioned in Chapter 5, the open-loop NSC for the new generator was created and simulated, as the figures Figure 5.9 to Figure 5.12 show for the existent generator. The equivalent to Figure 5.9 and Figure 5.14 for the new generator is seen in Figure 6.3 and Figure 6.4 respectively (Figure 6.3 represents a comparison of the SSM output and the simulated rotational speed and Figure 6.4 represents the model output and the tuned response and tuned PID parameters).
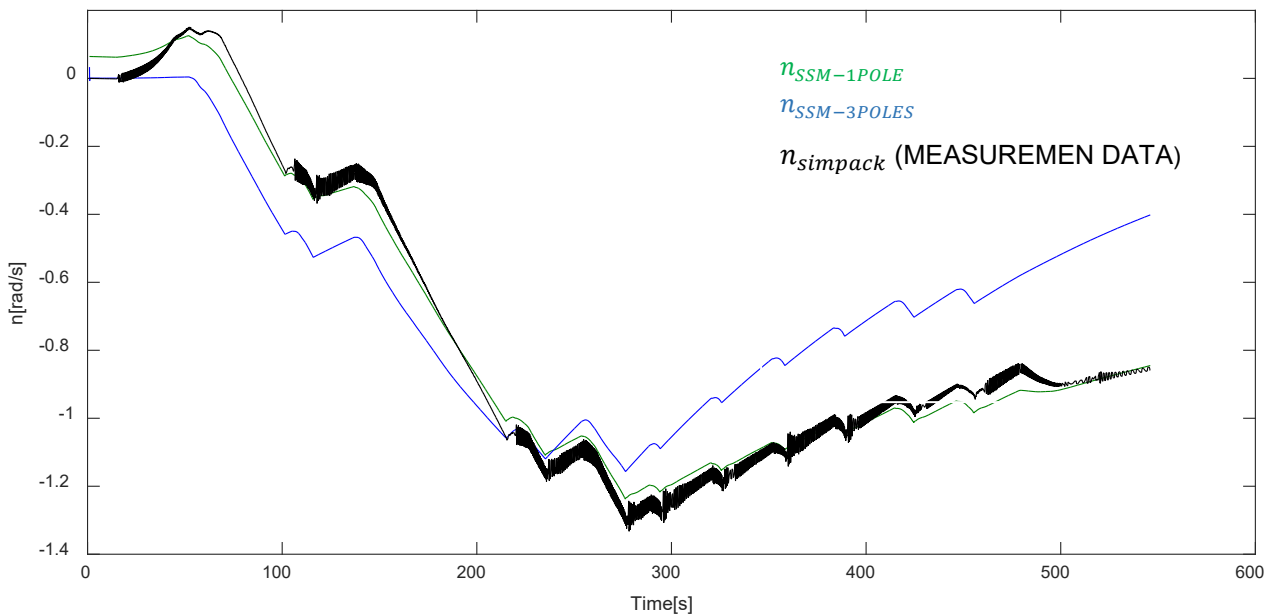
Figure 6.3: Designed continuous SSM response to measurement data (green and blue curves respectively).

Controller Parameters

	Tuned	Block
P	2004453.9489	2004453.9489
I	7080942.1584	7080942.1584
D	19033.427	19033.427
N	72.9365	72.9365

Performance and Robustness

	Tuned	Block
Rise time	0.0906 seconds	0.0906 seconds
Settling time	0.694 seconds	0.694 seconds
Overshoot	10.2 %	10.2 %
Peak	1.1	1.1
Gain margin	Inf dB @ NaN rad/s	Inf dB @ NaN rad/s
Phase margin	90 deg @ 20 rad/s	90 deg @ 20 rad/s
Closed-loop stability	Stable	Stable

Figure 6.4: Tuned step response parameters and tuned PID parameters.

Chair for Wind Power Drives
Univ.-Prof. Dr.-Ing. Georg Jacobs

64

However, since we get a worse *fit-value* between the SSM output and the measurement data (approximately 71%), this means that the SSM does not reproduce exactly the new generator's dynamic. Because of that, the simulations did not give satisfactory results (see Figure 6.5).

In Figure 6.5, the obtained rotational speed $n_{simpack}$ is very high in comparison with the measured one. That happens because the designed SSM for the new generator doesn't describe exactly the dynamic of the V52-SM, but only approximately. Another reason for this deviation in the rotational speed could be that the measurement data used to create the new state-space model corresponds to the existent generator, and not to the new one. During the thesis, it is supposed that the Simpack model is an LTI System (linear-time-invariant system), which means that the internal dynamic of the system (the differential equations that describe the model) does not depend on the inputs or the history of the system. Because of that, using the measurement data from the existent generator as input should determine the global dynamic of the new state-space model for the new generator. Furthermore, we do not have any measurement data from the new generator.
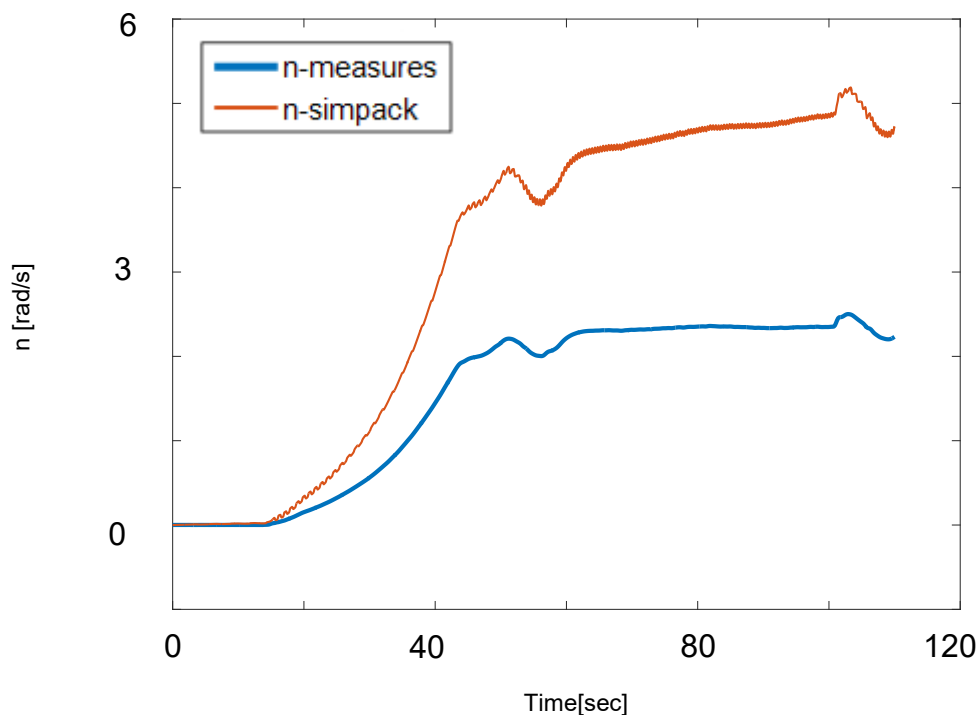
Figure 6.5:   Comparison of n-simpack and n-measures for the new generator's open-loop control strategy simulation with the modified NSC.

A sensitivity analysis was done to determine the value of the gain block situated before the feedback-loop (see Figure 5.7–Open loop-block after the input $n_{simpack}$) which better fits $n_{simpack}$ with $n_{measures}$. Gain values between 1/1.9 and 1/2.5 (Figure 6.6 and Figure 6.7 respectively) were tested (this range was determined after several simulations with different gain values), concluding finally that the value of 1/1.75 best fits the measurements. Despite this sensitivity analysis, the tendency of $n_{simpack}$ to grow higher during the run operation was not corrected.

Chair for Wind Power Drives
Univ.-Prof. Dr.-Ing. Georg Jacobs

65

If we now calculate the mean square root error for the results in Figure 6.6 we obtain an error of **0.7290 rad/s**, which is very big in comparison with the errors calculated in Chapter 5.
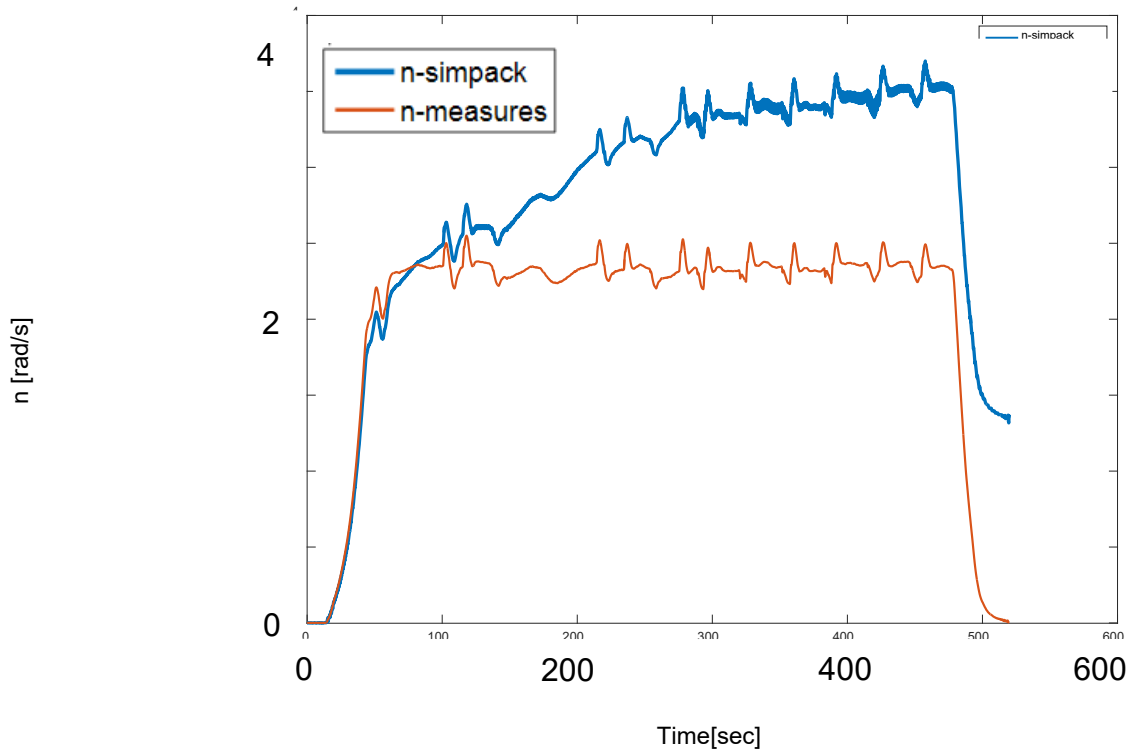
Figure 6.6: Open-loop behavior for the new generator's control strategy simulation with the modified NSC and a modified reference gain value of 1/1.9.
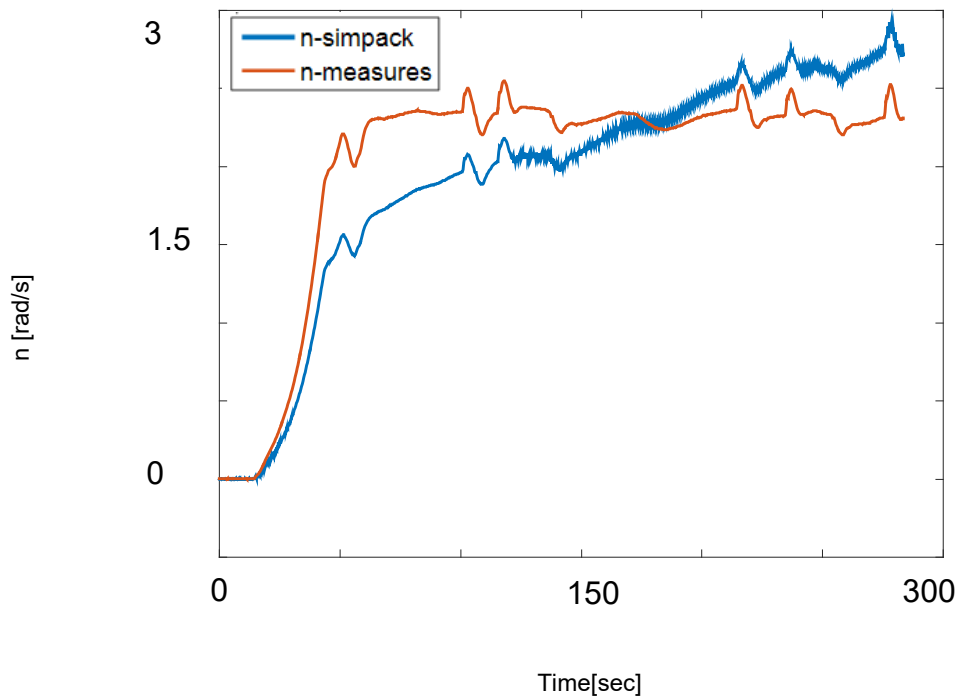
Figure 6.7: Open-loop behavior for the new generator's control strategy simulation with the modified NSC and a modified reference gain value of 1/2.5.

Chair for Wind Power Drives
Univ.-Prof. Dr.-Ing. Georg Jacobs

66

The rotational speed fits the measurement data at the beginning, when the measured rotational speed is zero, but then it goes very high upon it. For that reason, it is necessary to develop a strategy that can correct this error.

This strategy will be the following: a global state-space model (GSSM) of the open-loop simulation will be created. The GGSM will get T_m and $n_{measures}$ as input and will output the rotational speed $n_{simpack}$. The GSSM matrices and its response are shown in Figure 6.8 and Figure 6.9.

Then, as proceeded in Chapter 5, a PID Controller will be tuned with the control loop shown in Figure 6. 11 to produce the desired rotational speed reference $n_{measures}$ (see Figure 6.10). The obtained PID action will be then the new reference for the modified NSC.

```
ss_additional =
  Continuous-time identified state-space model:
      dx/dt = A x(t) + B u(t) + K e(t)
       y(t) = C x(t) + D u(t) + e(t)

  A =
                x1          x2          x3
    x1  -0.0004808     -0.3166   0.0004355
    x2      0.3073   -0.008766      -23.76
    x3    -0.06039       22.56      -59.65

  B =
               u1          u2
    x1  1.464e-07       0.142
    x2  2.828e-05        23.1
    x3  6.051e-05       47.84

  C =
                x1          x2          x3
    y1         405.7    -0.02189   0.0003239

  D =
          u1   u2
    y1     0    0

  K =
               y1
    x1     3.643
    x2     -1195
    x3      2511
```

Figure 6.8:   GSSM state matrixes.

Chair for Wind Power Drives
Univ.-Prof. Dr.-Ing. Georg Jacobs

67
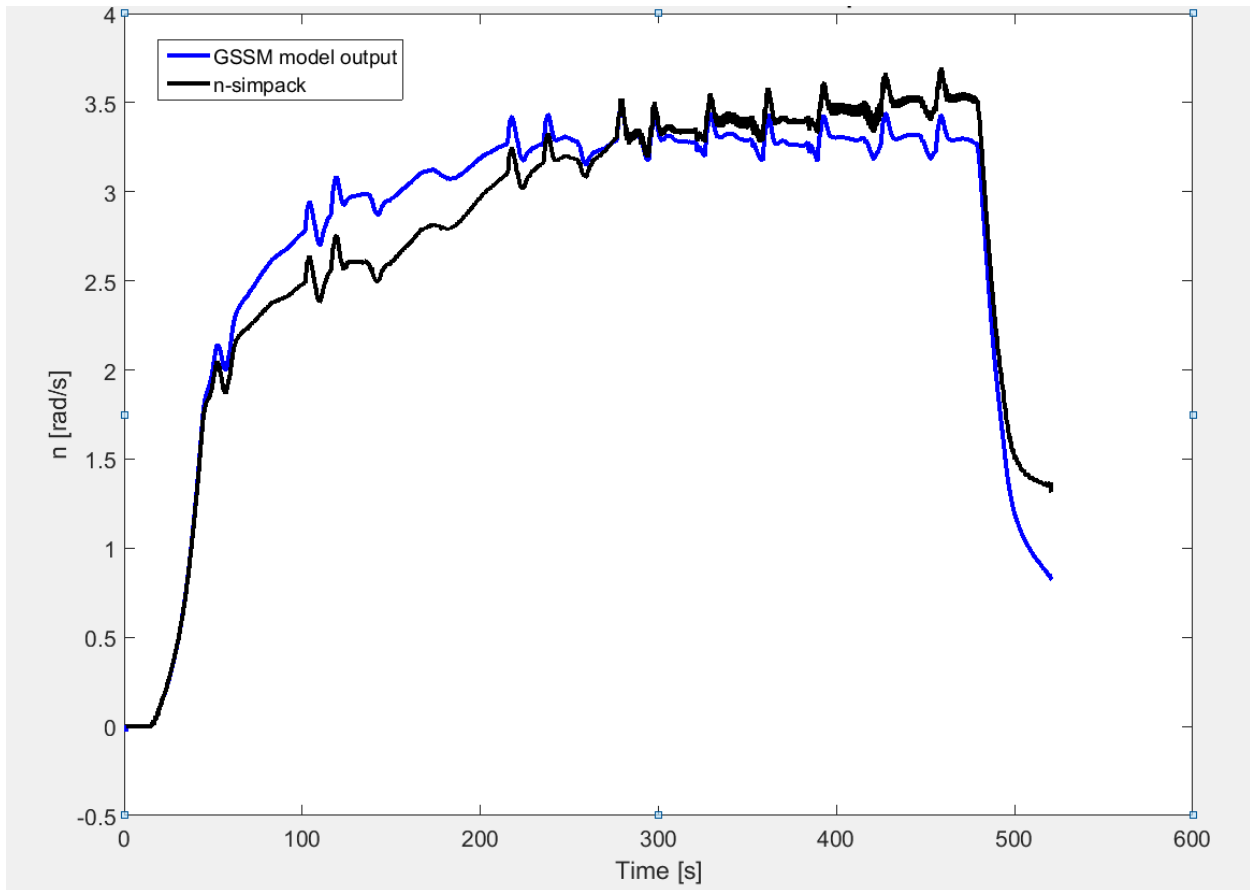
Figure 6.9:   Comparison between GSSM and real simulation outputs.

Controller Parameters

	Tuned	Block
P	11.6877	11.6877
I	2139.4635	2139.4635
D	0.0033595	0.0033595
N	1927.0792	1927.0792

Performance and Robustness

	Tuned	Block
Rise time	0.00259 seconds	0.00259 seconds
Settling time	0.0152 seconds	0.0152 seconds
Overshoot	8.31 %	8.31 %
Peak	1.08	1.08
Gain margin	Inf dB @ NaN rad/s	Inf dB @ NaN rad/s
Phase margin	90 deg @ 712 rad/s	90 deg @ 712 rad/s
Closed-loop stability	Stable	Stable

Figure 6.10: Adjusted PID parameters.
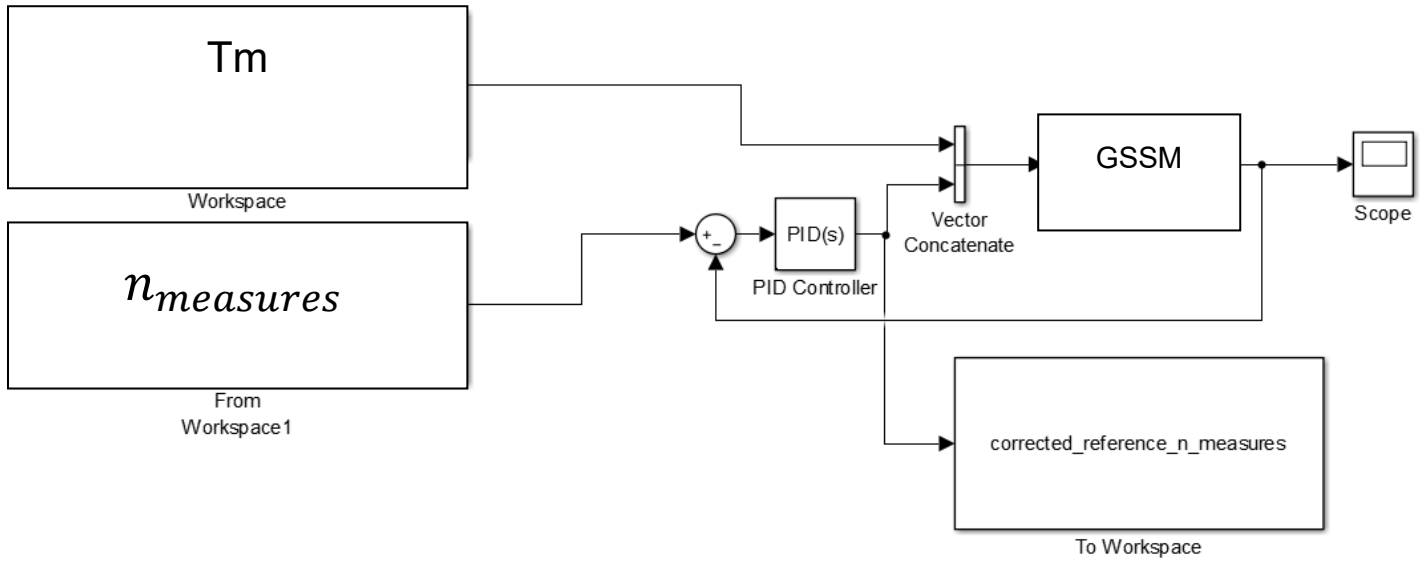
Figure 6.11: PID tuning scheme.

The ´´corrected reference $n_{measures}$ ´´ (see Figure 6. 11 and Figure 6.12) is the signal that, when inputted in the open-loop simulation, will produce the desired signal $n_{measures}$ as output.
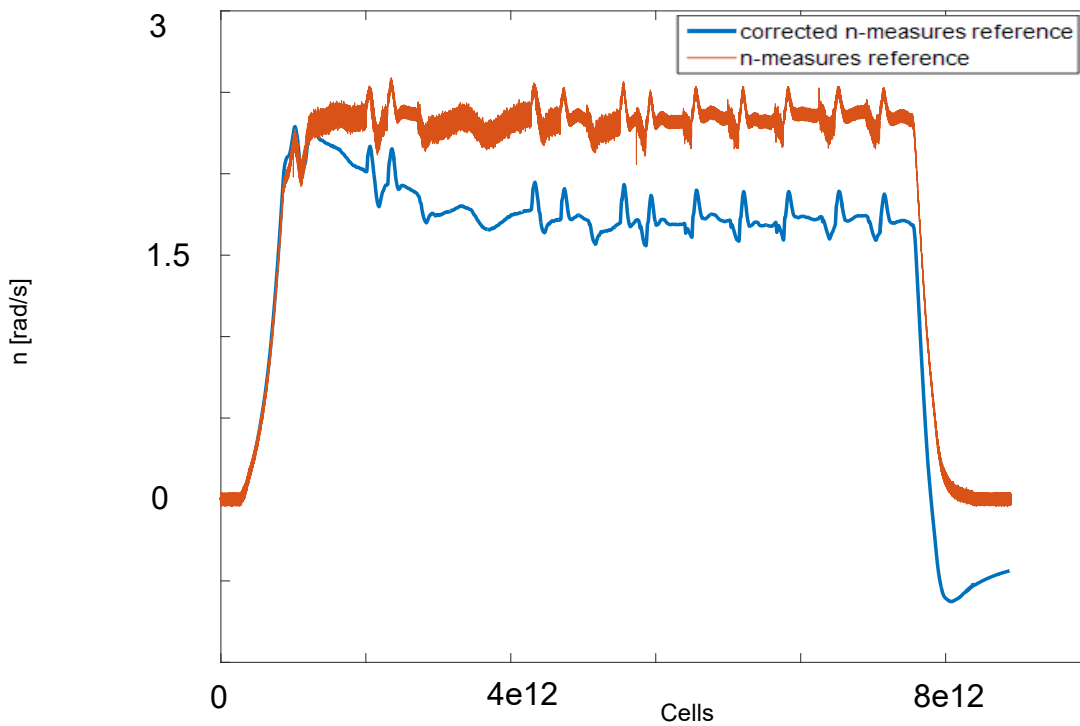
Figure 6.12: Corrected reference $n_{measures}$ (PID action) in comparison with the reference from measurement data. The horizontal axis represents the MATLAB-cells in which the data are sampled with a sampling frequency of 2000 Hz.

Chair for Wind Power Drives
Univ.-Prof. Dr.-Ing. Georg Jacobs

69

When inputting the signal ´´corrected reference $n_{measures}$´´ as reference, we obtain the rotational speed shown in Figure 6.13.

Looking at Figure 6.13, it is clear that $n_{simpack}$ follows the reference just at the beginning. In a certain point, it grows higher, but the behavior has improved significantly if we compare it with the one in Figure 6.6.
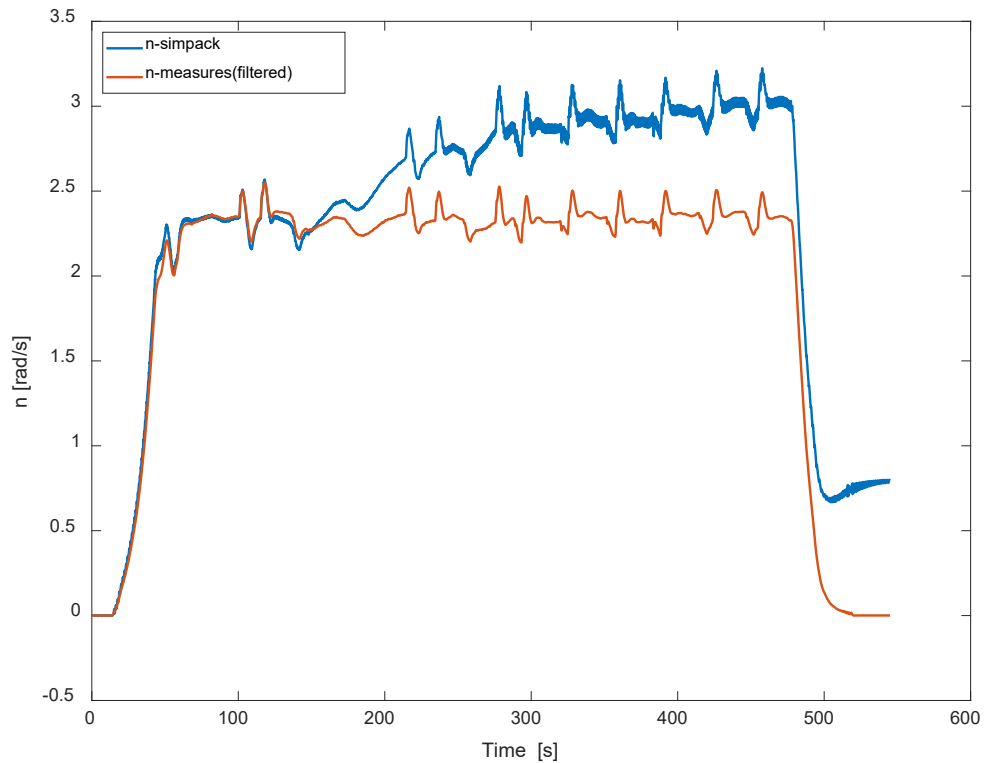
Figure 6.13: Results of the open-loop simulation for the new generator with the corrected reference $n_{measures}$ for a gain of 1/1.75.

The results in Figure 6.14 were obtained for further measurement data. There is still a tendency of $n_{simpack}$ to grow higher than $n_{measures}$.

Chair for Wind Power Drives
Univ.-Prof. Dr.-Ing. Georg Jacobs

70
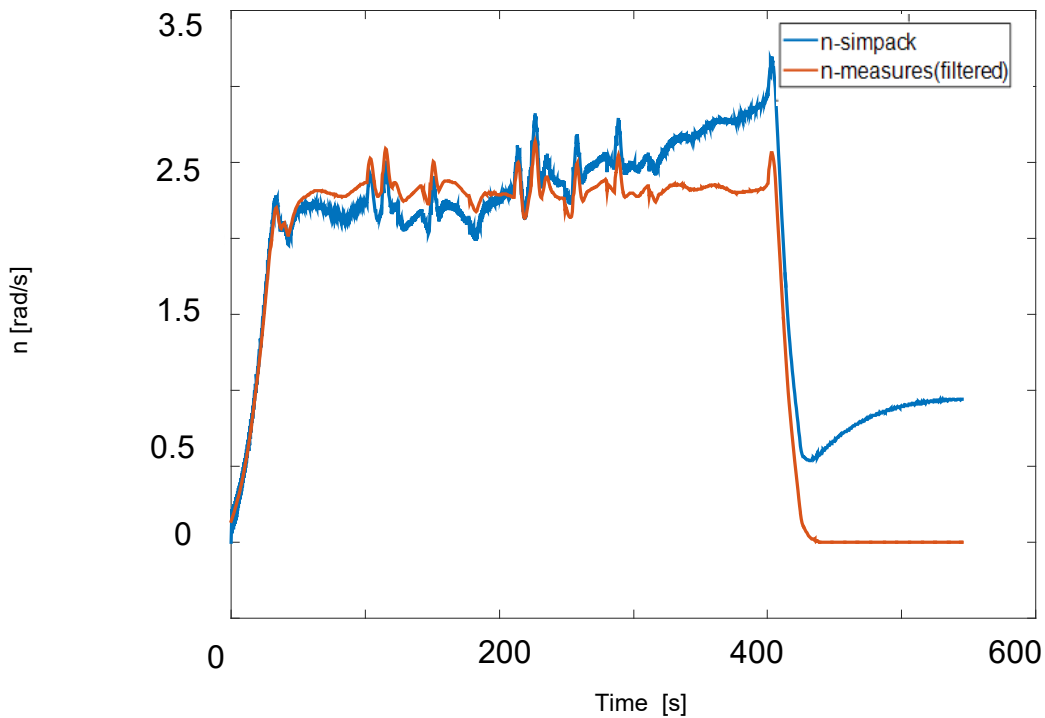
Figure 6.14: Results for further measurement data with the corrected reference $n_{measures}$ for a gain of 1/1.75.

To further improve the results, the same process explained in Figure 6. 11 was followed once again, but this time the reference signal used to tune the PID will be the corrected reference $n_{measures}$ and not $n_{measures}$ (see Figure 6.15). If we now use the *new corrected reference* $n_{measures}$ (new PID action obtained when inputting the corrected reference $n_{measures}$ as reference signal for the control loop in Figure 6.11) as the reference for the open-loop simulation the results are better (see Figure 6.16).
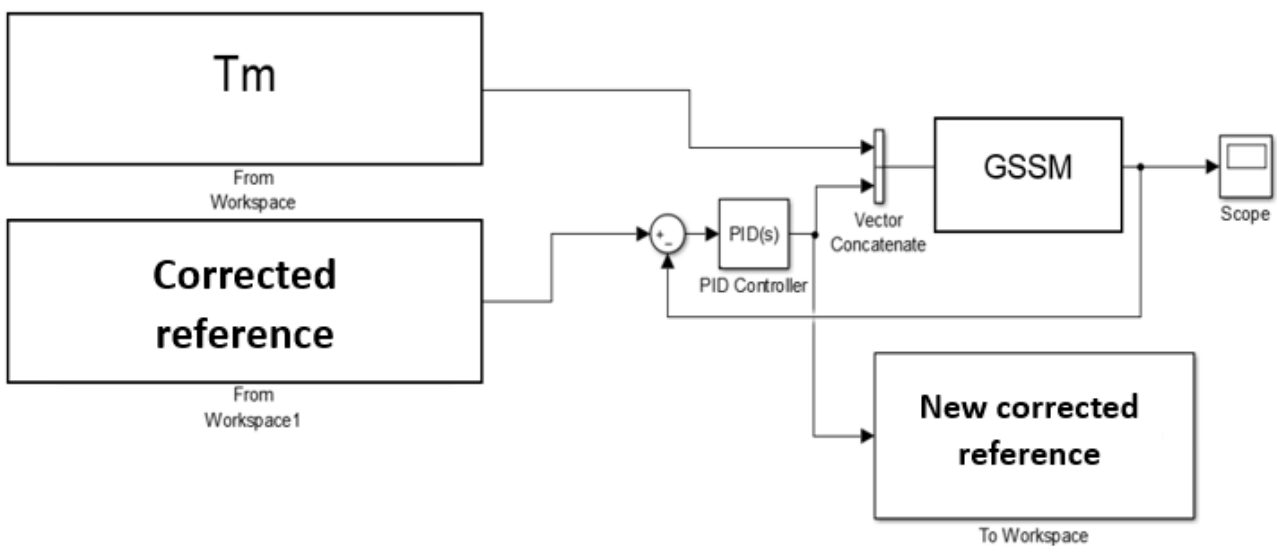
Figure 6.15: PID tuning scheme with the corrected reference as reference.

Chair for Wind Power Drives
Univ.-Prof. Dr.-Ing. Georg Jacobs

71
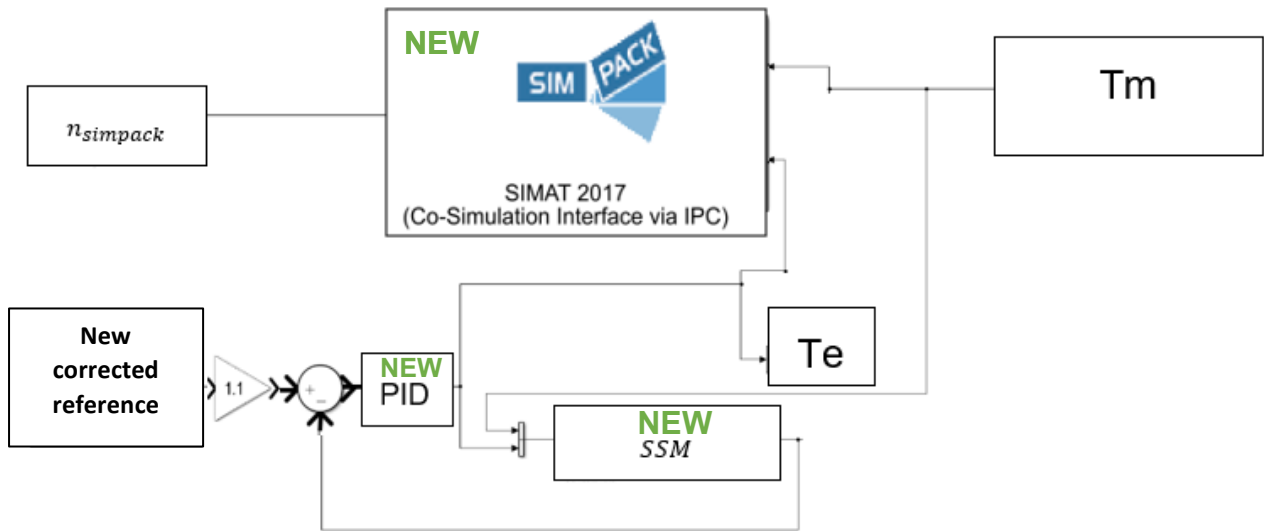
Figure 6.16: Open-loop simulation with the new corrected reference as reference.
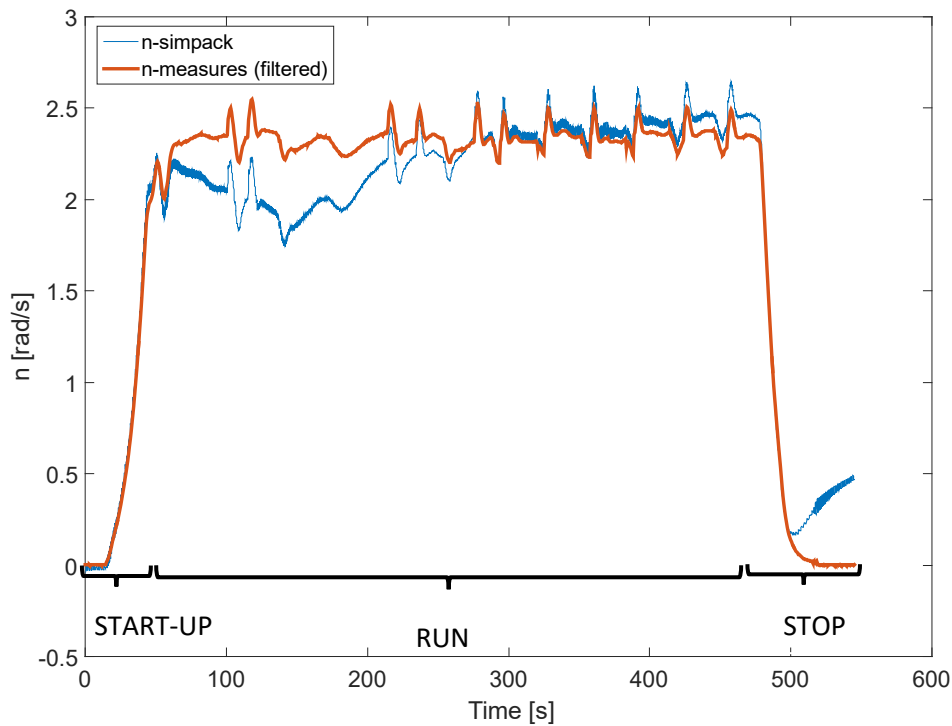
Figure 6.17: Results with the *new corrected reference* $n_{measures}$ for a gain of 1/1.75.

The results in Figure 6.17 are now better than in Figure 6.6 (a **mean-square root error of 0.048 rad/s** is estimated), which is a **93.4%** lower than the calculated for the results in Figure 6.6). Nevertheless, there is a higher error at the beginning of the run operation and after the stop operation. The error after the stop operation points out that the simulated rotational speed will keep growing higher than the measured one after the stop operation (see Figure 6.17). The fact that this error between $n_{simpack}$ and $n_{measures}$ exists is not relevant in this case, because we are more interested in estimating the dynamic of the generator torque in a global way during the test, and not after it.

Chair for Wind Power Drives
Univ.-Prof. Dr.-Ing. Georg Jacobs

72

Once the simulation is relatively successful, it is relevant to look at the difference between the corrected generator torques produced by the existent and upcoming generator, so that it is possible to analyze which is the effect of an increase of the inertia (new inertia for the new generator). Figure 6.18 shows that the torque in the new generator is much higher than the torque in the existent generator during start-up and stop (around 50 times higher) and some periods of the run operation (see Figure 6.18), where we don't see any relevant proportionality between both signals. It is then concluded that an increase of the inertia provokes also an increase of the torque in the generator in the V52-SM during the start-up and stop operation and some periods of the run operation.
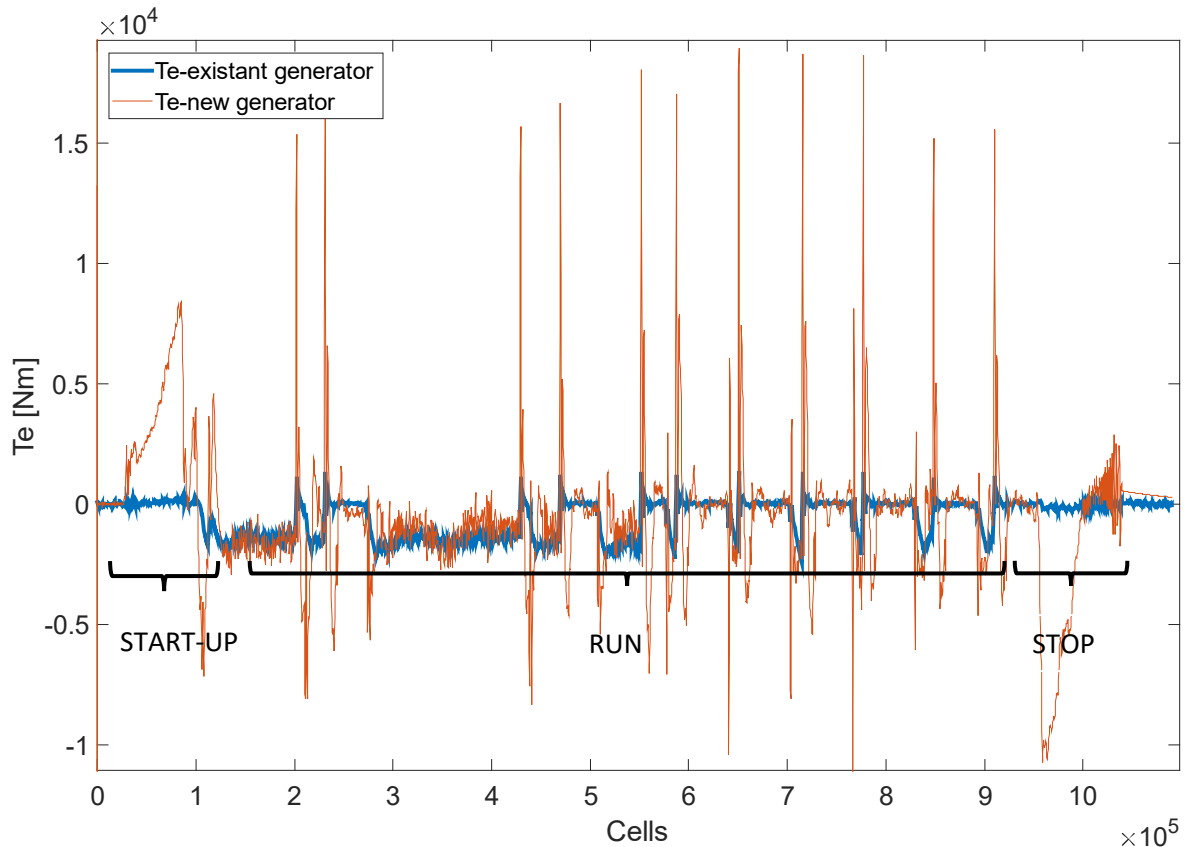
Figure 6.18: Comparison between the T_e signal obtained with the existent and the upcoming generator. The horizontal axis represents the MATLAB-cells in which the data are sampled with a sampling frequency of 2000 Hz.

The new generator was not tested in closed-loop because we simply don't have any measurement data of the rotational speed available yet, so there is still no way to compare the real data with the results from a closed-loop simulation (we do not know which rotational speed is produced by a rotor torque input T_m).

Chair for Wind Power Drives
Univ.-Prof. Dr.-Ing. Georg Jacobs

73

7. Development of a control strategy for the step and ramp reference ECS-input signal.

The objective of this chapter is mainly to introduce desired control signals like a step or a ramp (instead of the rotational speed measurement data) as the reference for the new simulated controller (NSC) and analyze the V52-SM output rotational speed ($n_{measures}$).

As input for the torque in the main shaft, the value of *100 kNm* was chosen, because in the measurement data this torque varies in a range of *0-200 kNm* approximately and stays constant during many periods in a range of *100-200 kNm*. The simulation interface is shown in Figure 7.1. The yellow block corresponds to a *Signal builder* block, used to generate the reference signals.
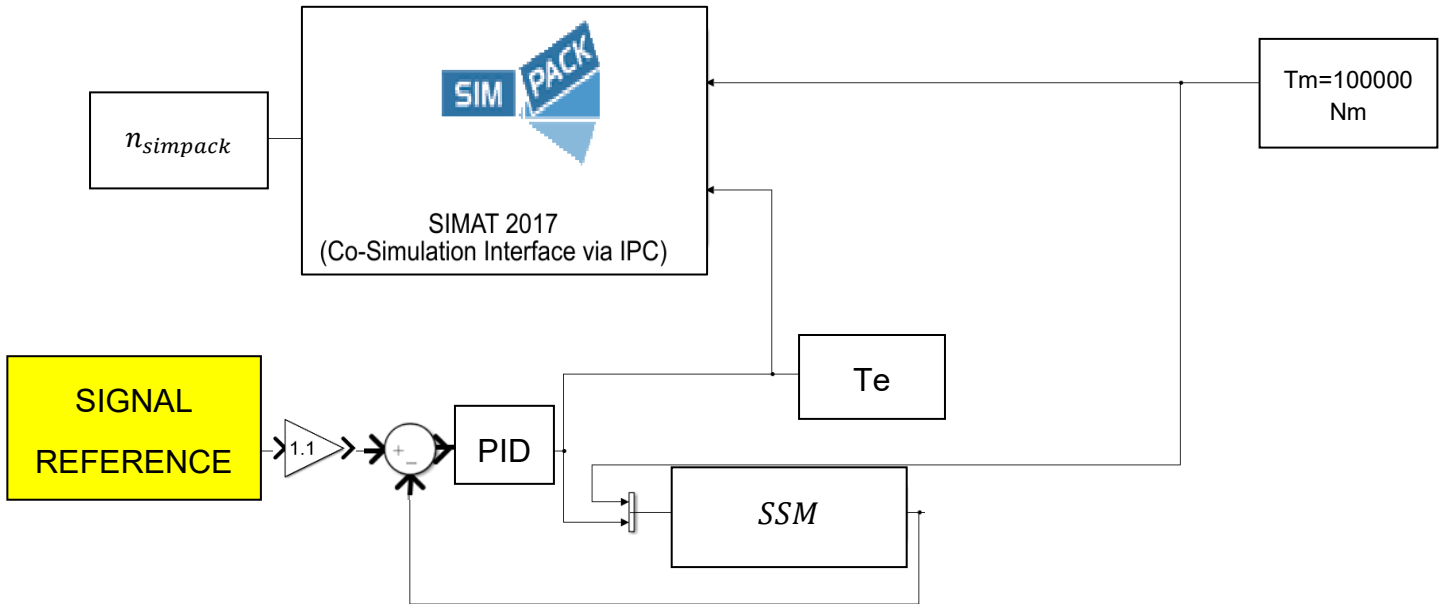
Figure 7.1:   Open-loop simulation with a reference input signal.

When inputting a ramp signal that reaches 2.5 rad/s at the time of 50 sec. and then stays constant (as shown in the red curve in Figure 7.2) we obtain:
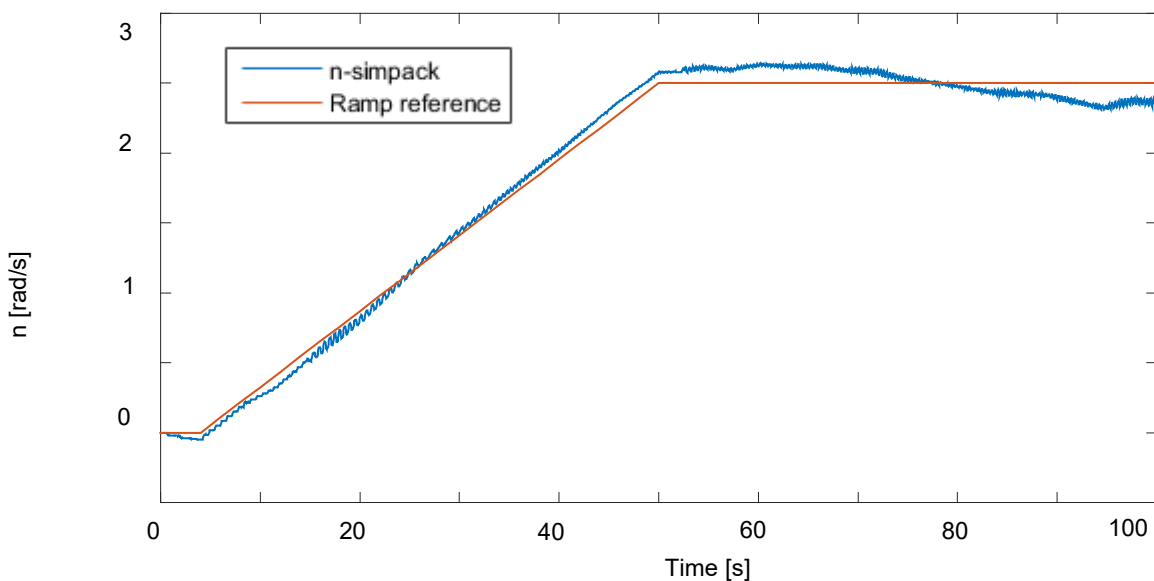
Figure 7.2:   Ramp reference and response of the V52-SM with NSC.

Chair for Wind Power Drives
Univ.-Prof. Dr.-Ing. Georg Jacobs

74

The mean-square root error between reference and output is **0.0075 rad/s.**

The same process was done with a step input of 2.5 rad/s, obtaining in this case an overshooting of almost 100%:
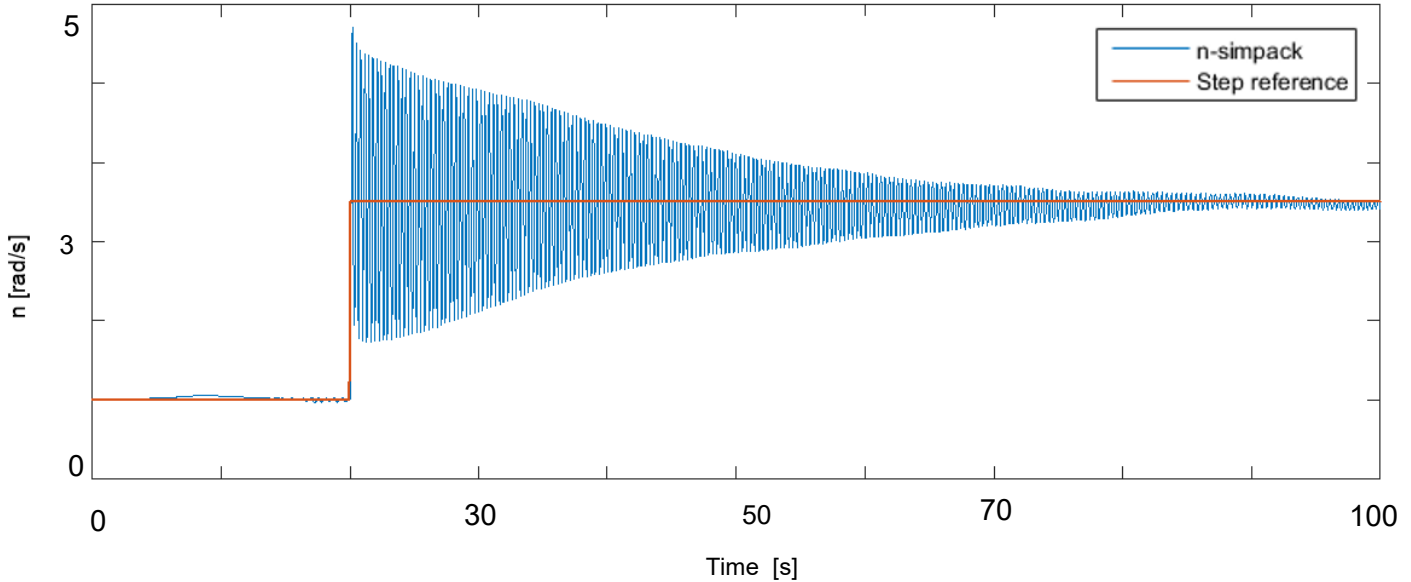
Figure 7.3:   Step reference and response of V52-SM with NSC.

To correct this overshooting the following method will be followed: a global state-space model (GSSM) of the whole NSC together with the V52-SM was created through the *Application Toolbox System Identification* of Matlab. Then, this model will be integrated in a control feedback loop containing another PID controller designed for this GSSM.This GSSM produces the following response (see Figure 7.5) and has the following characteristics (see Figure 7.4):

```
Continuous-time identified state-space model:
    dx/dt = A x(t) + B u(t) + K e(t)                      D =
     y(t) = C x(t) + D u(t) + e(t)
                                                               u1   u2
                                                          y1    0    0
  A =
             x1         x2         x3         x4          K =
    x1    -0.1246     -20.58    0.001774   -0.03065
    x2     20.58    -0.007397     61.01    -0.04668                 y1
    x3    0.06635     -60.95     -0.3659     165.2         x1      6.134
    x4    0.08146     -0.1575    -163.6     -1.061         x2     -414.2
                                                          x3      -2683
  B =                                                      x4      -3899
               u1         u2
    x1     5.45e-05  -0.0003502
    x2    -2.776e-05   -0.01969
    x3    0.0005575      0.1443
    x4    0.0002128     -0.197


  C =
             x1         x2         x3         x4
    y1     224.3      -1.15    -0.03101   -0.002665
```

Figure 7.4:   GSSM characteristics.

Chair for Wind Power Drives
Univ.-Prof. Dr.-Ing. Georg Jacobs

75
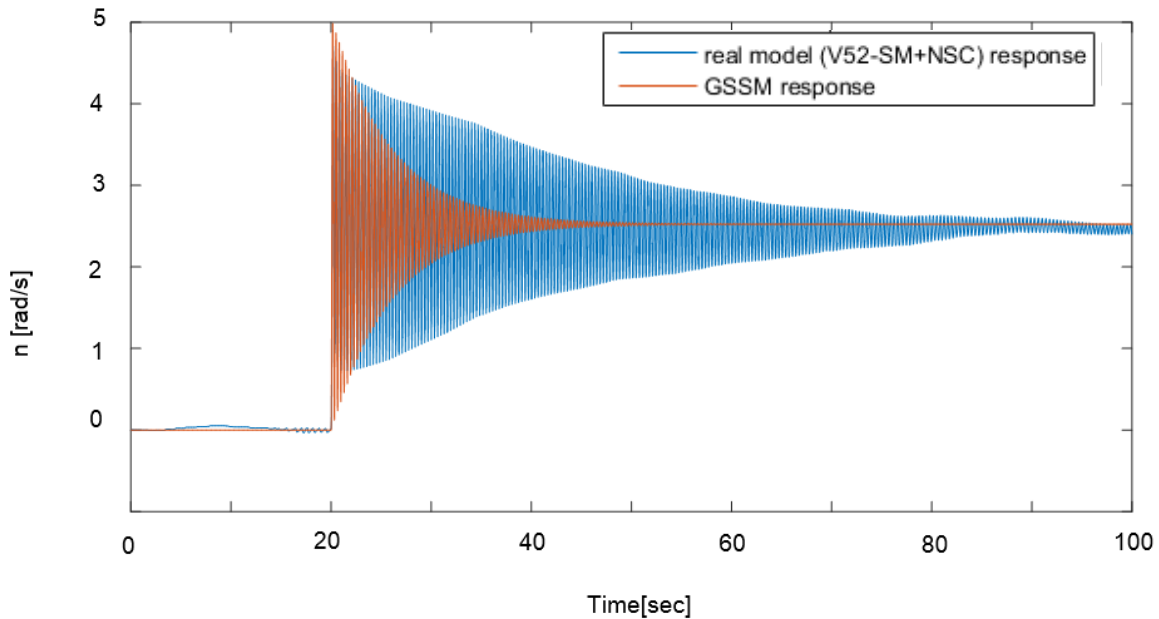
Figure 7.5:   GSSM step response and comparison with the real simulated response.

Once the GSSM is created, the parameters of the PID controller in the control feedback loop will be determined. The *Application Toolbox PID Tuning* will be used to tune a PID controller according to the dynamics determined by the GSSM.

When tuning the PID, it is determined that for response times lower than tr=11.7 sec. the step response becomes very oscillating and even unstable. For that reason, this minimum stable response time of tr=11.7 sec. was selected. In Figure 7.6 the PID parameters are shown. It is relevant to see that the PID doesn't have any derivative part. Therefore, from now on it will be called **PI**.

Controller Parameters

	Tuned	Block
P	0	0
I	0.18759	0.18759
D	0	0
N	100	100

Performance and Robustness

	Tuned	Block
Rise time	11.7 seconds	11.7 seconds
Settling time	20.9 seconds	20.9 seconds
Overshoot	0.0212 %	0.0212 %
Peak	1	1
Gain margin	4.82 dB @ 19.3 rad/s	4.82 dB @ 19.3 rad/s
Phase margin	90 deg @ 0.189 rad/s	90 deg @ 0.189 rad/s
Closed-loop stability	Stable	Stable

Figure 7.6:   Tuned PI parameters.

Chair for Wind Power Drives
Univ.-Prof. Dr.-Ing. Georg Jacobs

76

Figure 7.7 and Figure 7.8 show the whole simulation scheme. In Figure 7.7, the GSSM was represented by its state equations, while in Figure 7.8 this block contains the name of the open-loop simulation, which is what the GSSM is substituting.
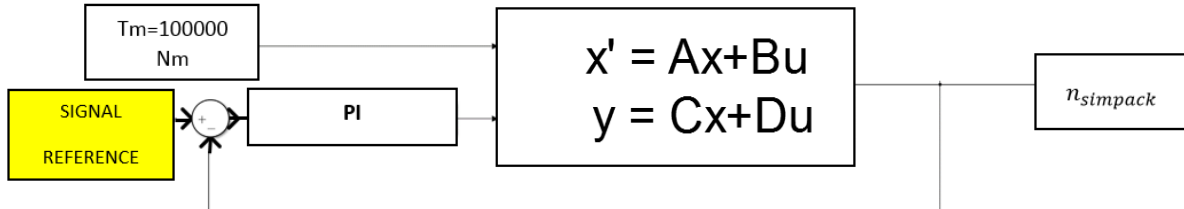
Figure 7.7:   Designed control feedback loop with the GSSM.
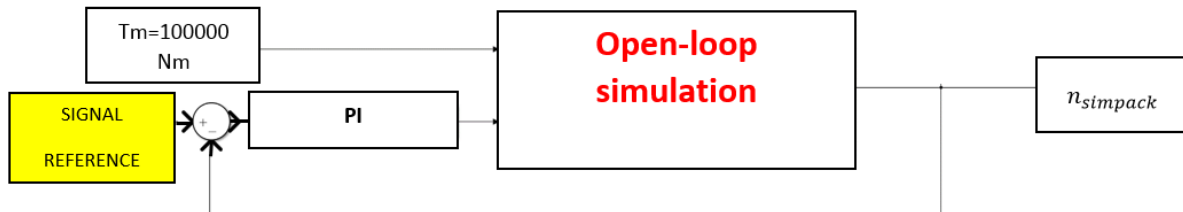
Figure 7.8:   Designed control feedback loop with the NSC+V52-SM as the ''plant'' (GSSM).

The results of the simulation are shown in Figure 7.9:
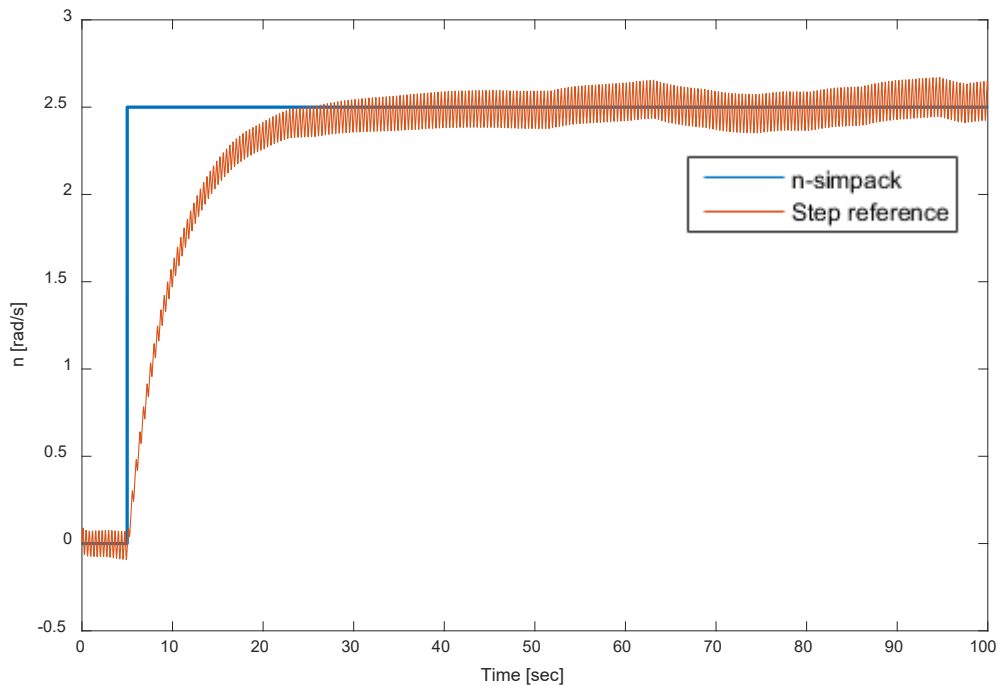
Figure 7.9:   Comparison of the simulated rotational speed with the step, obtained in the simulation in Figure 7.8.

Chair for Wind Power Drives
Univ.-Prof. Dr.-Ing. Georg Jacobs

77

We obtain no overshooting in the response and a response time of tr=20 sec, although the controller was designed for a tr=11.7, since the GSSM doesn't reproduce exactly the dynamic of the real model.

Furthermore, the possibility to reduce the high-frequency oscillation of the output rotational speed is investigated. For that, a low-pass filter (pass-band frequency= 1Hz, stop-band frequency=2Hz) was added after the PI controller, meaning that the controller action (generator torque) is filtered. The new control loop and response are shown in Figure 7.10 and Figure 7.11 .
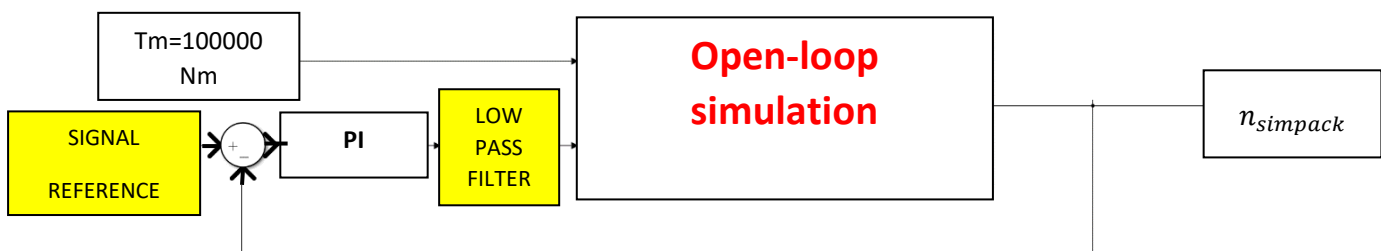
Figure 7.10: Designed control feedback loop with the NSC and V52-SM as the ''plant'', and the low-pass filter.
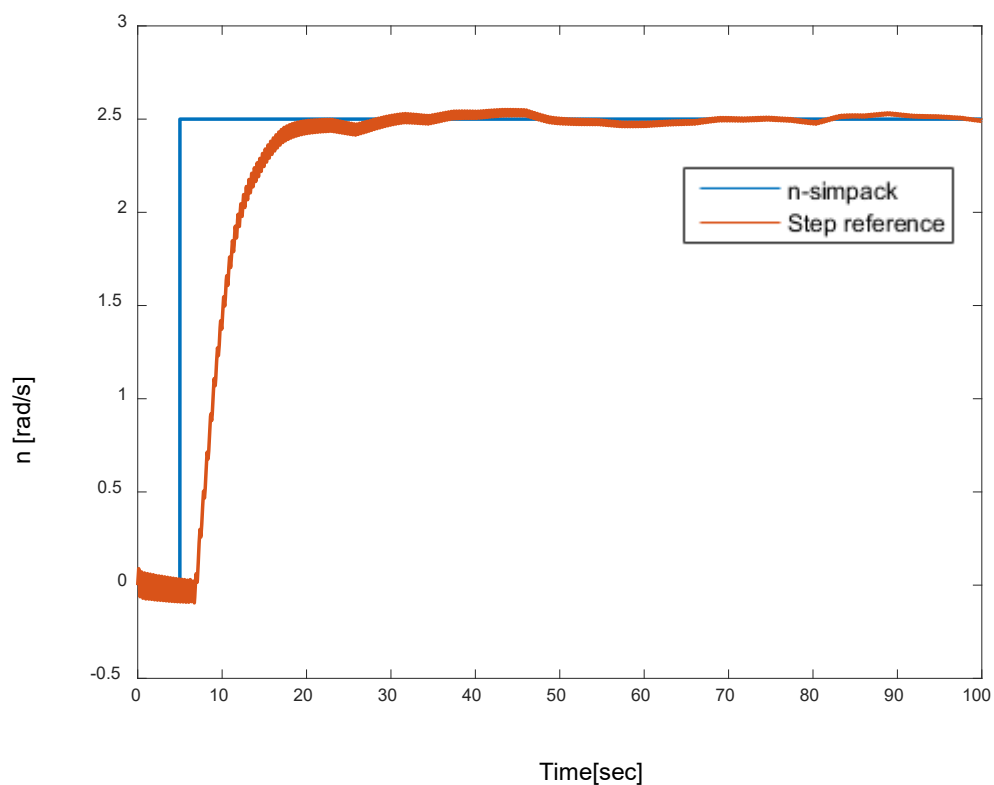
Figure 7.11: Step reference and rotational speed obtained in the simulation in Figure 7.10.

If we now try to input a ramp and run the simulation with the PI controller (see Figure 7.10), a delay of td=5 sec. with respect to the reference ramp appears (see Figure 7.12), but at least the step response has a much faster step response than before (the time response is considerably reduced).
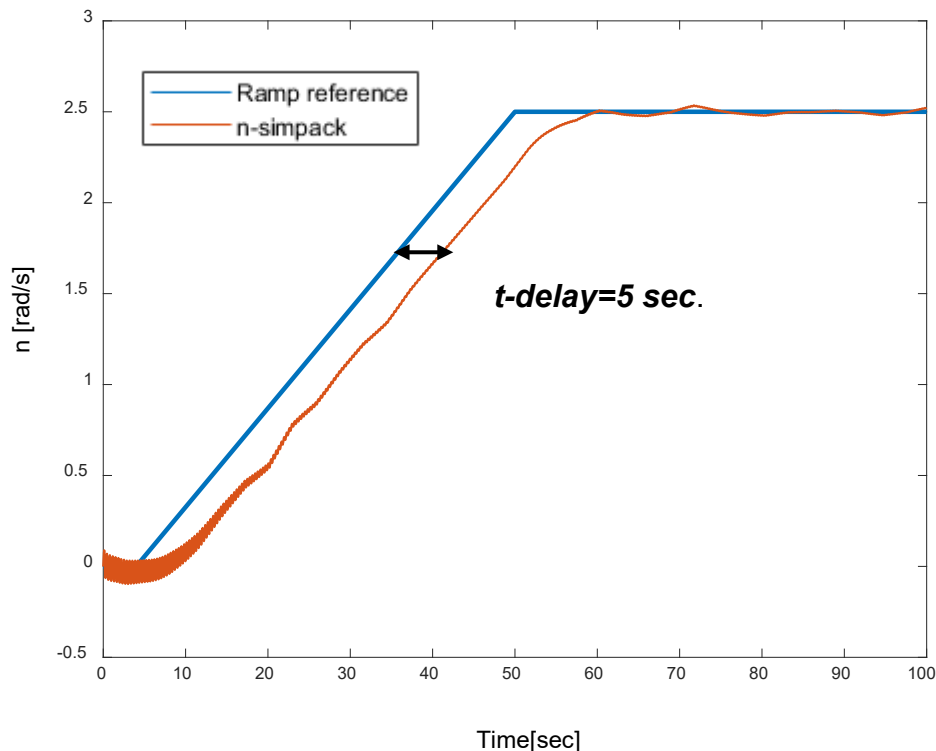
Figure 7.12: Ramp reference and rotational speed obtained in the simulation in Figure 7.10.

The NSC was tested with different input signals, and a new strategy was developed to adjust the output rotational speed to response time of 20 sec. and no overshoot.

Determining the real loads in the generator produced when inputting these reference signals becomes a relevant task because in this way, the behavior of the generator can be predicted (for example, the electrical current in the stator coils can be calculated by means of the generator torque T_e and the high-speed shaft rotational speed).

In Figure 7.13 it is possible to see how the torque in the generator changes to produce the desired rotational speed reference, which in this case is a step. Particularly, when the rotational speed is zero, a torque of about -1600 rad/s is generated. When the step rises, then the torque increases rapidly to reach approximately 500 Nm and then progressively decreases to reach a permanent value of about -1500 Nm.

Chair for Wind Power Drives
Univ.-Prof. Dr.-Ing. Georg Jacobs

79
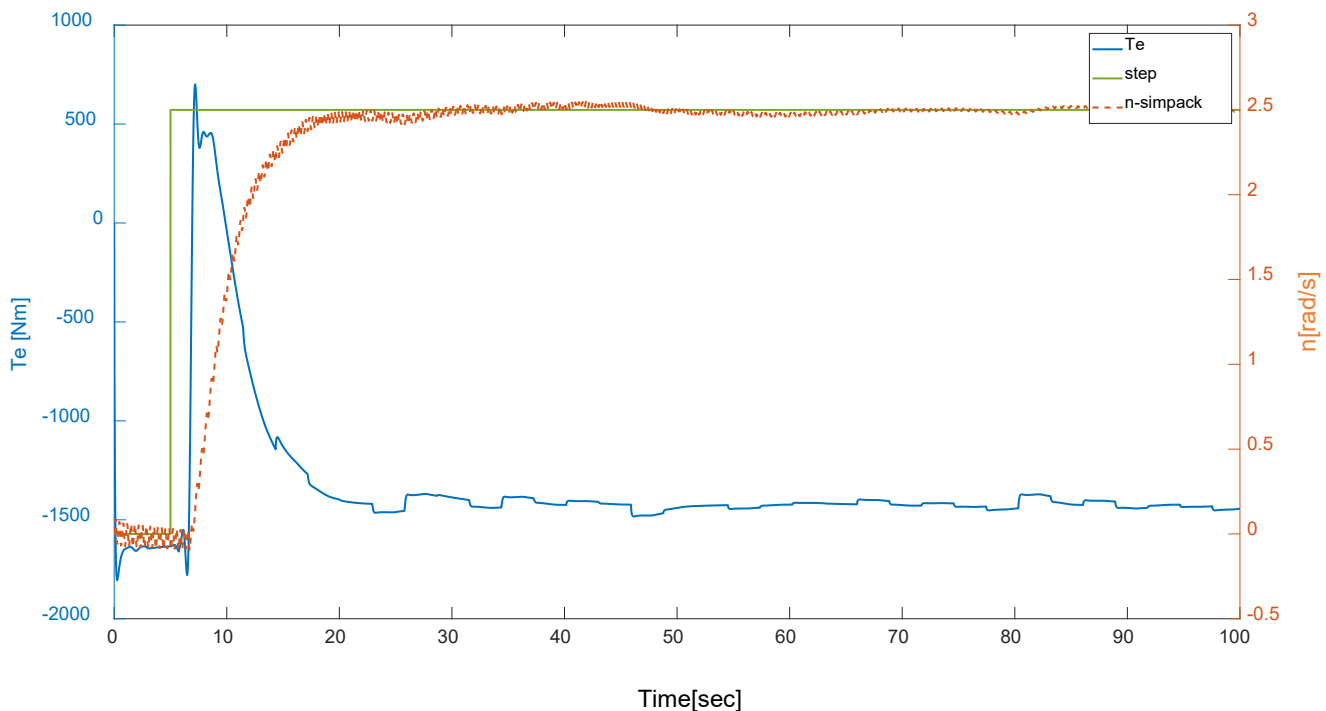
Figure 7.13: *Te* generated by NSC for a rotational speed step reference with the additional control strategy.

The generator torque in Figure 7.13 will be compared with Figure 3.5. For that, we must consider the sign of the generator torque in Figure 3.5 as the opposite because, as shown in Figure 5.3, the V52-SM requires that for its generator torque input. If we compare these two figures, it is possible to see that when the step is zero rad/s, the ESC outputs also a torque of zero Nm. However, the NSC outputs a torque of about -1600 Nm.

When the step changes to 2.5 rad/s, then ESC outputs -600 Nm, and the NSC outputs about 500 Nm.

After the 2.5 rad /s are reached, the torque in both controllers decreases rapidly, to zero in the ESC, and to -1500 in the NSC. The fact that the NSC must produce a constant generator torque (which is different from zero) during the periods where the rotational speed is constant or zero, is relevant if we compare it with the ESC, because the ESC does not produce any torque during these periods. This shows the great difference between the action produced by the NSC and the ECS. This difference lies on the fact that the NSC is a controller designed for the V52-SM, while the ESC does not seem to be designed specifically for the V52-SM.

We can see that the torque responses are very different from one another. However, the generator torque in Figure 7.13 is the one who produces the rotational speed response that fits the reference input (step or ramp).

Chair for Wind Power Drives
Univ.-Prof. Dr.-Ing. Georg Jacobs

80

8. Conclusion and Outlook

In this chapter, the most relevant results and conclusions achieved during the work of the thesis will be summarized. Furthermore, an evaluation of the outlook of the project will be made.

8.1 Conclusion

The most important results are:

✓ A star-delta switch control strategy was developed (Chapter 3) for its possible use on the implementation of the new simulated controller. Although it was not used afterwards for the creation of the new simulated controller, this strategy was integrated in the ESC (existing simulated controller).

✓ A NSC (new simulated controller) for the open-loop control strategy (Chapter 5) was created and tested with different rotational speed references from measurement data, obtaining an **error of 0.0137 rad/s, 0.0068 rad/s, 0.0857 rad/s and 0.0067 rad/s** between the measured rotational speed and the Simpack model rotational speed for each one of the four simulations done. The NSC was also tested with step and ramp references (Chapter 7) by means of the implementation of another PI controller working in parallel with the NSC, obtaining in this case a **response time of 20 sec. and no overshoot** for the Simpack rotational speed. The NSC proved in this way to calculate with high fidelity the T_e needed to run a realistic open-loop simulation with the V52-SM.

✓ The NSC was tested in closed-loop simulation (Chapter 5) and didn't work well. Because of that the NSC was modified by creating a Look-up table with a sliding mean instead of the former NSC. Therefore, it is possible to calculate the loads in the generator (T_e) by means of the measurement data input T_m, without the rotational speed measurement data $n_{measures}$ as a second reference, obtaining an **error of 0.0252 rad/s and 0.0270 rad/s** for the two simulations done.

✓ Furthermore, the NSC was modified for the upcoming generator in the V52-testbench (Chapter 6), and tested in open-loop simulation by changing some of its parameters and the value of the moment of inertia in the V52-SM. In this way, it is possible to predict and estimate which loads (T_e) will the new generator produce.

The fact that T_e (generator torque) can be calculated for rotational speed references and T_m (rotor torque) inputs can be useful to predict, by means of co-simulation, how the loads in the real generator during the tests in the V52-testbench will be. **The open and closed-loop controller created in the thesis will also make it possible to run a complete simulation of the V52-Simpack model that reproduces the real behavior of the V52-testbench in CWD.**

8.2 Outlook

The main improvements and research lines that could proceed the results of this work are:

✓ Analysis of the T_e signal generated by the NSC in comparison with the measured T_e.

✓ Correction of the delay that appears when inputting ramp references in the NSC.

✓ Further improvements on the closed-loop NSC look-up tables to minimize the error and.

Chair for Wind Power Drives
Univ.-Prof. Dr.-Ing. Georg Jacobs

81

✓ The NSC does not take into consideration any pitch angle measurement from the V52-SM. An improved simulated controller would also take these measurements into consideration, so that the T_e generated by the controller depends on the pitch angle as well. In this way, a more realistic simulation of the real operation strategy would be achieved.

Chair for Wind Power Drives
Univ.-Prof. Dr.-Ing. Georg Jacobs

82

9. Bibliography

[AE]   ANDERSON, D.; EBERHARDT, S. *How Airplanes Fly: A Physical Description of Lift*.

[Bi15]   BI, L. *Dynamic Simulation of Full-Scale Wind Turbine Nacelle System Test Benches*. RWTH RWTH, Dissertation vom 2015.

[CWD18]   CWD. *Measurement data. V52 Prüfstand., Veröffentlichungsdatum*.

[CWDECS]   CWD. *ECS (Existent simulatied generator), Veröffentlichungsdatum*.

[CWDSIM]   CWD. *V52-Simpack model, Veröffentlichungsdatum*.

[DMS15]   DIRSCHERL CHRISTIAN; M. HACKL, C.; SCHECHNER, K. *Modeling and control ofmodern wind turbine systems: An introduction*.

[Dut16]   DUTCHWIND. URL: http://dutchwind.com/products/vestas-v52-850-kw/.

[Ele16]   ELECTRICAL CONCEPTS. *Difference between Star and Delta ConnectionFacebookWhatsAppTwitterGooglDifference between Star and Delta ConnectionFacebookWhatsAppTwitterDifference between Star and Delta Connection*. URL: https://electricalbaba.com/difference-between-star-and-delta-connection/.

[FSK14]   FOKIANOU, P.; SAMARAKOU, M.; KANDIRD, D. *Star-Delta Switches Evaluation for Use in Grid-Connected WindFarm Installations*.

[FY10]   FLETCHER, J.; YANG, J. *Introduction to Doubly-Fed Induction Generatorfor Wind Power Applications*.

[Gam17]   GAMBIER, A. *Dynamic Modelling of the Rotating Subsystem of a Wind Turbine for Control Design Purposes*.

[GWE17]   GWEC - GLOBAL WIND ENERGY COUNCIL. URL: http://nejdetkanviinte.se/tag/vindkraft/.

[HK12]   HWAS ABDULHAMED; KATEBI, R. *Wind Turbine Control Using PI Pitch Angle Controller*.

[KAB]   KABATIC POWER. *Wind speed extrapolation*. URL: https://websites.pmc.ucsc.edu/~jnoble/wind/extrap/.

[KMD08]   KAWAI, H.; MICHISHITA, K.; DEGUCHI, A. *DESIGN WIND LOADS ON A WIND TURBINE FOR STRONG WIND*.

[LA07]   LI, S.; A. HASKEW, T. *Analysis of Decoupled d-q Vector Control in DFIGBack-to-Back PWM Converter*.

[LCK11]   LÆGAARD BERTHELSEN, T.; CORDERO, A.; KVERNØY DØHLIE, J.; UDENGAARD PEDERSEN, K. *Intelligent Start-up of Wind Turbines*. Aalborg Aalborg University. Institute of Electronic Systems, Project report vom 2011.

[MAT]   MATLAB R2018B. *compare*. URL: https://www.mathworks.com/help/ident/ref/compare.html.

[MAT18]   MATLAB. *Wind Farm - DFIG Detailed Model*. URL: https://www.mathworks.com/help/physmod/sps/examples/wind-farm-dfig-detailed-model.html.

[MMM02]   MANWELL; MANWELL, J. F.; MCGOWAN, J. G.; ROGERS, A. L. *Wind energy explained*. Chichester: Wiley 2002.

[MPP18]   M. HACKL, C.; PFEIFER, MARTIN, SCHECHNER; POL JANÉ-SONEIRA, K.; HOHMANN, S. *Full- & Reduced-Order State-Space Modeling ofWind Turbine Systems with Permanent-MagnetSynchronous Generator*.

[Pie06]   PIERRE-ELOUAN RÉTHORÉ. *Thrust and wake of a wind turbine: Relationship and measurements*Technical University of Denmark vom 2006.

[REA15]   REASEARCH HUBS. URL: http://researchhubs.com/post/engineering/wind-energy/pitch-regulated-and-stall-regulated-wind-turbine.html.

[RUT]   ROSYADI, M.; UMEMURA, A.; TAKAHASHI R.; TAMURA, J.; UCHIYAMA N.; IDE, K. *A New Simple Model of Wind Turbine Driven Doubly-FedInduction Generator for Dynamic Analysis of Grid ConnectedLarge Scale Wind FarmM*.

[RUT14]   ROSYADI, M.; UMEMURA, A.; TAKAHASHI, R.; TAMURA, J.; UCHIYAMA, N.; K. IDE. *A New Simple Model of Wind Turbine Driven Doubly-Fed Induction Generator for Dynamic Analysis of Grid Connected Large Scale Wind Farm*.

[ŞAE]   ŞEN, Z.; ALTUNKAYNAK, A.; ERDIK, T. *Wind Velocity Vertical Extrapolation by Extended Power Law*.

[Sel07]   SELVAM, K. *Individual Pitch Control for Largescale wind turbines*.

Bibliography

[SHY16]   SHANG, L.; HU, J.; YUAN, X.; CHI, Y. *Understanding Inertial Response of Variable-SpeedWind Turbines by Defined Internal Potential Vector*.

[Sim16]   SIMANI, S. *Overview of Modelling and Advanced Control Strategies for Wind Turbine Systems*.

[VES]   VESTAS. *V52-850 kW Pitch regulated wind turbine with OptiTip® and OptiSpeed®.* URL:http://www.orkneywind.co.uk/explore/Balnamoon/original%20report/ose2358%20Section%202.pdf.

[VES04]   VESTAS. *V52-850kW, VCS Frequency Converter, Veröffentlichungsdatum*.

[VES11]   VESTAS. *Control Systems, Veröffentlichungsdatum*.

[VESChar]   VESTAS, VERÖFFENTLICHUNGSDATUM.

[VESEL04]   VESTAS. *Electrical Data VMP 850 kW- 690 V- 50 Hz Controller, Veröffentlichungsdatum*.

[VEST]   VESTAS. *V52-850 kW The turbine that goes anywhere.* URL: https://www.epd.gov.hk/eia/register/report/eiareport/eia_1242006/html/EIA_Report/Annex%20A3.3.pdf.

[VESTCurve]   VESTAS, VERÖFFENTLICHUNGSDATUM.

[Wik]   WIKIPEDIA. *Variable speed wind turbine.* URL: https://en.wikipedia.org/wiki/Variable_speed_wind_turbine.

[WIN]   WIND-TURBINE-MODELS.COM. *VESTAS_DATASHEED.* URL: https://en.wind-turbine-models.com/turbines/71-vestas-v52.

Chair for Wind Power Drives
Univ.-Prof. Dr.-Ing. Georg Jacobs

84

10. Appendix

Appendix 1

<u>Functions used to implement the dependences on the wind of the generator's shaft speed, pitch angle, electrical power and electrical torque</u>.

DREHZAHL

```
function Drehzahl =fcn(v_wind)
%#codegen
if ((v_wind >=3)&&(v_wind <=4))
    y=900;
elseif ((v_wind >4)&&(v_wind <=9))
    y = 144* v_wind + 324;
elseif ((v_wind >9)&&(x<=25))
    y=1620;
else y=0;

end
```

HIGH-SPEED SHAFT SPEED

```
function Drehzahl =fcn(v_wind)
%#codegen
if ((v_wind >=3)&&(v_wind <=4))
    Drehzahl =900;
elseif ((v_wind >4)&&(v_wind <=9))
    Drehzahl = 144* v_wind + 324;
elseif ((v_wind >9)&&(x<=25))
    Drehzahl =1620;
else Drehzahl =0;

end
```

PITCH

```
function Pitch =fcn(v_wind)
%#codegen
if ((v_wind >=3)&&(v_wind <=4))
    Pitch =-2* v_wind +7;
elseif ((v_wind >4)&&(v_wind <=9))
    Pitch =-1;
elseif ((v_wind >9)&&(v_wind <=14))
    Pitch =0.272*(v_wind ^2)-6.256*
v_wind +33.272;
elseif ((v_wind >14)&&(v_wind <=25))
    Pitch =sqrt(abs(64.3236*(v_wind -
14)))-1;
else Pitch =0;

end
```

ELECTRICAL TORQUE

```
function Drehmoment = fcn(v_wind)
%#codegen
if ((v_wind>=3)&&(v_wind <=4))
  Drehmoment =(6902.77* v_wind ^2-
40074.4* v_wind +58098.4)/900;
elseif ((v_wind >4)&&( v_wind <=9))
  Drehmoment =(6902.77* v_wind ^2-
40074.4* v_wind +58098.4)/(144*
v_wind + 324);
elseif ((v_wind >9)&&( v_wind <=14))
  Drehmoment =(217.949* v_wind ^2-
40074.4* v_wind +58098.4)/1620;
elseif (v_wind >=14)
  Drehmoment = 850000/(1620*(pi/30));
else
  Drehmoment =0;
end

end
```

ELECTRICAL POWER

```
function Leistung = fcn(v_wind)
%#codegen
if ((v_wind >=3)&&( v_wind <=14))
  Leistung =6902.77* v_wind ^2-
40074.4* v_wind +58098.4;
else if (v_wind >=14)
  Leistung =850000;
else  Leistung=0;
    end
end
```

CP-FUNCTION
```
%cp-Calculator
function cp = fcn( Pitch, v_wind,
w_rotor)
%#codegen
rt=52/2; %[m]
lambda= v_wind/(w_rotor*rt)
c1=0.5176; c2=116; c3=0.4; c4=0;
x=0; c5=5; c6=21; c7=0.08; c8=0.035;
c9=0.0068;
f=((1/(lambda+c7*Pitch))-
(c8/((Pitch^3)+1)))
cp = (c1*(c2*f-c3*Pitch-
c4*(Pitch^x)-c5)*exp(-
c6*f)+c9*lambda);
```

CP-PLOT
```
%cp; 3D-plot

function cp=fcn(Pitch, lambda)
syms Pitch
syms lambda
c1=0.5176; c2=116; c3=0.4; c4=0;
x=0; c5=5; c6=21; c7=0.08;
c8=0.035; c9=0.0068;
f=((1/(lambda+c7*Pitch))-
(c8/((Pitch^3)+1)))
c1=0.5176; c2=116; c3=0.4; c4=0;
x=0; c5=5; c6=21; c7=0.08;
c8=0.035; c9=0.0068;
f=((1/(lambda+c7*Pitch))-
(c8/((Pitch^3)+1)))
cp =(c1*(c2*f-c3*Pitch-
c4*(Pitch^x)-c5)*exp(-
c6*f)+c9*lambda);

ezsurf(cp,[-5*(pi/180)
25*(pi/180)], [0 15]);
```

Appendix 2

Construction of the generator characteristics

The characteristics $P(v_{wind}) - M(v_{wind})$ will be built up in the following way:

Assuming that $P(v_{wind})$ and $M(v_{wind})$, $n(v_{wind})$ are respectively the output electrical power, electrical torque and high-speed shaft rotational speed, all of them depending on the wind speed v_{wind}, it is possible to find a relation of the type:

$$P = f(M) = f(P/n)$$

Dividing the behavior in intervals depending on the wind speed:

➤ $3 < v_{wind} < 4 \; m/s$

$$P(v_{wind}) = 6902.77 v_{wind}^2 - 40074.4 v_{wind} + 58098.4 \; [kW]$$

$$n(v_{wind}) = 900 \; [rpm]$$

$$P(v_{wind}) = 900 \frac{\pi}{30} M(v_{wind})$$

Interval limit values.

$P(v_{wind} = 3) = 0 \quad M(v_{wind} = 3) = 0 \; [Nm]$

$P(v_{wind} = 4) = 8245.12 \quad M(v_{wind} = 4) = 87.4832 [Nm]$

➤ $4 < v_{wind} < 9 \; m/s$

$$P(v_{wind}) = 6902.77 v_{wind}^2 - 40074.4 v_{wind} + 58098.4 \; [kW]$$

$$n(v_{wind}) = 144 \, v_{wind} + 324 \; [rpm]$$

$$v_{wind} = (n(v_{wind}) - 324)/144)$$

$$n(v_{wind}) = P(v_{wind})/M(v_{wind})$$

$$v_{wind} = ((\frac{P(v_{wind})}{M(v_{wind})} - 324)/144)$$

$$P(v_{wind}) = 6902.77 \left(\frac{\frac{P(v_{wind})}{M(v_{wind})} - 324}{144} \right)^2 - 40074.4 \left(\frac{\frac{P(v_{wind})}{M(v_{wind})} - 324}{144} \right) + 58098.4 = c1 \left(\frac{P(v_{wind})}{M(v_{wind})} - 324 \right)^2 + c2 \left(\frac{P(v_{wind})}{M(v_{wind})} - 324 \right) + c3$$

$If \; y = P(v_{wind}) \; and \; x = M(v_{wind}) \; and \; c1 = 0.3329, c2 = -278.2944 \; and \; c3 = 58098.4$

Interval limit values.

$$P(v_{wind} = 4) = 8245.12 \quad M(v_{wind} = 4) = 9.16 \frac{30}{\pi} = 87.525 [Nm]$$

$$P(v_{wind} = 9) = 256553.17 \quad M(v_{wind} = 9) = 158 \frac{30}{\pi} = 1512.2865 [Nm]$$

➢ $9 < v_{wind} < 14 \ m/s$

$$P(v_{wind}) = 6902.77 v_{wind}^2 - 40074.4 v_{wind} + 58098.4 \ [kW]$$

$$n(v_{wind}) = 1620 \ [rpm]$$

$$P(v_{wind}) = 1620 \frac{\pi}{30} M(v_{wind})$$

Intervals limit values.

$$P(v_{wind} = 9) = 256553.17 \quad M(v_{wind} = 9) = 1512.2865 \ [Nm]$$

$$P(v_{wind} = 14) = 850000 \quad M(v_{wind} = 14) = 5010.433 [Nm]$$

➢ $14 < v_{wind} < 25 \ m/s$

$$P(v_{wind}) = 850000 \ [kW]$$

$$n(v_{wind}) = 1620 \ [rpm]$$

$$P(v_{wind}) = 1620 \frac{\pi}{30} M(v_{wind})$$

Interval limit values.

$$P(v_{wind} = 14 - 25) = 850000 \quad M(v_{wind} = 14 - 25) = 5010.433 \ [Nm]$$

The characteristic $M(v_{wind}) - n(v_{wind})$ will be built up in the following way:

➢ $3 < v_{wind} < 4 \ m/s$

$$M(v_{wind}) = P(v_{wind})/n(v_{wind}) = 0 - 87.525$$

➢ $4 < v_{wind} < 9 \ m/s$

$$M(v_{wind}) = P(v_{wind})/n(v_{wind}) = P(v_{wind}) = \frac{c1(n(v_{wind}) - 324)^2 + c2(n(v_{wind}) - 324) + c3}{n(v_{wind})}$$

$If \ c1 = 0.3329, c2 = -278.2944 \ and \ c3 = 58098.4$

Chair for Wind Power Drives
Univ.-Prof. Dr.-Ing. Georg Jacobs

88

Interval limit values

$$M(n(v_{wind}) = 900) = 9.16\frac{30}{\pi} = 87.525 \text{ [Nm]}$$

$$M(n(v_{wind}) = 1620) = 158.378\frac{30}{\pi} = 1512.402 \text{ [Nm]}$$

➤ $9 < v_{wind} < 14 \ m/s$

$$M(v_{wind}) = P(v_{wind})/n(v_{wind}) = P(v_{wind}) = \frac{c1(n(v_{wind}) - 324)^2 + c2(n(v_{wind}) - 324) - c3}{n(v_{wind})}$$

$$n(v_{wind}) = 1620 \text{ [rpm]}$$

Interval limit values.

$$M(n(v_{wind}) = 1620) = 158.378\frac{30}{\pi} = 1512.402 \text{ [Nm]} - 5010.43 \text{ [Nm]}$$

➤ $14 < v_{wind} < 25 \ m/s$

$$P(v_{wind}) = 850000 \text{ [kW]}$$

$$n(v_{wind}) = 1620 \text{ [rpm]}$$

$$M(n(v_{wind}) = \frac{850000}{1620\frac{\pi}{30}} = 5010.43 \ N/m$$

Appendix 3

Chair for Wind Power Drives
Univ.-Prof. Dr.-Ing. Georg Jacobs

89

Appendix

The following information was used to develop the star-delta switch strategy. (0), (1), (2) and (3) are found in [VES11], VES04, VESEL04, [VES11] respectively. The lines remarked in green correspond to important information used in the thesis.

[VES11]-(0)

	unit	VMP name	V52-850 kW
P_{rtd}	kW	PowerNominelPx^2	850
V_{on}	m/s	-*)	3
V_{off}	m/s	HighWindLimitPx	25
rpm_{rtd}	rpm	NomTorqRPMPx	1620
rpm_{min}	rpm	G2MinConnectSpeed Px (replacing G2MinRPMPx)	900
$rpm_{min,\Delta}$	rpm	G1MinConnectSpeed Px (replacing G1MinRPMPx)	1200
$P_{max,\lambda}$	kW	G2PowerRefMaxPx	425

VES04-(1)

Every line highlighted in green refers information used during the thesis.

The generator stator is coupled directly to the 690 V grid. The generator can be coupled in star (K500 and K502) or delta (K500 and K501) connection.

The generator is coupled in star mode if the total power is low (equivalent to a small generator); in the case of high total power the generator is coupled in delta mode. The advantage of the star coupling is that the speed range is increased and the losses in generator and converter are reduced.

Chair for Wind Power Drives
Univ.-Prof. Dr.-Ing. Georg Jacobs

90

VESEL04-(2)

The V52-850 kW wind turbine is able to operate in fixed power factor mode with a power factor range in the interval from 0.98 capacitive to 0.95 inductive measured on the 690 V generator side and with 100% of rated active power. It is possible to choose other power factor values, however, with reduced active power.

The V52-850 kW wind turbine is also able to operate in fixed reactive power mode. In the fixed reactive power mode, the wind turbine will generate or absorb reactive power up to 500 kVAr, when the generator stator winding is coupled in delta, however, with decreased reactive power close to the rated power output (see the red line in the attached diagram). When the stator winding is in star connection, the maximum reactive power is 250 kVAr.

The turbine will automatically change the generator stator connection from star to delta and vice versa, depending on the actual active power production.
The criteria are as follows:

- From star to delta: Active power must be above 300 kW for more than 30 seconds
- From delta to star: Active power must be below 100 kW for more than 15 seconds

This means that if the turbine is adjusted to generate e.g. 400 kVAr, the turbine will automatically decrease the reactive power to 250 kVAr, when the generator is in star connection.

Please note that the area marked with ▨ indicates that the generator can be in either star or delta, depending on the actual conditions.

Please note that the generator can be in star connection producing active power above 300 kW, if the wind speed increases rapidly during the 30 seconds time delay. The active power in star is limited to 450 kW.
This can also happen at low wind speed, so that the generator can be in delta below 100 kW, if the wind speed is decreasing rapidly (faster than the 15 seconds time delay).

[VES11]-(3)

4.3 Star-/Delta Connection

In order to maximize efficiency, the generator' stator can be operated in two different connections:

    a) Star connection (λ).

    b) Delta connection (Δ).

At star connection, the generator rpm can cover the whole area from rpm_{min} to rpm_{rtd}, while the generator power is limited to $P_{max, \lambda}$ (see Figure 4-3, p. 12 /Table 4-1, p. 10 & Table 4-2, p. 10). At delta connection, the power is unlimited, while the rpm is restricted to be higher than $rpm_{min, \Delta}$. The control system selects the generator connection dependent on the wind speed. In order to shift connection, the turbine is transferred to the respective connect speed while ramping down the power to zero. Then the generator is disconnected, re-synchronized to the grid and connected in the new configuration. Finally, the power is ramped up again.

Chair for Wind Power Drives
Univ.-Prof. Dr.-Ing. Georg Jacobs

91

Code needed to run the star-delta switch control strategy.

Block *Connection.*

```matlab
function y = fcn(Leistung,gen_speed)
%#codegen
P_max_star= 4.5e5; %W;
rpm_min_delta=1200; %rpm;
if ((Leistung < P_max_star))
    y=0; %star
elseif ((gen_speed > rpm_min_delta))
    y=1; %delta
else
    y=2; %terminate
```

Block *Case Star-Delta Switch Subsystem.*

```matlab
function y  = fcn(Leistung,clock,Speed_rate)

%#codegen
global j
persistent i
    if isempty(i)
        i = 0;
    end


if ((mod(clock,30)==0)&&(Leistung~=0))
    if ((Leistung>=3e5))
        i=1
    else   i=0

    end

end


if ((i==1)|| (Speed_rate==1))
    y=1 %star-delta
    disp('star-delta')

else y=0
    disp('no more change in connection(remains star)')%no change in
connection(remains star)
end

end
```

Block *Case Delta-Star Switch Subsystem.*

```matlab
function y  = fcn(Leistung,clock,Speed_rate)

%#codegen
persistent i
    if isempty(i)
```

Chair for Wind Power Drives
Univ.-Prof. Dr.-Ing. Georg Jacobs

92

```matlab
        i = 0;
    end

if ((mod(clock,15)==0)&& (Leistung~=0))
    if (Leistung<=1e5)
        i=1
    else  i=0 %%i=0 means that it is not going to be switching at this execution

    end

end


if ((i==1)||(Speed_rate==0))
    y=1 ; %delta-star
    disp('delta-star')

else
    y=0 ; %terminate
    disp('no change in connection(remains delta)')%no change in
connection(remains delta)

end

end
```

Chair for Wind Power Drives
Univ.-Prof. Dr.-Ing. Georg Jacobs

93

Appendix 4

TREATMENT AND ANALYSIS OF THE MEASUREMENT DATA

20180830_170000_173000

(Measurement data from the test made on 30-08-2018, from 17:00 to 17:30 h.)

```matlab
woelfel_signals{1,10}(1,3)=0;% es fängt eine Minute später als der Schalter

for i=2:3600000
    woelfel_signals{1,10}(i,3)= woelfel_signals{1,10}(i-1,3)+(1/2000);
end

for j=1:3600000
    woelfel_signals{1,10}(j,4)=-4;
end
for m=2:3600000
    woelfel_signals{1,10}(m,2)=
woelfel_signals{1,10}(m,1)*woelfel_signals{1,10}(m,4);
end
woelfel_signals{1,11}(1,2)=0;
for n=2:3600000
    woelfel_signals{1,11}(n,2)= woelfel_signals{1,11}(n-1,2)+(1/2000);
end
for n=2:3600000
    woelfel_signals{1,11}(n,3)= ((woelfel_signals{1,11}(n,1))+0.285)*70;
end

Channel_12_Data(1,2)=941.4595+1.55;
for y=2:1077497
Channel_12_Data(y,2)=Channel_12_Data(y-1,2)+(1/300);
end

Channel_11_Data(1,2)=941.4595+1.55;
for y=2:1077497
Channel_11_Data(y,2)=Channel_11_Data(y-1,2)+(1/300);
end

Channel_10_Data(1,2)=941.4595+1.55;
for o=2:1077497
Channel_10_Data(o,2)=Channel_10_Data(o-1,2)+(1/300);
end
Channel_13_Data(1,2)=941.4595+1.55;

for p=2:1077497
Channel_13_Data(p,2)=Channel_13_Data(p-1,2)+(1/300);
end

Channel_9_Data(1,2)=941.4595+1.55;
for s=2:1077497
Channel_9_Data(s,2)=Channel_9_Data(s-1,2)+(1/300);
end


%LEISTUNG
```

Chair for Wind Power Drives
Univ.-Prof. Dr.-Ing. Georg Jacobs

94

```matlab
for u=1:3600000
Leistung_calculated(u,1)=woelfel_signals{1,10}(u,2)*(2*pi/60)*woelfel_signals{1,
11}(u,3)*1000;
end

%% mit den Definitionen aus: https://www.elektronik-
kompendium.de/sites/grd/1006061.htm
% written by Brian Rieckhoff,until %%%

U_st_1=woelfel_signals{24};
U_st_2=woelfel_signals{25};
U_st_3=woelfel_signals{26};
U_st=[U_st_1;U_st_2;U_st_3];

%Leiterspannung
U=U_st*sqrt(3);
U_1=U(1,:);U_2=U(2,:);U_3=U(3,:);

%Leiterstrom
I_1=woelfel_signals{21};
I_2=woelfel_signals{22};
I_3=woelfel_signals{23};
I=[I_1;I_2;I_3];

%% Effektivwerte
f=50;
U_eff_1=[];U_eff_2=[];U_eff_3=[];
I_eff_1=[];I_eff_2=[];I_eff_3=[];

for ii=1:f:length(U)
        U_eff_1(ii:ii+f-1)=rms(U(1,ii:ii+f-1));
        U_eff_2(ii:ii+f-1)=rms(U(2,ii:ii+f-1));
        U_eff_3(ii:ii+f-1)=rms(U(3,ii:ii+f-1));
        I_eff_1(ii:ii+f-1)=rms(I(1,ii:ii+f-1));
        I_eff_2(ii:ii+f-1)=rms(I(2,ii:ii+f-1));
        I_eff_3(ii:ii+f-1)=rms(I(3,ii:ii+f-1));
end
U_eff=[U_eff_1;U_eff_2;U_eff_3];
I_eff=[I_eff_1;I_eff_2;I_eff_3];


P_el=transpose(U_eff.*I_eff.*sqrt(3)); %kW

%%%

Drehzahl=woelfel_signals{1,10}(:,2);
Drehmoment=woelfel_signals{1,11}(:,3);
Time_Drehzahl=woelfel_signals{1,10}(:,3);
Time_Drehmoment=woelfel_signals{1,11}(:,2);
Leistung_plot=Leistung_calculated(:,1);
Time_Schalter_K537=Channel_9_Data(:,2);
Prozent_Schalter_K537=Channel_9_Data(:,1);
Time_Schalter_K536=Channel_10_Data(:,2);
Prozent_Schalter_K536=Channel_10_Data(:,1);
Time_Schalter_K500=Channel_11_Data(:,2);
Prozent_Schalter_K500=Channel_11_Data(:,1);
Time_Schalter_K501=Channel_12_Data(:,2);
Prozent_Schalter_K501=Channel_12_Data(:,1);
Time_Schalter_K502=Channel_13_Data(:,2);
Prozent_Schalter_K502=Channel_13_Data(:,1);
```

Chair for Wind Power Drives
Univ.-Prof. Dr.-Ing. Georg Jacobs

95

```matlab
Drehzahl_rotor_generator=Drehzahl*((20/129*21*29/74/79)^-1); %rpm

Drehmoment_generator=[]; %kNm

for i=1:length(Drehzahl)
    if (Drehzahl(i,1)~=0)

Drehmoment_generator(i,1)=P_el(i,1)./(Drehzahl_rotor_generator(i,1)*(2*pi/60));
%kNm

    else
    Drehmoment_generator(i,1)=0;

    end

end

f_tp=1;
[b,a]=butter(5,f_tp/(0.5*(2000)),'low');

Drehmoment_filtered=filter(b,a,Drehmoment); %kNm
Leistung_filtered=filter(b,a,Leistung_plot); %W
Drehzahl_filtered=filter(b,a,Drehzahl); %rpm
Drehzahl_rotor_generator_filtered=filter(b,a,Drehzahl_rotor_generator); %rpm
P_el_filtered=filter(b,a,P_el(:,1)); %kW
Drehmoment_generator_filtered=filter(b,a,Drehmoment_generator); %kNm

Drehmoment_abtriebswelle_filtered=Drehmoment_filtered/((20/129*21*29/74/79)^-1);
difference=Drehmoment_abtriebswelle_filtered-Drehmoment_generator_filtered;
difference_filtered=filter(b,a,difference);
acel=diff(Drehzahl_filtered*2*pi/60)./diff(Time_Drehzahl);
acel_filtered=filter(b,a,acel);
t_acel=Time_Drehzahl(2:end);

%PLOT

subplot(10,1,1)
plot(Time_Drehzahl,Drehzahl)
xlim([540 1800])

subplot(10,1,2)
plot(Time_Drehmoment, Drehmoment)
xlim([540 1800])

subplot(10,1,3)
plot(Time_Drehmoment, Leistung_plot)
xlim([540 1800])

subplot(10,1,4)
plot(Time_Schalter_K537, Prozent_Schalter_K537)
xlim([540 1800])

subplot(10,1,5)
plot(Time_Schalter_K536, Prozent_Schalter_K536)
xlim([540 1800])

subplot(10,1,6)
plot(Time_Schalter_K500, Prozent_Schalter_K500)
xlim([540 1800])
```

Chair for Wind Power Drives
Univ.-Prof. Dr.-Ing. Georg Jacobs

96

```
subplot(10,1,7)
plot(Time_Schalter_K501, Prozent_Schalter_K501)
xlim([540 1800])

subplot(10,1,8)
plot(Time_Schalter_K502, Prozent_Schalter_K502)
xlim([540 1800])

subplot(10,1,9)
plot(Time_Drehzahl, P_el(:,3)*1000)
xlim([540 1800])

figure;

plot(Time_Drehzahl,Drehzahl)
hold on
plot(Time_Drehmoment, Drehmoment)
hold on
plot(Time_Drehmoment, Leistung_plot/1000)
hold on
plot(Time_Drehzahl, P_el(:,1));
hold on
legend('n_xrotor[rpm]','M_xrotor[kNm]','Leistung[kW]')
xlim([540 1800])
```

Calculation of the moment of inertia

```
acel_filtered_corrected(1,1)=acel_filtered(1,1);
for i=2:length(acel_filtered)+1
    acel_filtered_corrected(i,1)=acel_filtered(i-1,1)*(1/((20/129*21*29/74/79)^-
1));
end
J_Inertia=difference_filtered*1000./(acel_filtered_corrected);
d=designfilt
J_Inertia_filtered=filter(d,J_Inertia); %kNm

plot(Time_Drehzahl,J_Inertia_filtered/100); ylim([0 100]); hold on;
plot(Time_Drehzahl,Drehzahl_rotor_generator_filtered/10);
hold on;  plot(Time_Schalter_K501, Prozent_Schalter_K501*2);
hold on;  plot(Time_Schalter_K502, Prozent_Schalter_K502*1.7);
hold on; plot(Time_Drehzahl,Drehmoment_generator_filtered*15);
hold on; plot(Time_Drehzahl,Drehmoment_abtriebswelle_filtered*15);
hold on; plot(Time_Drehzahl,P_el_filtered(:,1)/5);
figure;
plot(Time_Drehzahl, difference_filtered); hold on;
plot(Time_Drehzahl,acel_filtered_corrected*100)
```

Graphic in Figure 4.1

```
plot(Time_Drehzahl,Drehmoment_abtriebswelle_filtered);
hold on; plot(Time_Drehzahl,Drehmoment_generator_filtered);
hold on; plot(Time_Schalter_K501, Prozent_Schalter_K501/100);
hold on; plot(Time_Drehzahl,Drehzahl*100*pi/30);
hold on; plot(Time_Drehzahl,Drehzahl_rotor_generator_filtered/100);
hold on; plot(t_acel, acel_filtered*10);
legend('Drehmoment-abtriebswelle-filtered','Drehmoment-generator-
filtered[kNm]','K_Schaler/10','n_xrotor[rpm]','acel')
```

Chair for Wind Power Drives
Univ.-Prof. Dr.-Ing. Georg Jacobs

97

```
figure;
hold on; plot(Time_Drehzahl,Drehzahl_filtered*10*pi/30);
hold on;  plot(Time_Schalter_K501, Prozent_Schalter_K501*2.3/10);
hold on;  plot(Time_Schalter_K502, Prozent_Schalter_K502*2.3/10);

hold on; plot(Time_Drehzahl,Drehmoment_abtriebswelle_filtered*10);
hold on; plot(Time_Drehzahl,P_el_filtered(:,1)/10);
```

Co-simulation with measurement data 20180830_170000_173000

```
% written by Brian Rieckhoff,until %%%


pfad = 'C:\Program Files\SIMPACK-2017\partners\mathworks\simat';
addpath(pfad)
% simat
%%%


for i=1660002:2.75e6
    Time_Simulink(i-1660001,1)=Time_Drehzahl(i,1)-8.300004999838291e+02;
end
for i=1660002:2.75e6
    Drehmoment_generator_Simulink(i-1660001,1)=Drehmoment_generator(i,1);

end
for i=1660002:2.75e6
    Drehmoment_Simulink(i-1660001,1)=Drehmoment(i,1);

end
for i=1660002:2.75e6
    Drehzahl_Simulink(i-1660001,1)=Drehzahl_filtered(i,1);
end
for i=1660002:2.75e6
    P_el_Simulink(i-1660001,1)=P_el_filtered(i,1);
end
```

20180830_153000_160000

(Measurement data from the test made on 30-08-2018, from 15:30 to 16:00 h.)

```
woelfel_signals{1,10}(1,3)=4800;% es fängt eine Minute später als der Schalter.

for i=2:4800000
    woelfel_signals{1,10}(i,3)= woelfel_signals{1,10}(i-1,3)+(1/2000);
end

for j=1:4800000
    woelfel_signals{1,10}(j,4)=-4;
end
for m=2:4800000
```

Chair for Wind Power Drives
Univ.-Prof. Dr.-Ing. Georg Jacobs

98

```matlab
    woelfel_signals{1,10}(m,2)=
woelfel_signals{1,10}(m,1)*woelfel_signals{1,10}(m,4);
end
woelfel_signals{1,11}(1,2)=4800;
for n=2:4800000
    woelfel_signals{1,11}(n,2)= woelfel_signals{1,11}(n-1,2)+(1/2000);
end
for n=1:4800000
    woelfel_signals{1,11}(n,3)= (woelfel_signals{1,11}(n,1)+0.285)*70;
end


Channel_12_Data(1,2)=60+401.4595+25-0.035+1.3+1.37+0.3425-0.9783;
for y=2:2125337
Channel_12_Data(y,2)=Channel_12_Data(y-1,2)+(1/300);
end
Channel_11_Data(1,2)=60+401.4595+25-0.035+1.3+1.37+0.3425-0.9783;

for l=2:2125337
Channel_11_Data(l,2)=Channel_11_Data(l-1,2)+(1/300);
end
Channel_10_Data(1,2)=60+401.4595+25-0.035+1.3+1.37+0.3425-0.9783;
for o=2:2125337
Channel_10_Data(o,2)=Channel_10_Data(o-1,2)+(1/300);
end
Channel_13_Data(1,2)=60+401.4595+25-0.035+1.3+1.37+0.3425-0.9783;

for p=2:2125337
Channel_13_Data(p,2)=Channel_13_Data(p-1,2)+(1/300);
end


Channel_9_Data(1,2)=60+401.4595+25-0.035+1.3+1.37+0.3425-0.9783;
for s=2:2125337
Channel_9_Data(s,2)=Channel_9_Data(s-1,2)+(1/300);
end



%LEISTUNG

for u=1:4800000
Leistung_calculated(u,1)=woelfel_signals{1,10}(u,2)*(2*pi/60)*woelfel_signals{1,
11}(u,3)*1000; %W
end

%% mit den Definitionen aus: https://www.elektronik-
kompendium.de/sites/grd/1006061.htm
%first load signal-.mat-files
% Spannungen
%Strangspannung
% written by Brian Rieckhoff,until %%%

U_st_1=woelfel_signals{24};
U_st_2=woelfel_signals{25};
U_st_3=woelfel_signals{26};
U_st=[U_st_1;U_st_2;U_st_3];

%Leiterspannung
U=U_st*sqrt(3);
U_1=U(1,:);U_2=U(2,:);U_3=U(3,:);

%Leiterstrom
I_1=woelfel_signals{21};
```

Chair for Wind Power Drives
Univ.-Prof. Dr.-Ing. Georg Jacobs

99

```matlab
I_2=woelfel_signals{22};
I_3=woelfel_signals{23};
I=[I_1;I_2;I_3];

%% Effektivwerte
f=50;
U_eff_1=[];U_eff_2=[];U_eff_3=[];
I_eff_1=[];I_eff_2=[];I_eff_3=[];

for ii=1:f:length(U)
        U_eff_1(ii:ii+f-1)=rms(U(1,ii:ii+f-1));
        U_eff_2(ii:ii+f-1)=rms(U(2,ii:ii+f-1));
        U_eff_3(ii:ii+f-1)=rms(U(3,ii:ii+f-1));
        I_eff_1(ii:ii+f-1)=rms(I(1,ii:ii+f-1));
        I_eff_2(ii:ii+f-1)=rms(I(2,ii:ii+f-1));
        I_eff_3(ii:ii+f-1)=rms(I(3,ii:ii+f-1));
end
U_eff=[U_eff_1;U_eff_2;U_eff_3];
I_eff=[I_eff_1;I_eff_2;I_eff_3];

P_el=transpose(U_eff.*I_eff.*sqrt(3)); %kW
%%%

Drehzahl=woelfel_signals{1,10}(:,2);
Drehmoment=woelfel_signals{1,11}(:,3);
Time_Drehzahl=woelfel_signals{1,10}(:,3);
Time_Drehmoment=woelfel_signals{1,11}(:,2);
Leistung_plot=Leistung_calculated(:,1);
Time_Schalter_K537=Channel_9_Data(:,2);
Prozent_Schalter_K537=Channel_9_Data(:,1);
Time_Schalter_K536=Channel_10_Data(:,2);
Prozent_Schalter_K536=Channel_10_Data(:,1);
Time_Schalter_K500=Channel_11_Data(:,2);
Prozent_Schalter_K500=Channel_11_Data(:,1);
Time_Schalter_K501=Channel_12_Data(:,2);
Prozent_Schalter_K501=Channel_12_Data(:,1);
Time_Schalter_K502=Channel_13_Data(:,2);
Prozent_Schalter_K502=Channel_13_Data(:,1);

Drehzahl_rotor_generator=Drehzahl*((20/129*21*29/74/79)^-1); %rpm

Drehmoment_generator=[]; %kNm

for i=1:length(Drehzahl)
    if (Drehzahl(i,1)~=0)

Drehmoment_generator(i,1)=P_el(i,1)./(Drehzahl_rotor_generator(i,1)*(2*pi/60));
%kNm

    else
    Drehmoment_generator(i,1)=0;

    end

end

f_tp=1;
[b,a]=butter(5,f_tp/(0.5*(2000)),'low');

Drehmoment_filtered=filter(b,a,Drehmoment); %kNm
Leistung_filtered=filter(b,a,Leistung_plot); %W
```

Chair for Wind Power Drives
Univ.-Prof. Dr.-Ing. Georg Jacobs

100

```matlab
Drehzahl_filtered=filter(b,a,Drehzahl); %rpm
Drehzahl_rotor_generator_filtered=filter(b,a,Drehzahl_rotor_generator); %rpm
P_el_filtered=filter(b,a,P_el(:,1)); %kW
Drehmoment_generator_filtered=filter(b,a,Drehmoment_generator); %kNm

Drehmoment_abtriebswelle_filtered=Drehmoment_filtered/((20/129*21*29/74/79)^-1);
difference=Drehmoment_abtriebswelle_filtered-Drehmoment_generator_filtered;
difference_filtered=filter(b,a,difference);
acel=diff(Drehzahl_rotor_generator_filtered*pi/30)./diff(Time_Drehzahl);
acel_filtered=filter(b,a,acel);
t_acel=Time_Drehzahl(2:end);


%PLOT


subplot(8,1,1)
plot(Time_Drehzahl,Drehzahl)
xlim([4800 7200])
ylabel('n_xrotor[rpm]');

subplot(8,1,2)
plot(Time_Drehmoment, Drehmoment)
xlim([4800 7200])
ylabel('M_xrotor[kNm]');
subplot(8,1,3)
plot(Time_Drehmoment, Leistung_plot)
xlim([4800 7200])
ylabel('Leistung[W]');
subplot(8,1,4)
plot(Time_Schalter_K537, Prozent_Schalter_K537)
xlim([4800 7200])
ylabel('K537');
subplot(8,1,5)
plot(Time_Schalter_K536, Prozent_Schalter_K536)
xlim([4800 7200])
ylabel('K536');
subplot(8,1,6)
plot(Time_Schalter_K500, Prozent_Schalter_K500)
xlim([4800 7200])
ylabel('K500');
subplot(8,1,7)
plot(Time_Schalter_K501, Prozent_Schalter_K501)
xlim([4800 7200])
ylabel('K501');
subplot(8,1,8)
plot(Time_Schalter_K502, Prozent_Schalter_K502)
xlim([4800 7200])
ylabel('K502');

figure;

plot(Time_Drehzahl,Drehzahl)
hold on
plot(Time_Drehmoment, Drehmoment)
hold on
plot(Time_Drehmoment, Leistung_plot/1000)
hold on
legend('n_xrotor[rpm]','M_xrotor[kNm]','Leistung[kW]')
xlim([4800 7200])
```

Chair for Wind Power Drives
Univ.-Prof. Dr.-Ing. Georg Jacobs

101

Appendix

Co-simulation with measurement data 20180830_170000_173000

```matlab
% written by Brian Rieckhoff,until %%%
pfad = 'C:\Program Files\SIMPACK-2017\partners\mathworks\simat';
addpath(pfad)
% simat
%%%




for i=1619420:1833578
    Time_Simulink(i-1619419,1)=Time_Drehzahl(i,1)-5.609709500164960e+03;
end
for i=1619420:1833578
    Drehmoment_generator_Simulink(i-
1619419,1)=Drehmoment_generator_filtered(i,1);

end
for i=1619420:1833578
    Drehmoment_Simulink(i-1619419,1)=Drehmoment_filtered(i,1);

end
for i=1619420:1833578
    Drehzahl_Simulink(i-1619419,1)=Drehzahl_filtered(i,1);
end
for i=1619420:1833578
    P_el_Simulink(i-1619419,1)=P_el_filtered(i,1);
End
```

Chair for Wind Power Drives
Univ.-Prof. Dr.-Ing. Georg Jacobs

102

Appendix 5

To create the start-up & run and stop operation look-up tables, Appendix 5.Figure 1 and Appendix 5.Figure 2 were used respectively. In this figures, $n_{measures}$ and two torques, T_e from measurement data and T_e *corrected* (generated by the open-loop simulation NSC- see Chapter 5), are shown. It is relevant to mention that the look-up table was done using T_e *corrected*, and not T_e from measurement data, because T_e *corrected* is the input variable that fits the dynamic of the V52-SM, as explained in Chapter 5.

Looking at Appendix 5. Figure 1 and Appendix 5. Figure 2, it is possible to see that while T_e from measurement data is zero during the start-up and stop operation, T_e *corrected* grows negative or positive respectively, and during run operation it is observed that T_e *corrected* is lower than T_e from measurement data. These effects proved to be very significant in the simulation and were considered in the designed look-up tables. For that reason, we can say that the design of the open-loop simulation NSC determined considerably the design of the closed-loop simulation NSC. In other words, the PID-action generated by the open-loop simulation NSC is tried to be reproduced by the closed-loop simulation NSC.

To create the start-up and stop operation look-up tables, values from $n_{measures}$ and its correspondent T_e *corrected* were collected (a sample rate was not necessary assumed). However, building the look-up table for the run operation proved to be a more difficult task, since in a look-up table it is not permitted to assign two different values of T_e *corrected* to a single $n_{measures}$ point. Therefore, and since during the run operation the rotational speed is almost constant, just three significant points were selected and included in the look-up table, expecting that they would describe this quasi-static regime. The election of these points turned out to be successful at the end, since the simulated rotational speed fitted the measurement data.
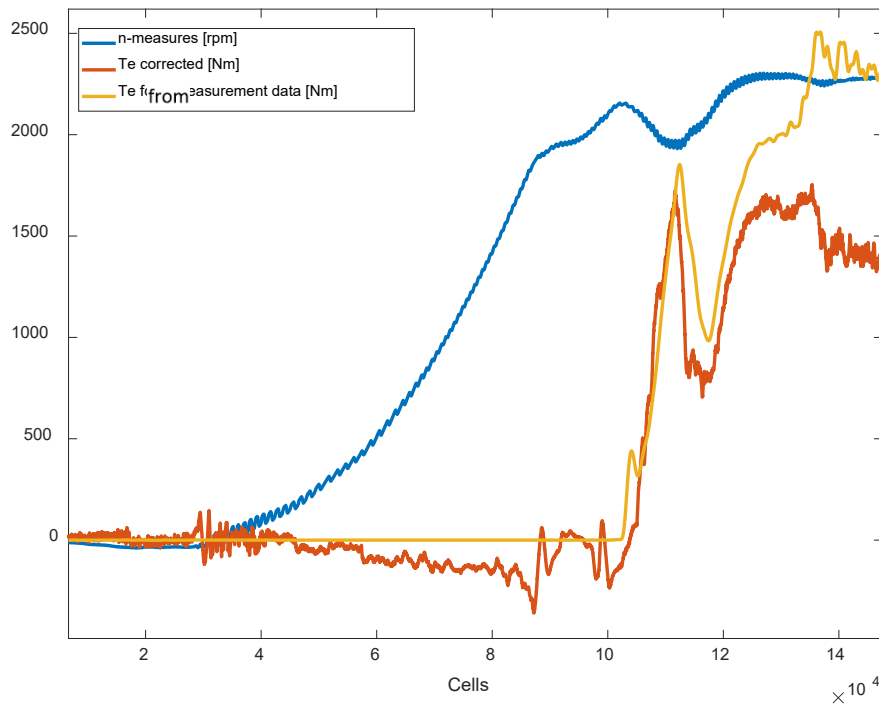
Appendix 5.Figure 1: Plot used to build start-up & run operation look-up table (T_e from measurement data was filtered).The horizontal axis represents the MATLAB-cells in which the data are sampled with a sampling frequency of 2000 Hz.
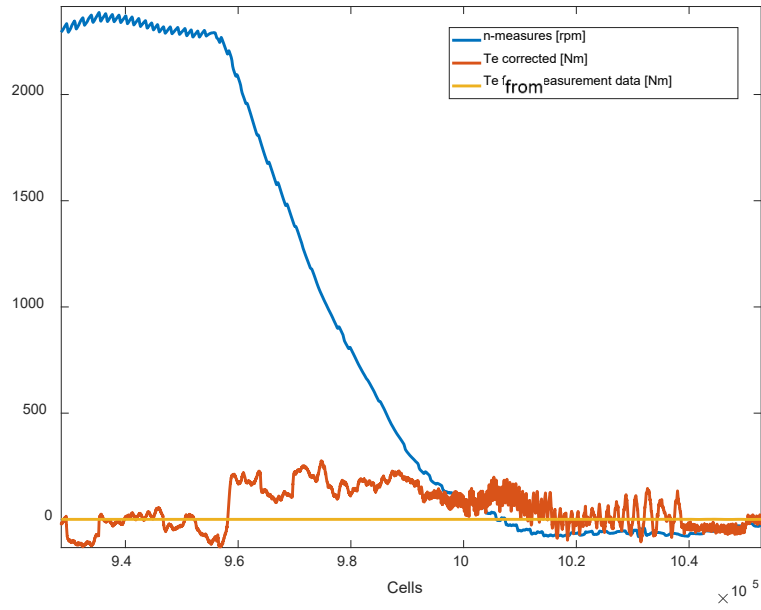
Appendix 5.Figure 2: The horizontal axis represents the MATLAB-cells in which the data are sampled with a sampling frequency of 2000 Hz.

Chair for Wind Power Drives
Univ.-Prof. Dr.-Ing. Georg Jacobs

104